Dynamics of Oceans:
Pt 1: Vast & Diverse

Professor Baylor Fox-Kemper

Brown University
Dept. of Earth, Environmental, and Planetary Sciences
(Formerly U. Colorado Atmospheres and Oceans)
Supported by NASA (NNX09AF38G), NSF (0934737, 1245944, 2220280), ONR (N00014-17-1-2963), NOAA (NA19OAR4310366), Gulf of Mexico Research Initiative, Schmidt Futures

Boulder School for Condensed Matter and Materials Physics
July 18, 2022

For Today

- Vast & Diverse
  - Turbulence
  - Waves
- Breakpoints at the Grid Scale
- Mesoscale, Submesoscale, Boundary Layer
- Navier-Stokes
- Boussinesq
  - Hydrostatic or Not?
- Quasi-Geostrophic?
- Wave-Averaged Equations for Boundary Layer to capture Langmuir turbulence

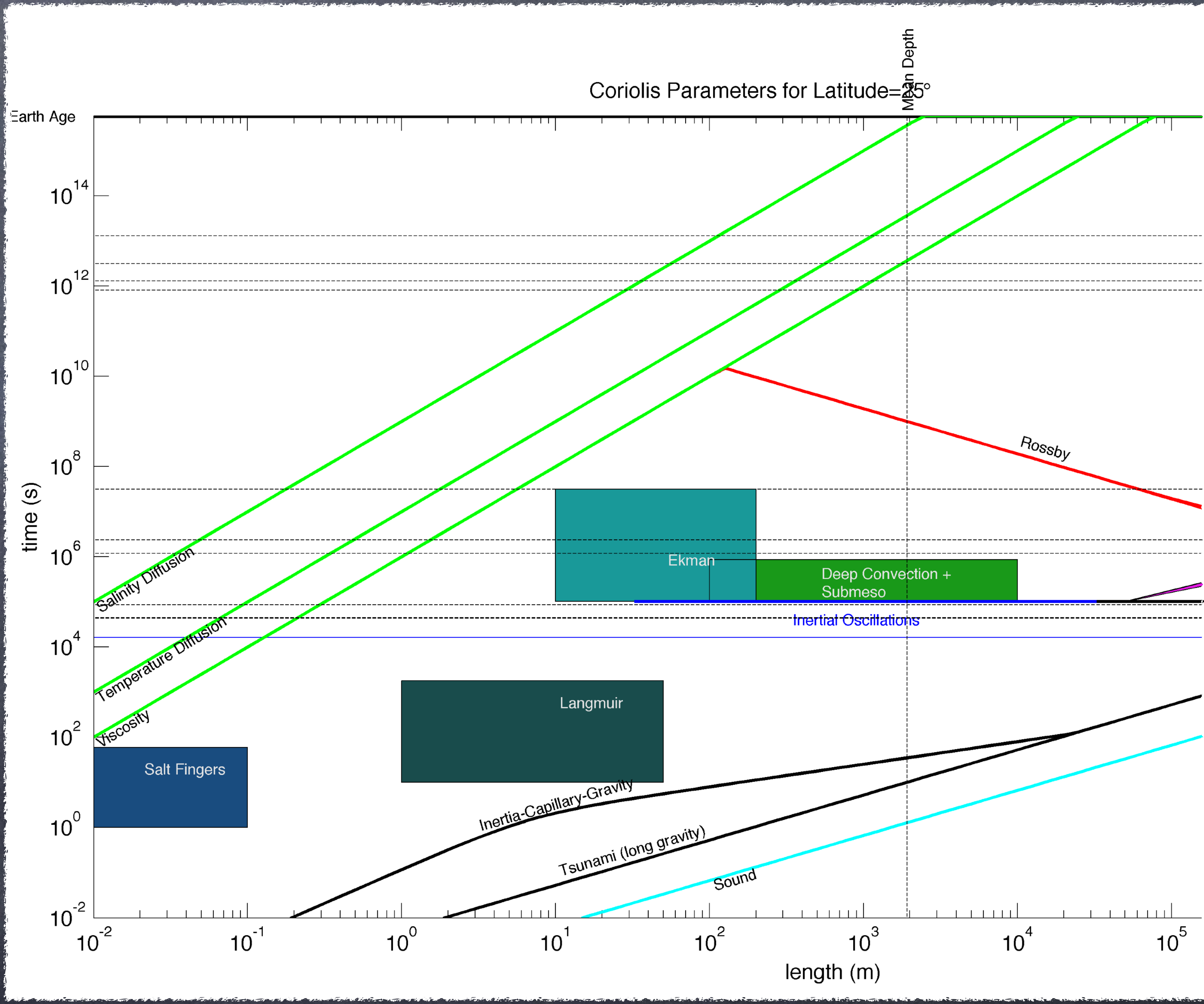

Estimating the Circulation & Climate of the Ocean

LLC4320 Model

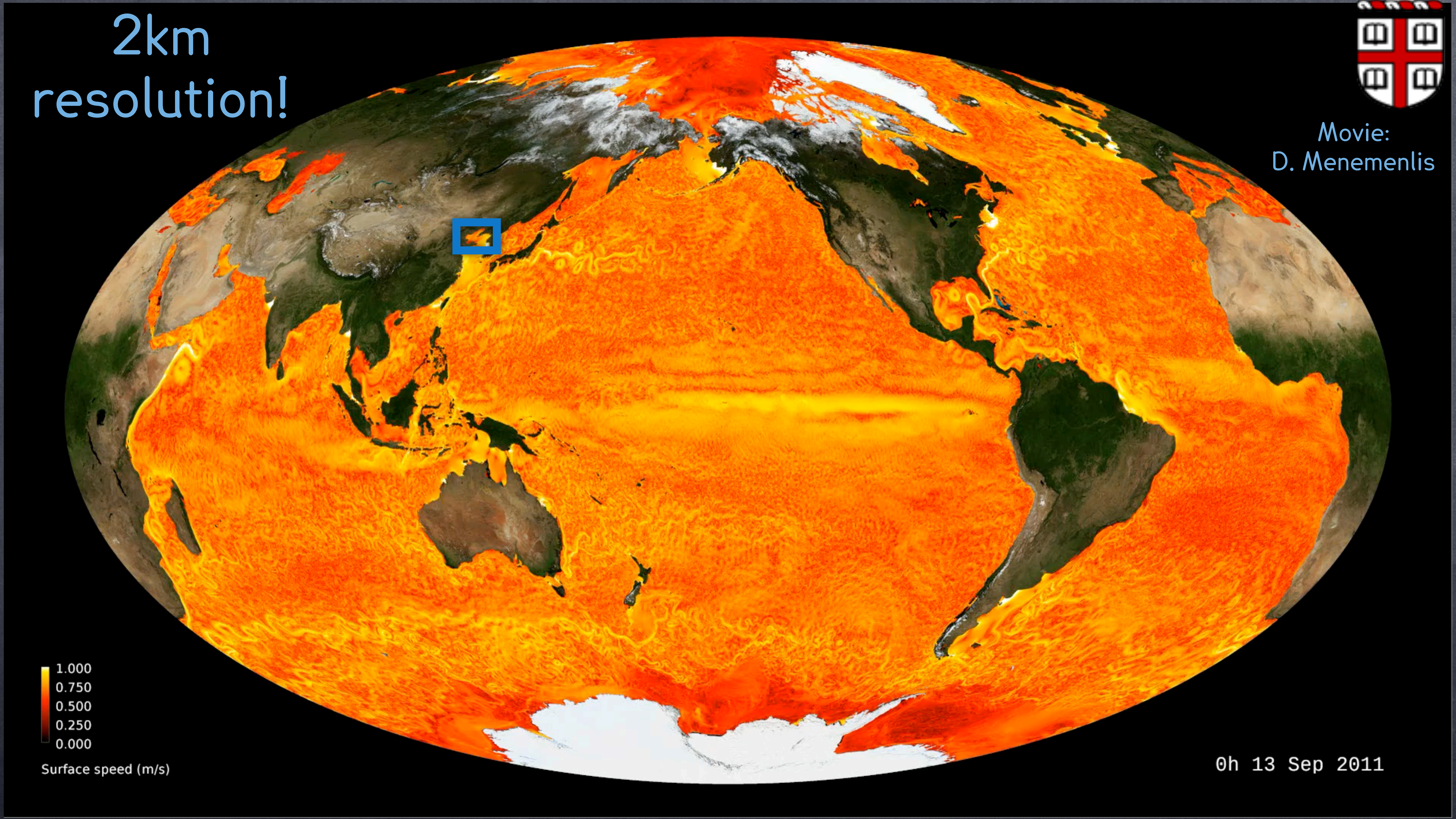

BFK, S. Bachman, B. Pearson, and S. Reckinger. Principles and advances in subgrid modeling for eddy-rich simulations. CLIVAR Exchanges, 19(2):42-46, 2014.

Estimating the Circulation & Climate of the Ocean LLC4320 Model

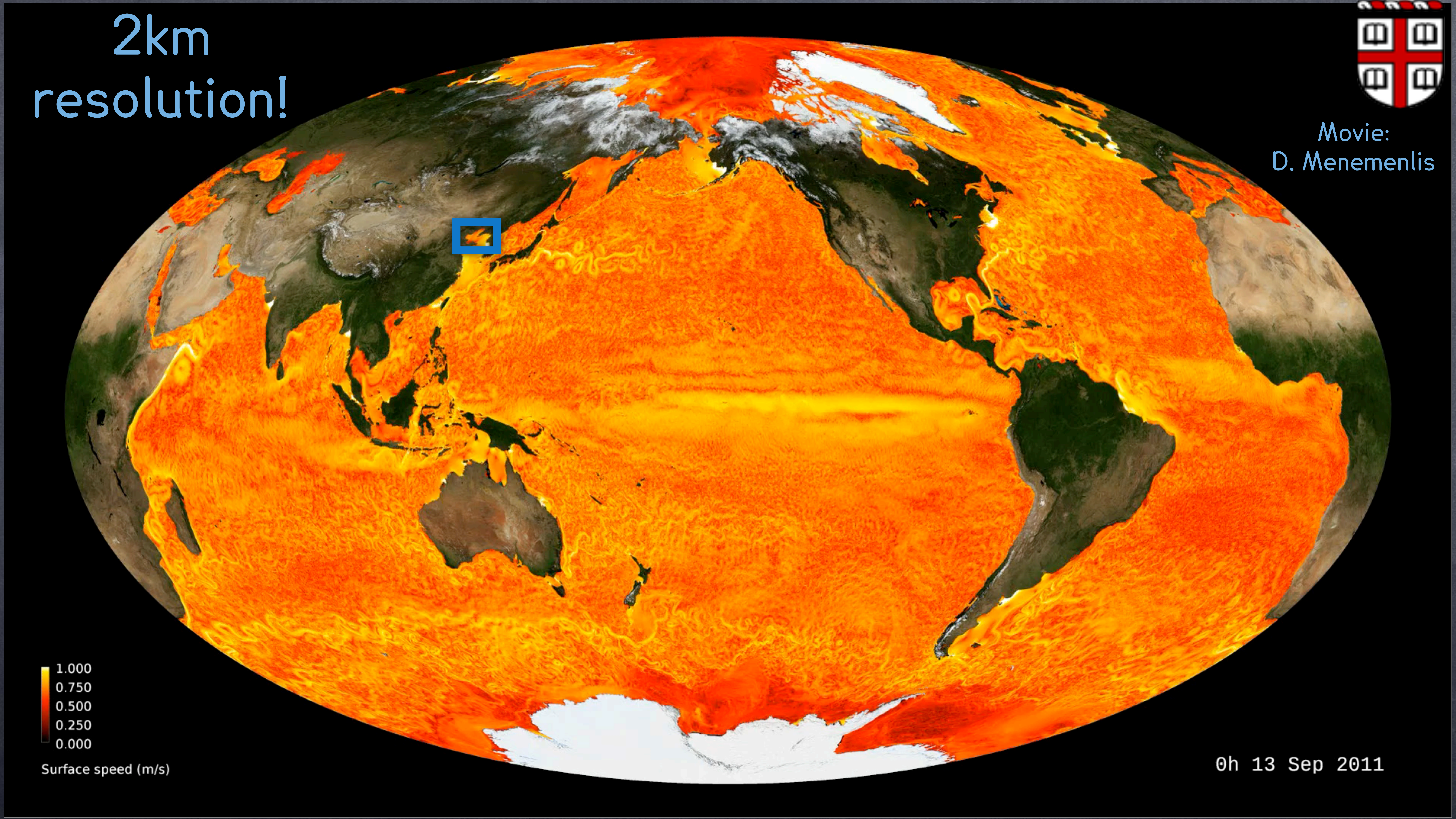

BFK, S. Bachman, B. Pearson, and S. Reckinger. Principles and advances in subgrid modeling for eddy-rich simulations. CLIVAR Exchanges, 19(2):42-46, 2014.

Estimating the Circulation & Cl

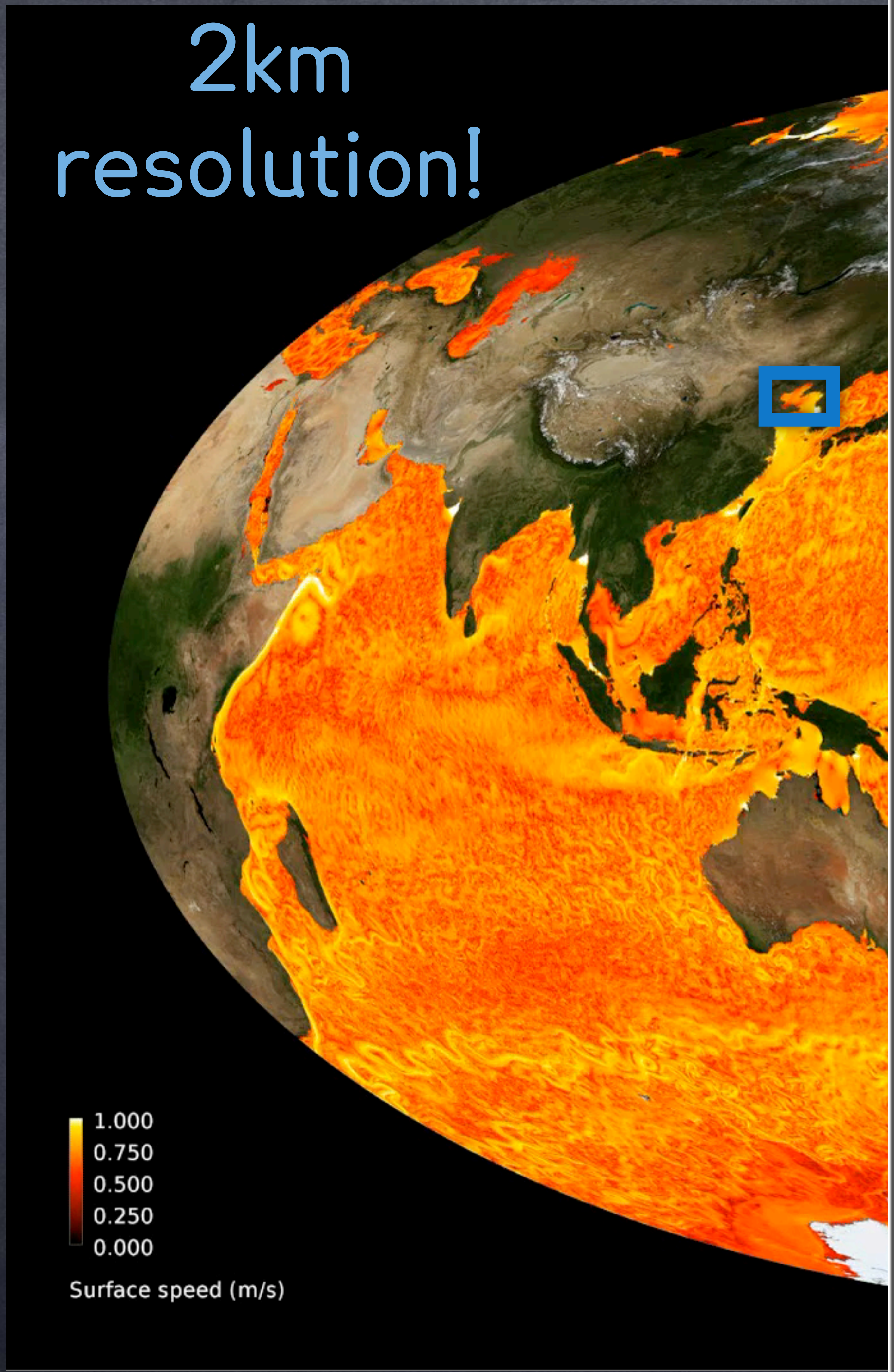

BFK, S. Bachman, B. Pearson, and S. R
simulations. CLIVAR Exchanges, 19(2)

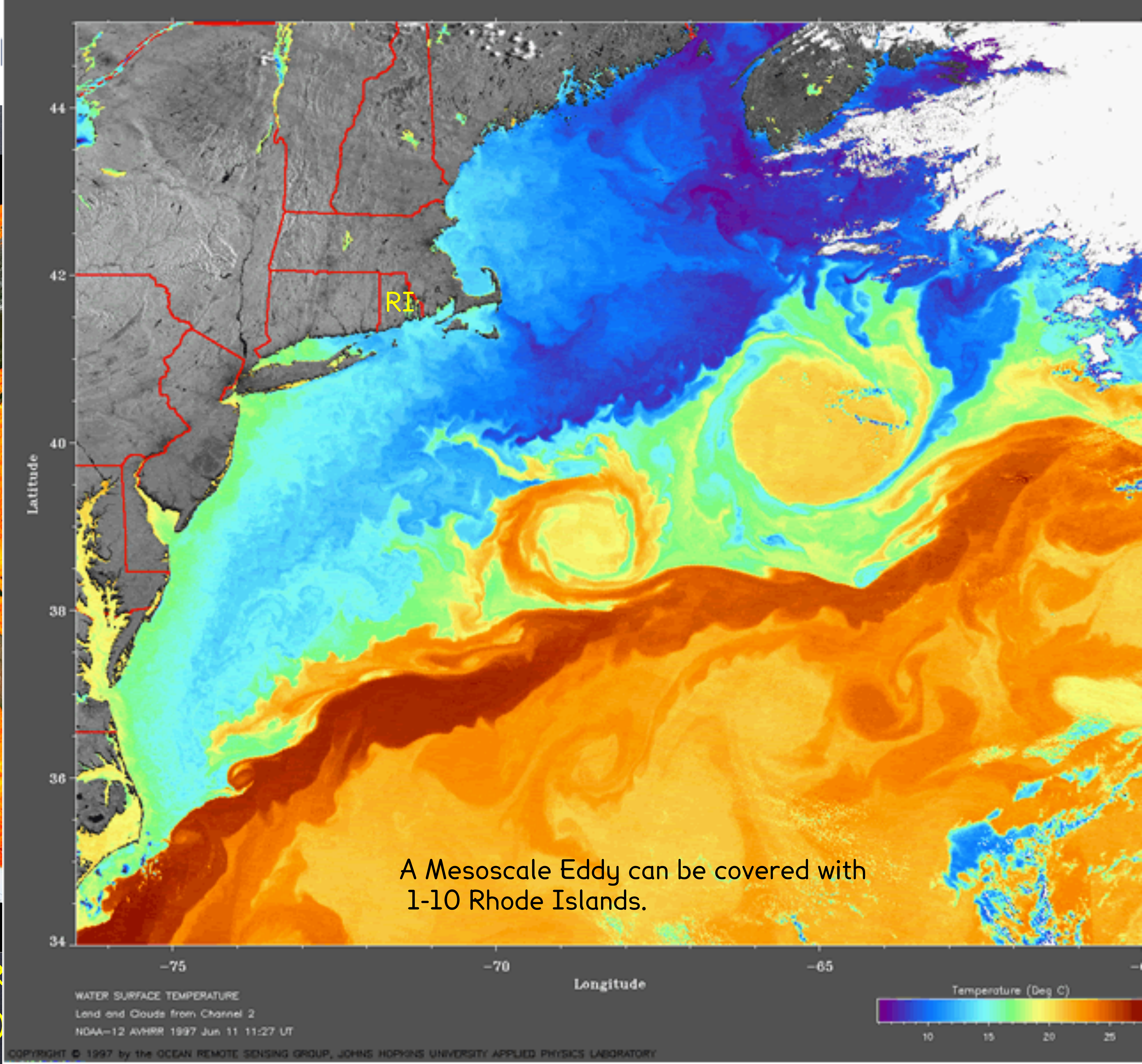

Estimating the Circulation & Climate of the Ocean LLC4320 Model

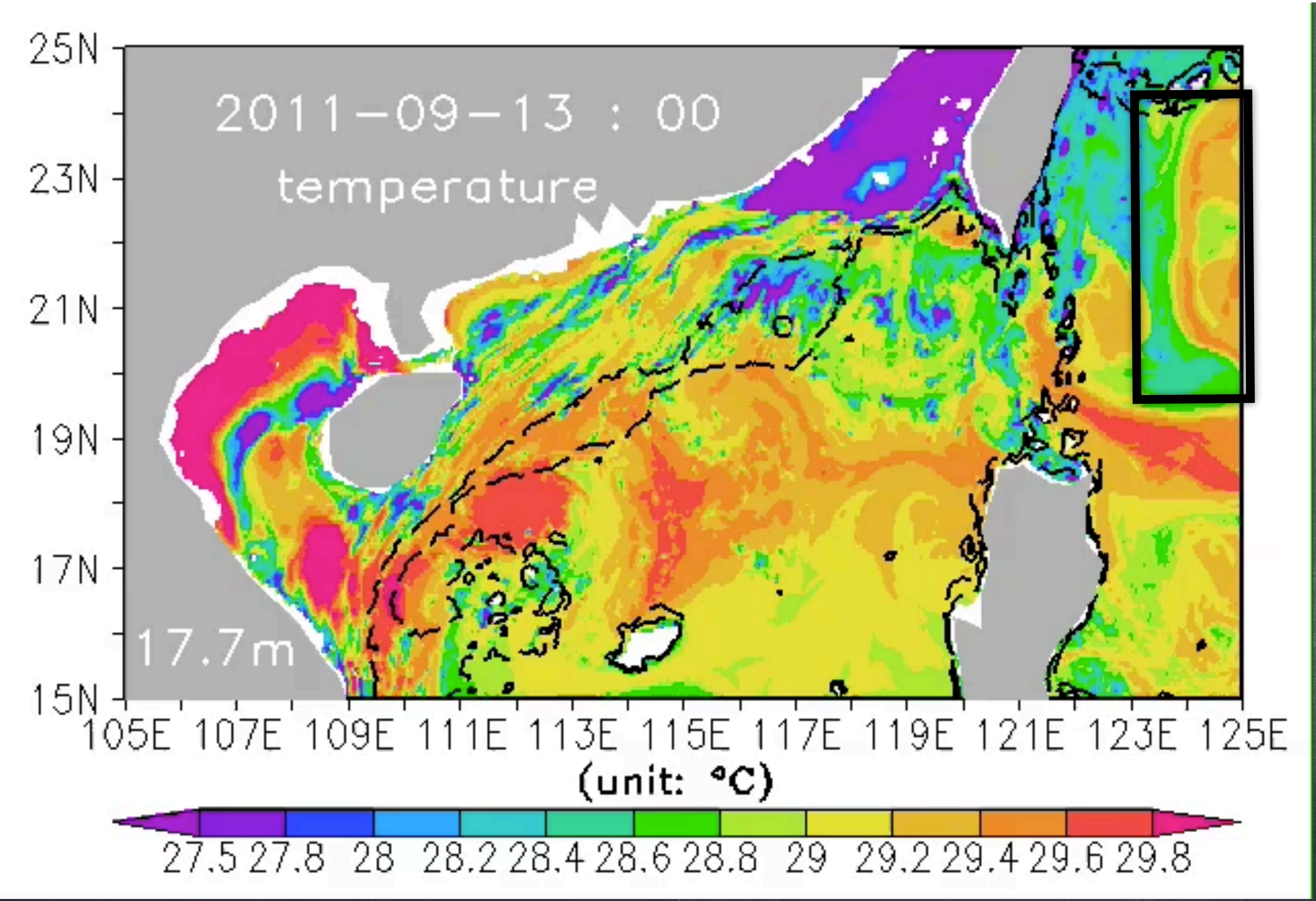

Local Analysis and Movie: Z. Jing, Y. Qi, BFK, Y. Du, and S. Lian. Seasonal thermal fronts and their associations with monsoon forcing on the continental shelf of northern South China Sea: Satellite measurements and three repeated field surveys in winter, spring and summer. JGR-Oceans, 121:1914-1930, 2016.

H. Cao, Z. Jing, BFK, T. Yan, and Y. Qi. Scale transition from geostrophic motions to internal waves in the northern South China Sea. JGR-Oceans, 124, 2019.

Estimating the Circulation & Climate of the Ocean LLC4320 Model

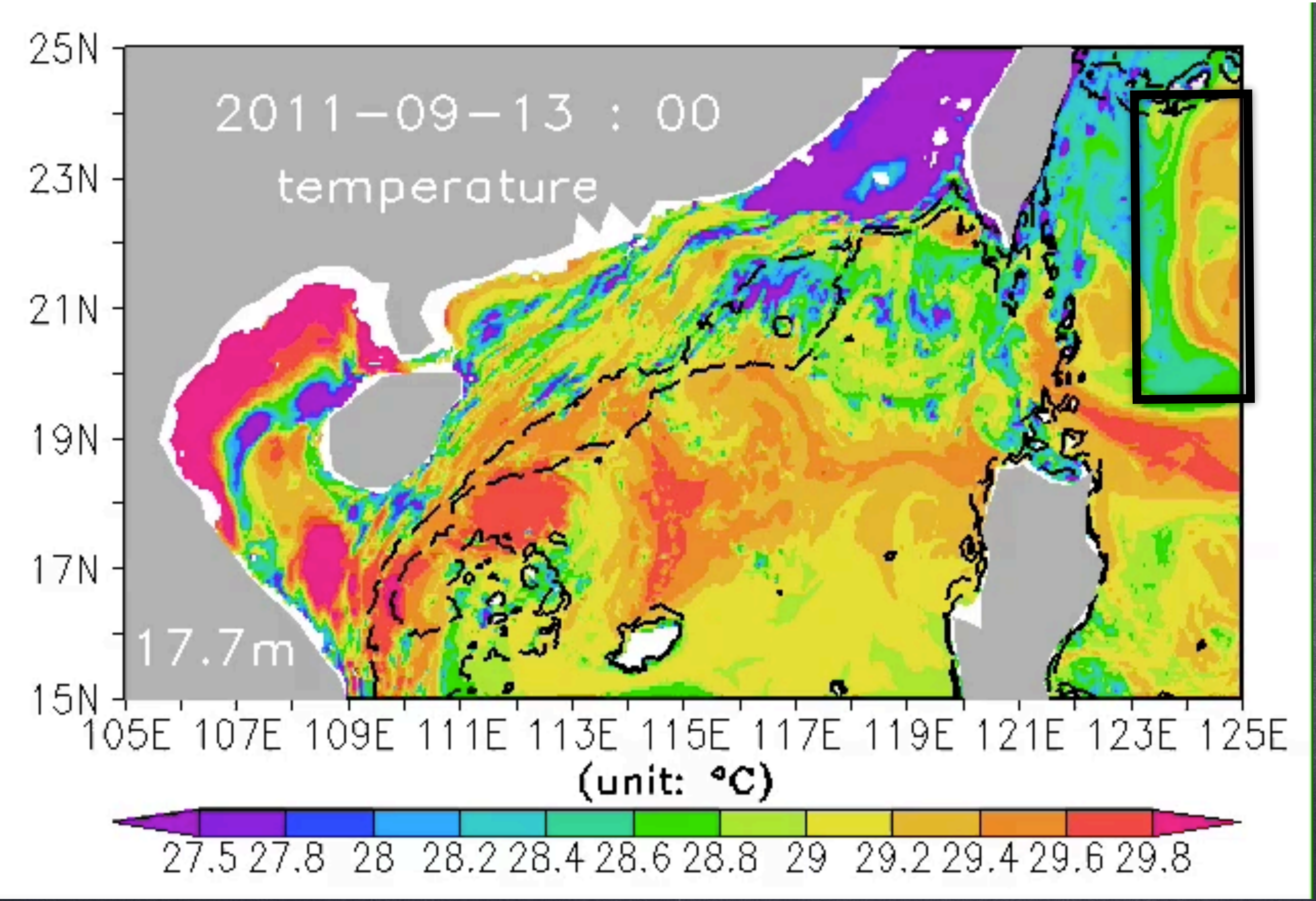

Local Analysis and Movie: Z. Jing, Y. Qi, BFK, Y. Du, and S. Lian. Seasonal thermal fronts and their associations with monsoon forcing on the continental shelf of northern South China Sea: Satellite measurements and three repeated field surveys in winter, spring and summer. JGR-Oceans, 121:1914-1930, 2016.

H. Cao, Z. Jing, BFK, T. Yan, and Y. Qi. Scale transition from geostrophic motions to internal waves in the northern South China Sea. JGR-Oceans, 124, 2019.

200km x 600km
x 700m
domain

1000 Day
Simulation

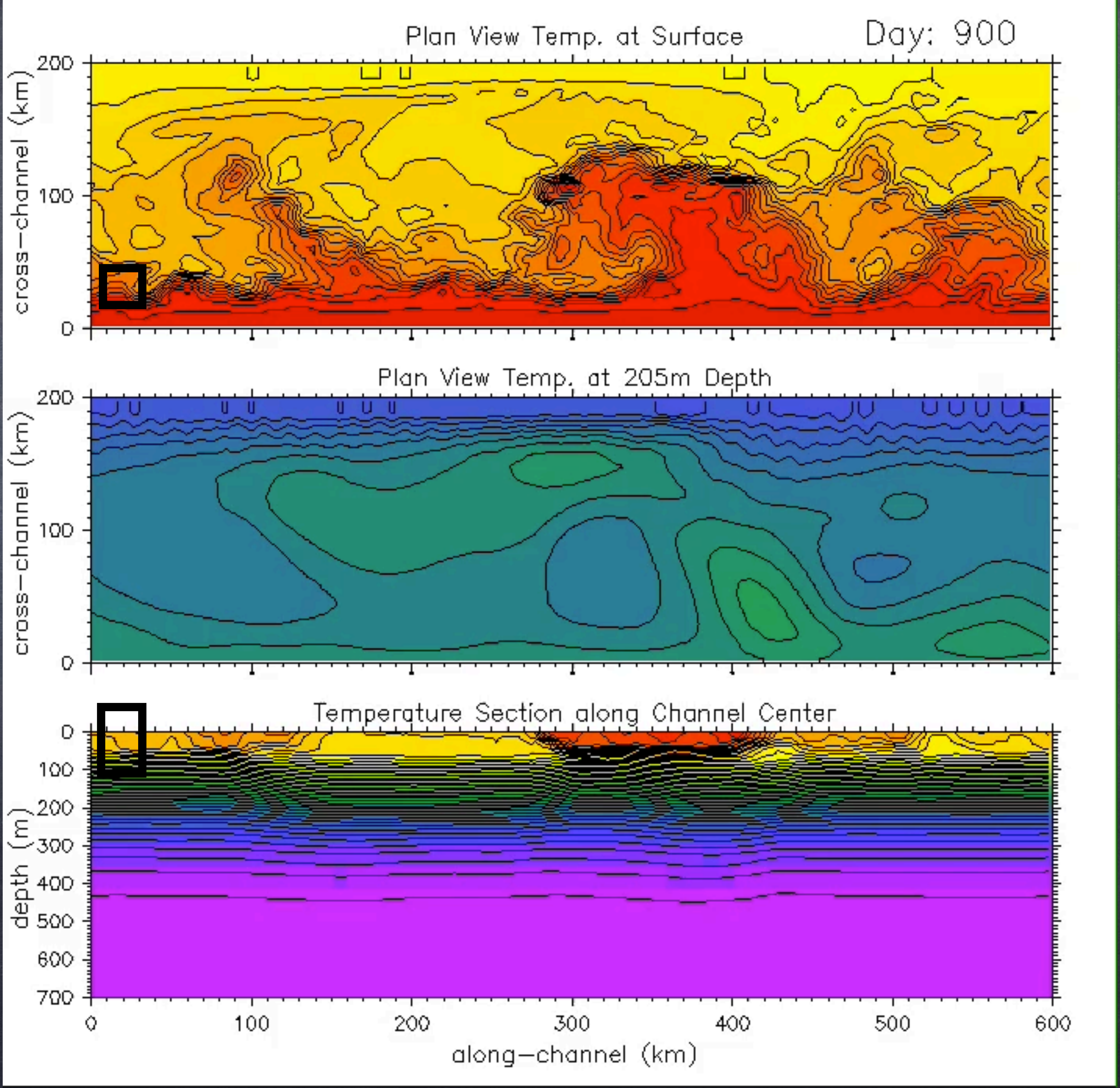

G. Boccaletti, R. Ferrari, and BFK. Mixed layer instabilities and restratification. Journal of Physical Oceanography, 37(9):2228-2250, 2007.

200km x 600km x 700m domain

1000 Day Simulation

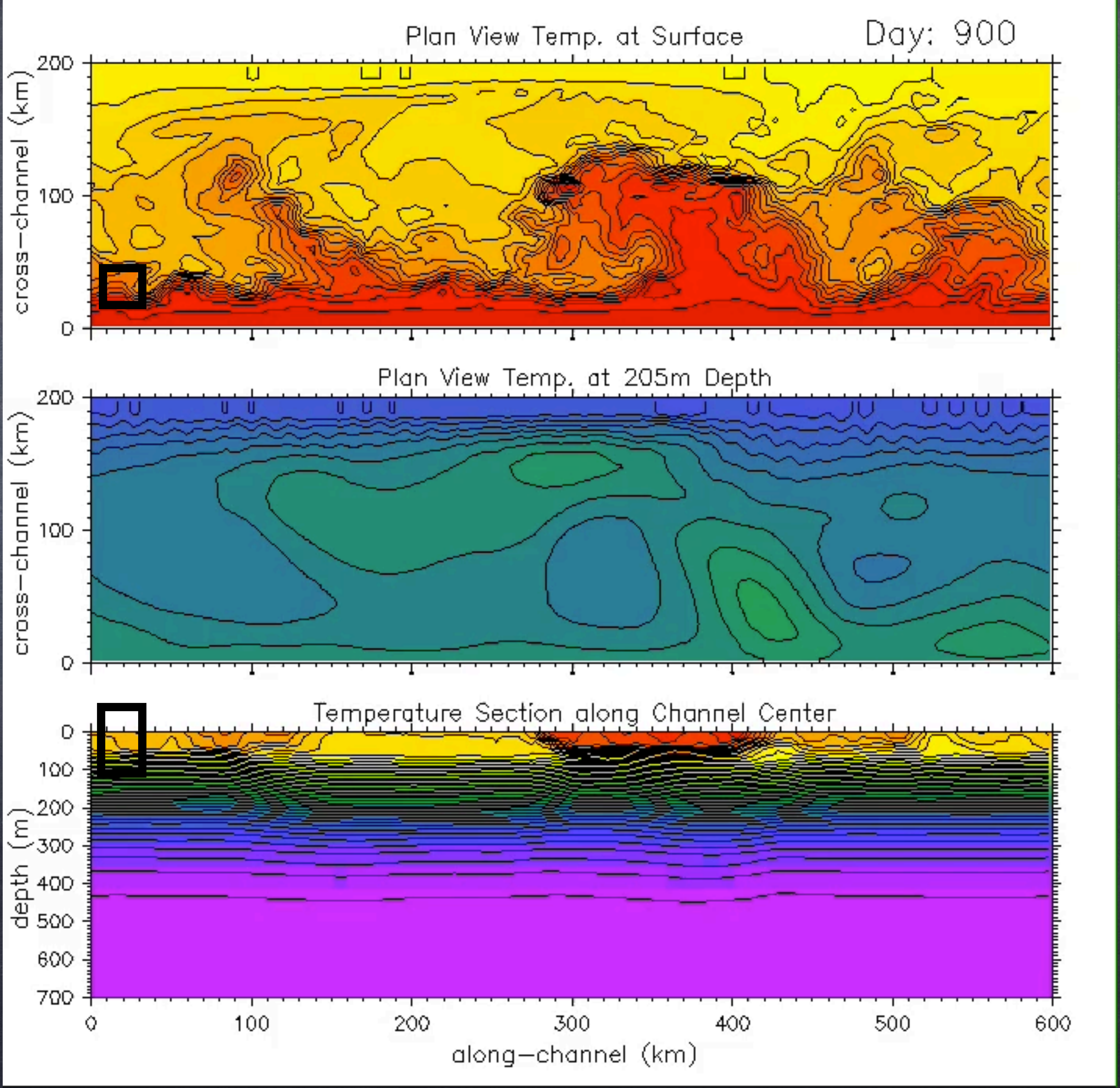

G. Boccaletti, R. Ferrari, and BFK. Mixed layer instabilities and restratification. Journal of Physical Oceanography, 37(9):2228-2250, 2007.

20km x 20km x 150m domain

15 Day Simulation

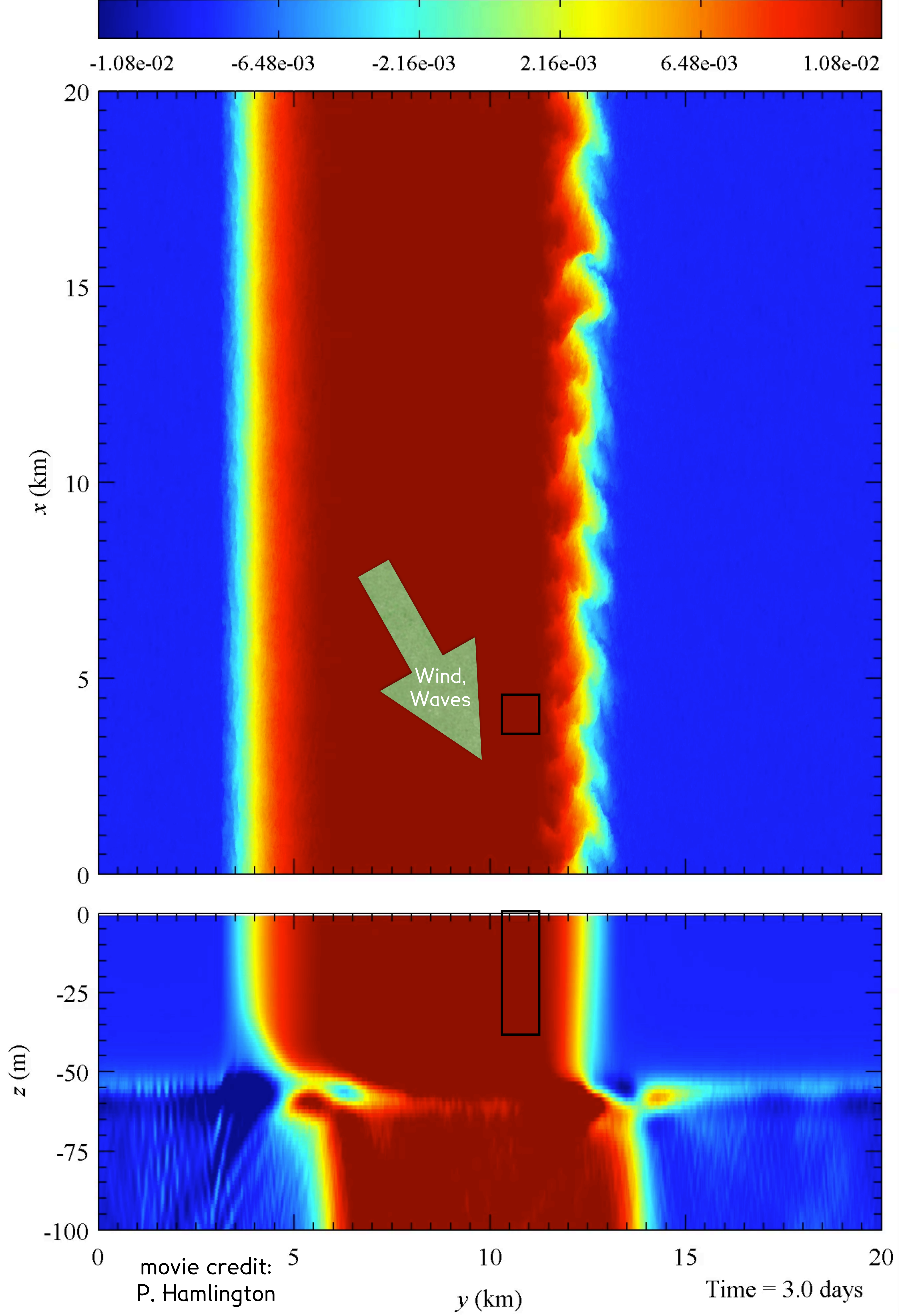

P. E. Hamlington, L. P. Van Roekel, BFK, K. Julien, and G. P. Chini. Langmuir-submesoscale interactions: Descriptive analysis of multiscale frontal spin-down simulations. Journal of Physical Oceanography, 44(9):2249-2272, September 2014.

University of Colorado at Boulder

20km x 20km x 150m
domain

15 Day Simulation

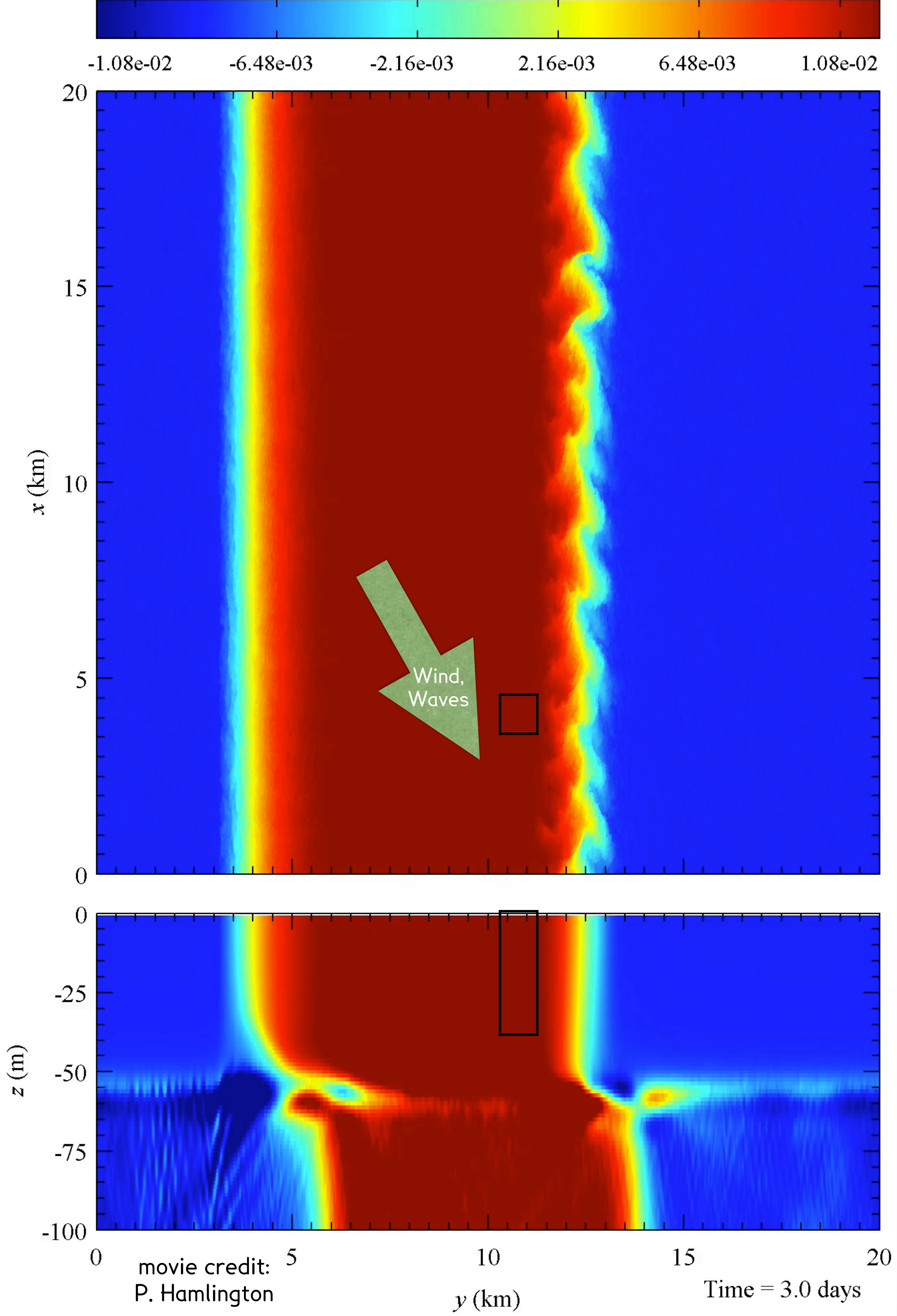

P. E. Hamlington, L. P. Van Roekel, BFK, K. Julien, and G. P. Chini. Langmuir-submesoscale interactions: Descriptive analysis of multiscale frontal spin-down simulations. Journal of Physical Oceanography, 44(9):2249-2272, September 2014.

Colorado
University of Colorado at Boulder

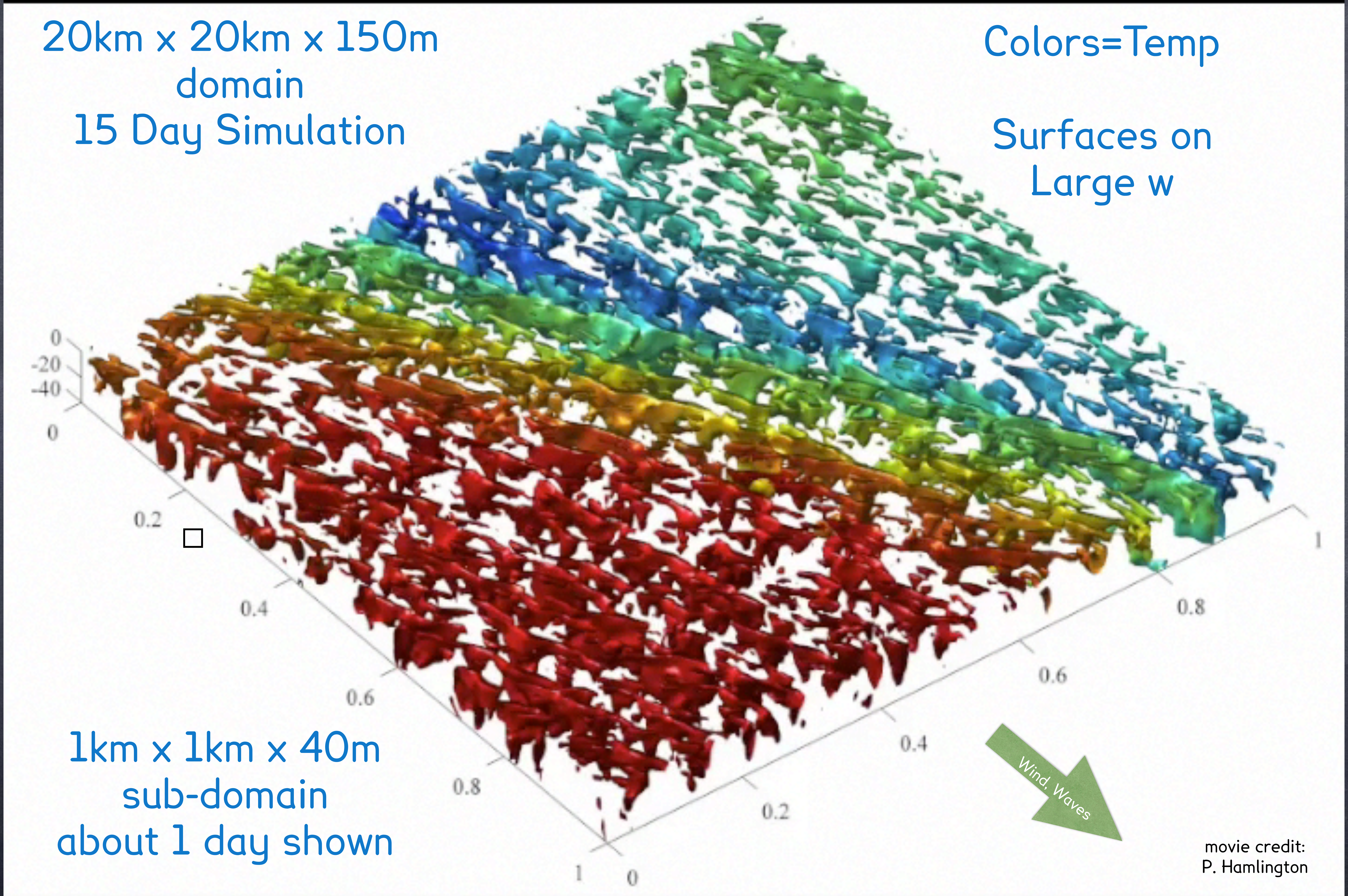

P. E. Hamlington, L. P. Van Roekel, BFK, K. Julien, and G. P. Chini. Langmuir-submesoscale interactions: Descriptive analysis of multiscale frontal spin-down simulations. Journal of Physical Oceanography, 44(9):2249-2272, September 2014.

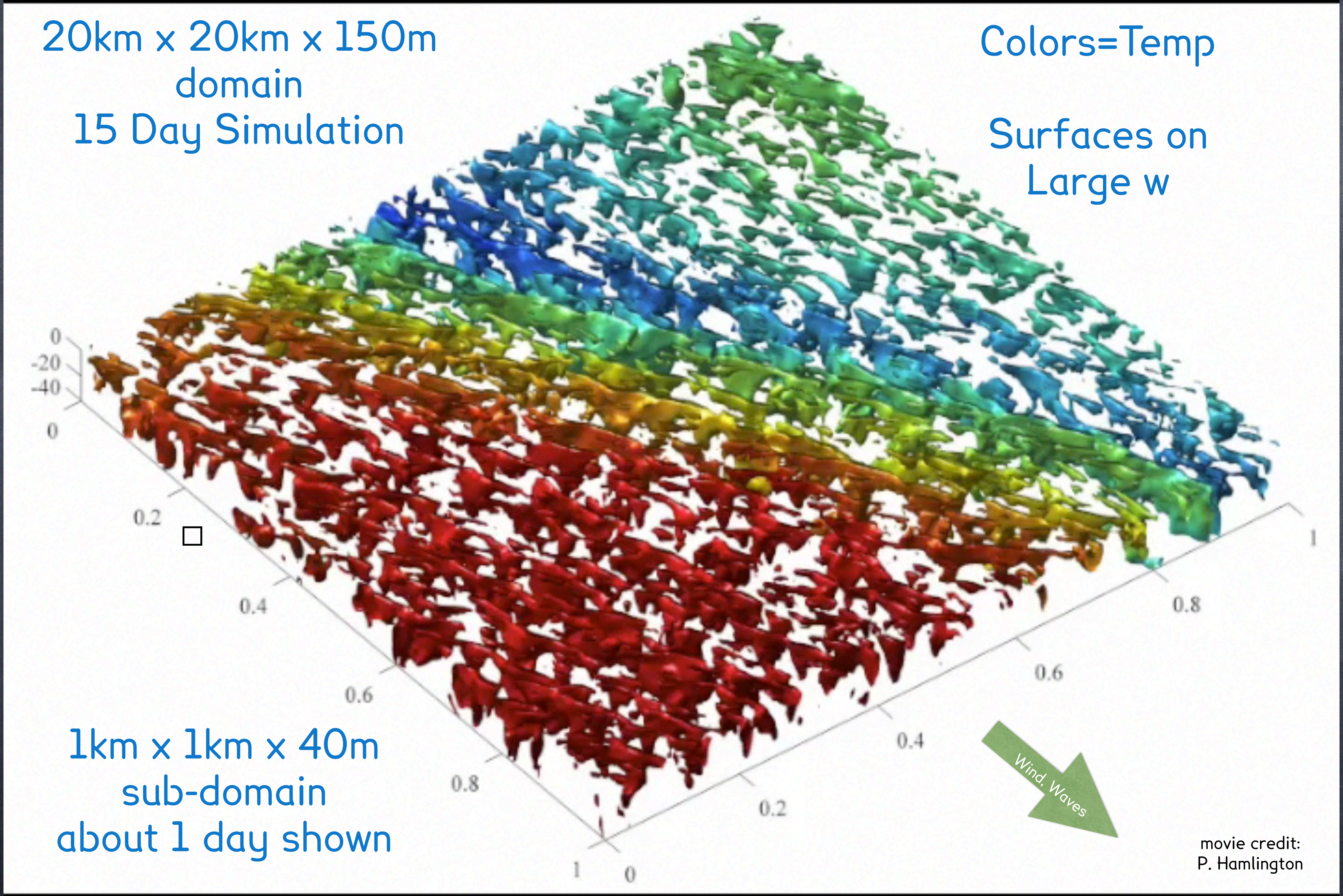

P. E. Hamlington, L. P. Van Roekel, BFK, K. Julien, and G. P. Chini. Langmuir-submesoscale interactions: Descriptive analysis of multiscale frontal spin-down simulations. Journal of Physical Oceanography, 44(9):2249-2272, September 2014.

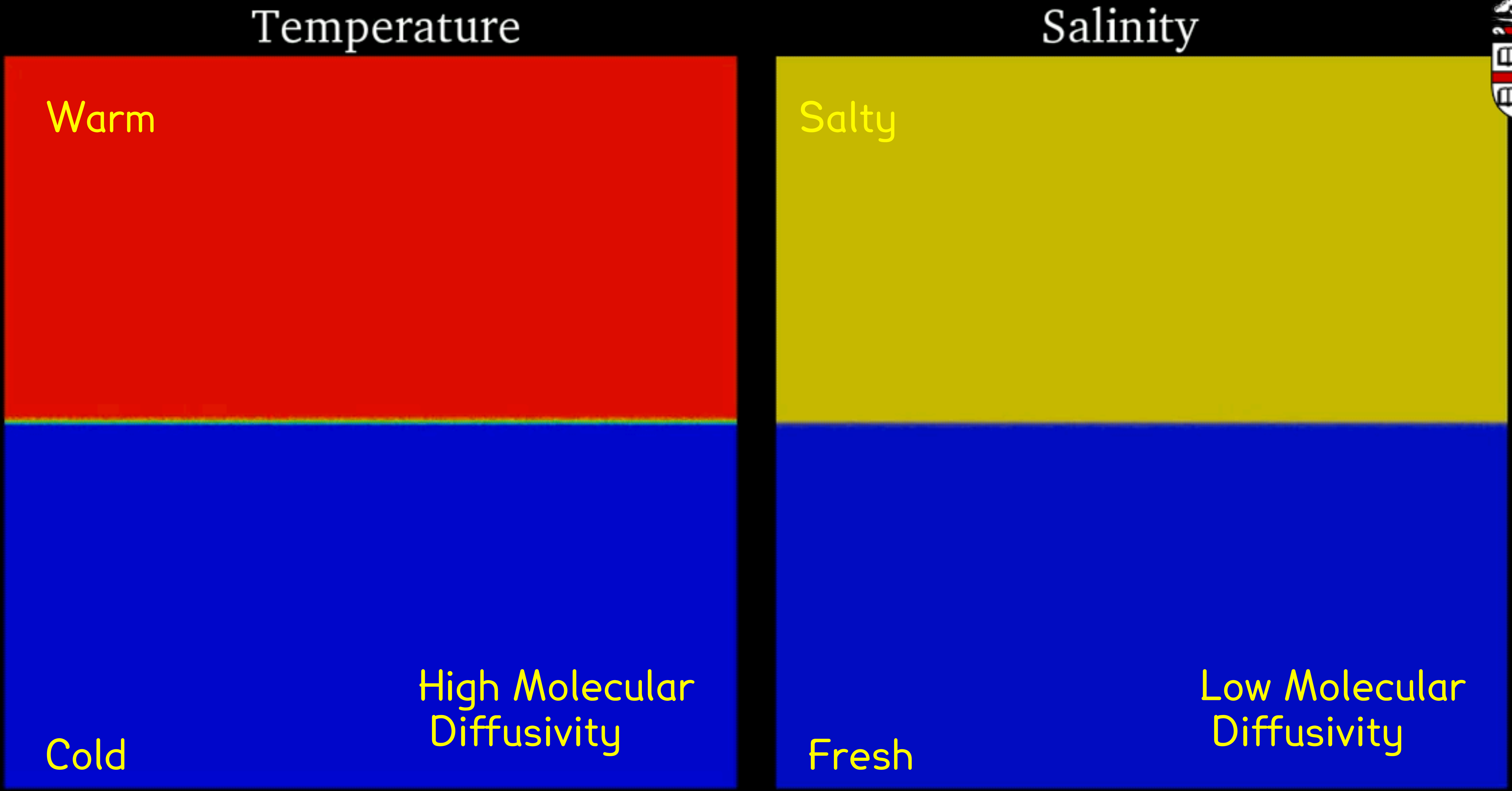

Top: Warm, salt water
Bottom: Cold, fresh water

Movie Credit: mmnasr on YouTube.

Temperature

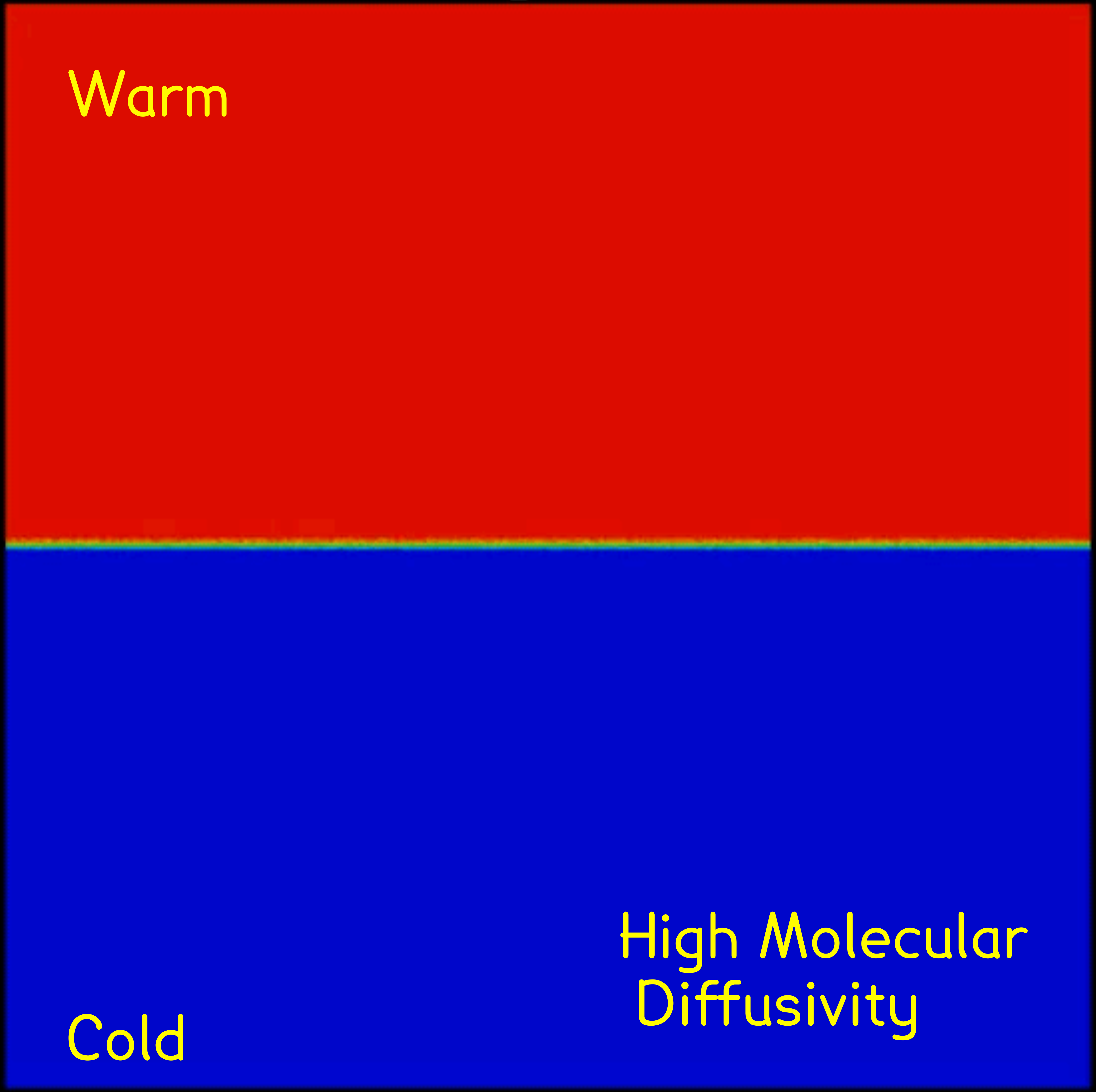

Salinity

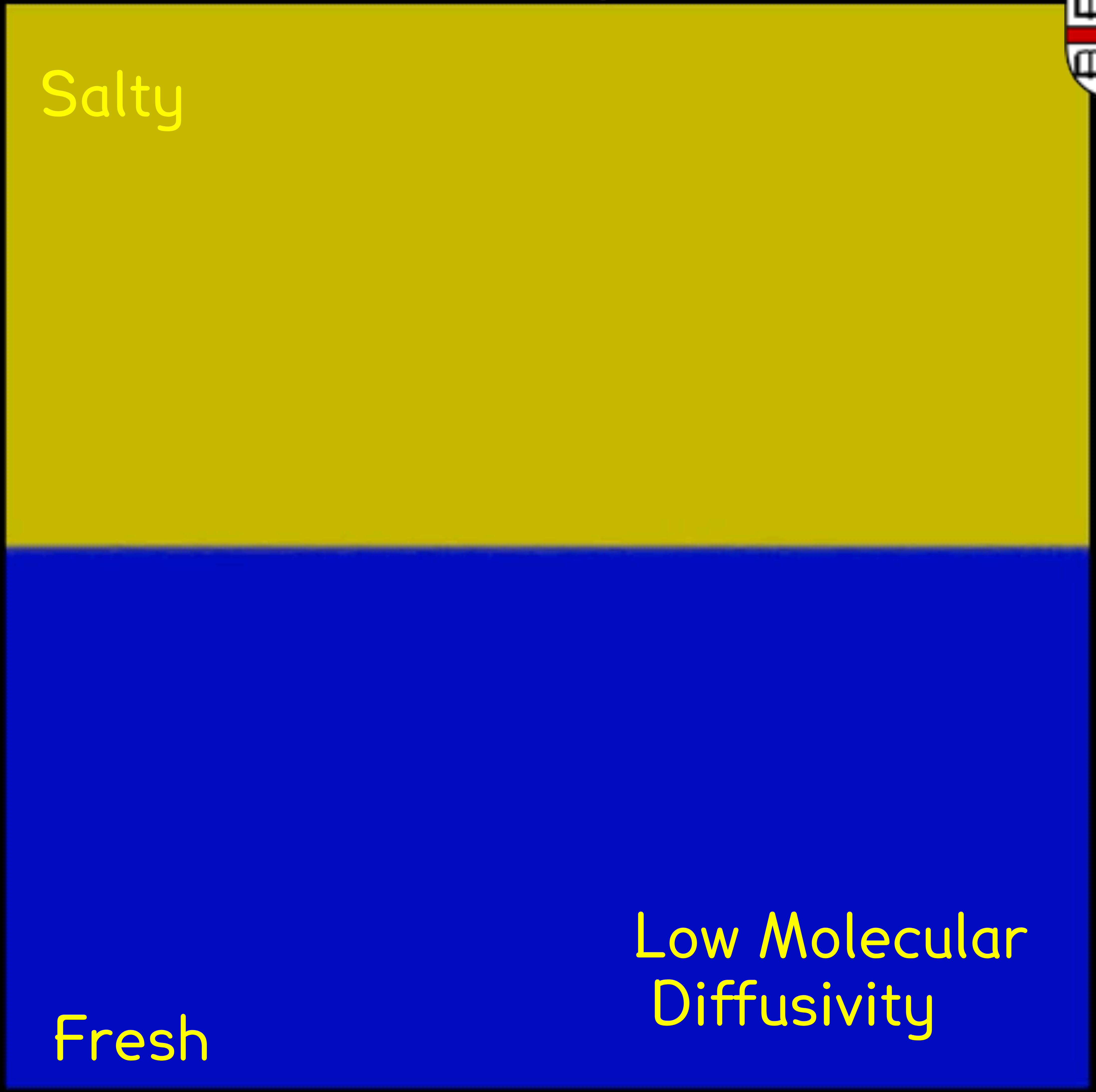

Top: Warm, salt water
Bottom: Cold, fresh water

Movie Credit: mmnasr on YouTube.

The Ocean is Vast & Diverse

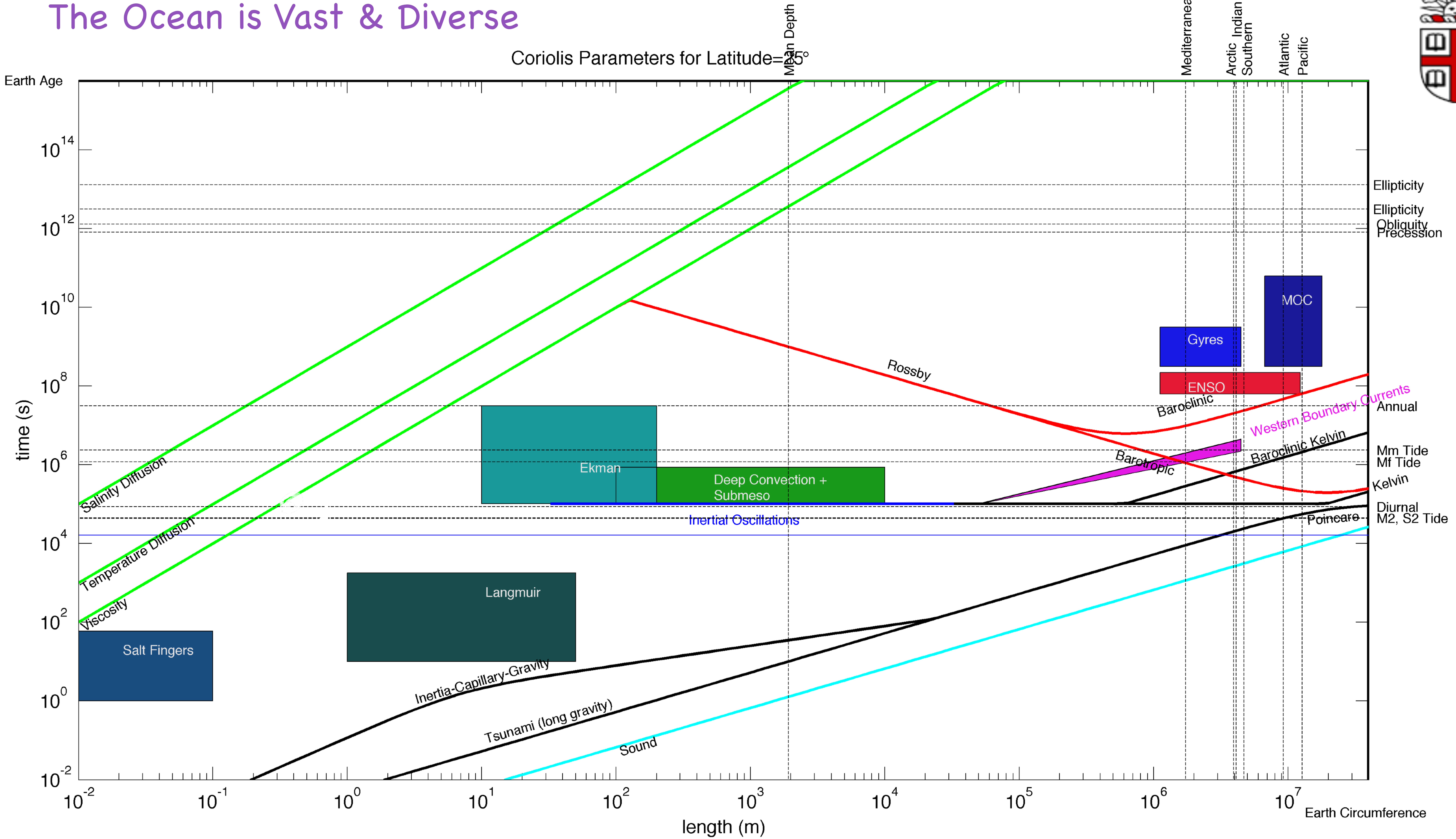

The small scales of the ocean may hold the key to surprises

Sharp fronts and eddies that are ubiquitous in the world ocean, as well as features such as shelf seas and under-ice-shelf cavities, are not captured in climate projections. Such small-scale processes can play a key role in how the large-scale ocean and cryosphere evolve under climate change, posing a challenge to climate models.

Helene Hewitt, Baylor Fox-Kemper, Brodie Pearson, Malcolm Roberts and Daniel Klocke

Hewitt et al., *Nature Climate Change*, 2022

But, global models won't resolve these small processes for decades.

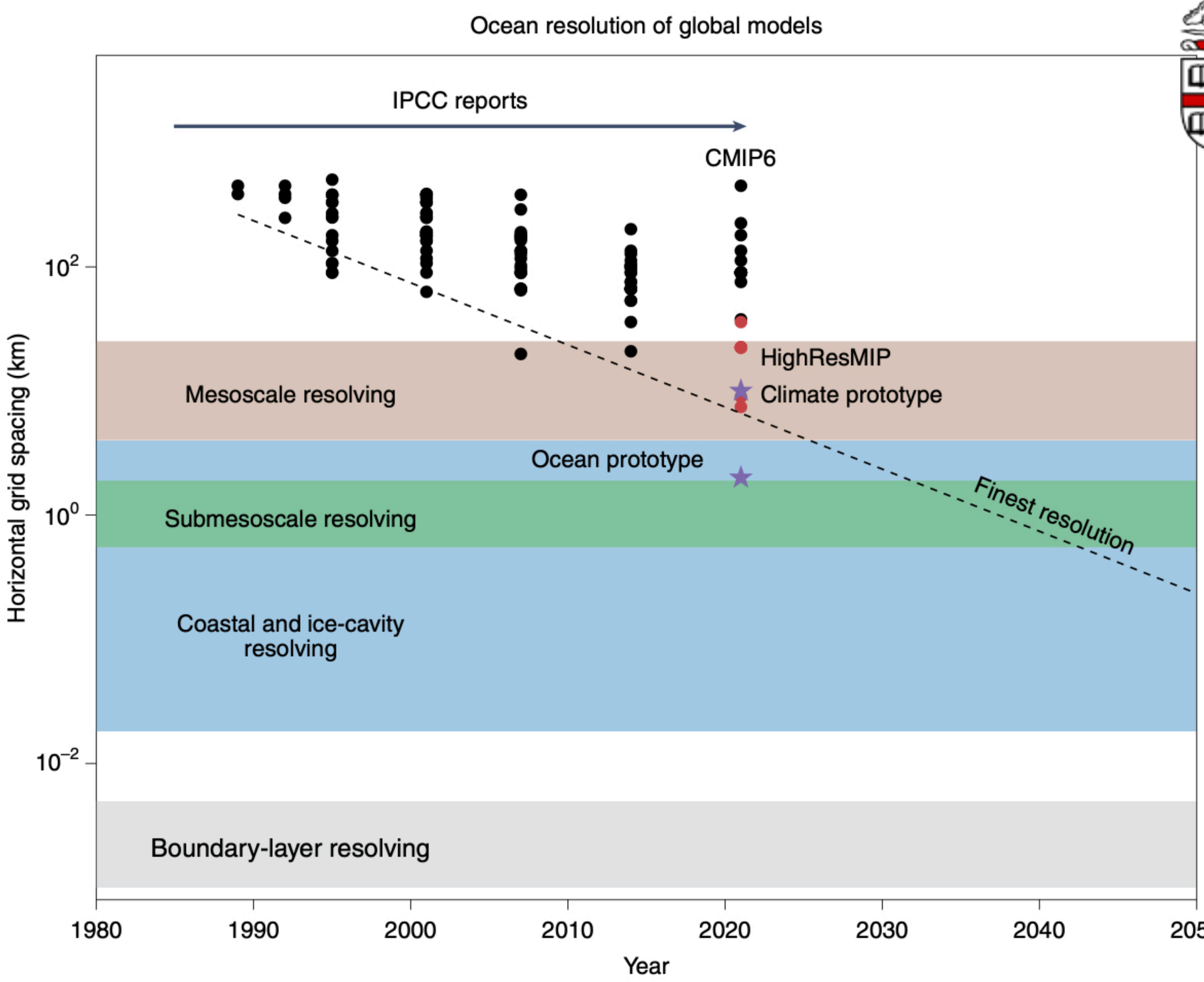

Fig. 2 | The evolution of global ocean model resolution by publication year. Shown are models from

Hewitt et al., *Nature Climate Change*, 2022

Nesting/Overlapping

- OK, can simulate global down to molecular scale in 4-5 single-scale nestings, each 1 teragrid (10^{12} space+time units), so could simulate effects of climate change on any chosen small domain fully.

- A teragrid is an accessible amount of computing (e.g., a PhD thesis could contain many with normal resources, possibly more with good code & gpus).

- If a simulation spans more than one scale, they simulations are much more expensive O(10-1000 teragrids)).

- But, what equations for each nest?

Don't we already know the equations?

- Euler, 1757
- Laplace et al., 1829
- Navier, 1822
- Fourier, 1822
- Stokes, 1845
- Fick, 1855
- Onsager, 1931

Yes, but...

Not how to solve them!

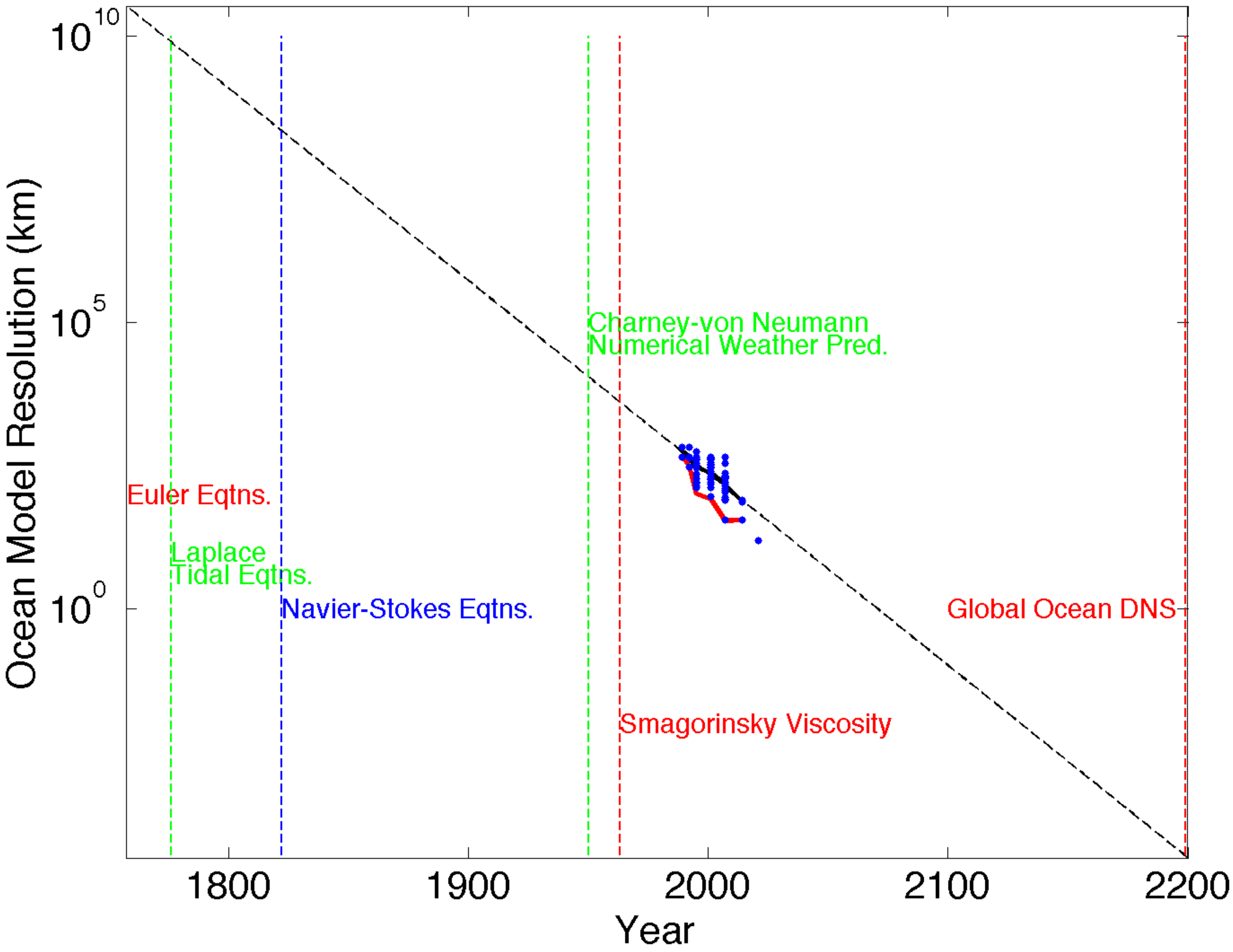

The Ocean is Vast & Diverse:

Vast scales, diverse phenomena, e.g.,
Global, Mesoscale, Submesoscale, Langmuir,
Double Diffusion

- Understanding each scale is needed as we can't afford to resolve all of the scales at once.
- At each grid resolution, we need to parameterize the smaller scales (subgrid modeling).
- Fronts appear at each scale, with varying intensity and varying characters of frontal instabilities/ turbulence
- What equations are appropriate at each scale?

BFK. New Frontiers in Operational Oceanography, chapter Notions for the Motions of the Oceans, pages 27-73. GODAE OceanView, 2018.

The New Schools:

Reduced Models

- Boussinesq, 1897
- Charney, 1947
- Longuet-Higgins, 1962
- Hasselmann, 1971
- Craik-Leibovich, 1976
- Blumen, 1982
- Samelson & Vallis, 1997
- McWilliams, Sullivan, & Moeng, 1997
- Pierrehumbert, Held, & Swanson, 1994
- Julien & Knobloch, 2007

Parameterizations

- Stommel, 1948
- Munk, 1950
- Smagorinsky, 1963
- Mellor & Yamada, 1982
- Gent & McWilliams, 1990
- Large, McWilliams, Doney, 1994
- Leith, 1996
- McDougall, 2003
- Kantha & Clayson, 2004
- Fox-Kemper, Ferrari, Hallberg 2008
- Harcourt, 2013
- Bachman, Fox-Kemper, Pearson 2017
- Reichl & Li, 2019
- Bodner et al. 2022...

Key Concept:

Gridscale* Dimensionless Parameters

Gridscale Reynolds[1]:

$$Re^* = \frac{U^* \Delta x}{\nu^*}$$

Gridscale Péclet[1]:

$$Pe^* = \frac{U^* \Delta x}{\kappa^*}$$

Gridscale Rossby:

$$Ro^* = \frac{U^*}{f \Delta x}$$

Gridscale Richardson:

$$Ri^* = \frac{\Delta b^* \Delta z}{\Delta U^{*2}}$$

Gridscale Burger:

$$Bu^* = \frac{N^{*2} \Delta z^2}{f^2 \Delta x^2} = \frac{L_d^2}{\Delta x^2} \sim Ro^{*2} Ri^*$$

Asterisks denote *resolved* quantities, rather than true values

[1] Gridscale Reynolds and Péclet numbers MUST be O(1) for numerical stability

BFK. New Frontiers in Operational Oceanography, chapter Notions for the Motions of the Oceans, pages 27-73. GODAE OceanView, 2018.

B. Fox-Kemper and D. Menemenlis. Can large eddy simulation techniques improve mesoscale-rich ocean models? In M. Hecht and H. Hasumi, editors, Ocean Modeling in an Eddying Regime, volume 177, pages 319-338. AGU Geophysical Monograph Series, 2008.

Navier-Stokes+, Fundamental Continuum Ocean Eqtns, Following Müller (2006)

$$\frac{D\rho}{Dt} = -\rho \underbrace{\nabla \cdot \mathbf{u}}_{\text{divergence}},$$

$$D_{ij} = \frac{1}{2}(\nabla_i u_j + \nabla_j u_i)$$

$$\rho \frac{D\mathbf{u}}{Dt} = \nabla \cdot \underbrace{\left(-p\mathbf{I} + \sigma^{\mathrm{mol}}\right)}_{\text{stress tensor}} - \underbrace{2\rho\mathbf{\Omega} \times \mathbf{u}}_{\text{Coriolis}} - \underbrace{\rho\nabla(\phi)}_{\text{geopotential}},$$

$$\frac{DT}{Dt} = \underbrace{\left(\frac{\partial T}{\partial p}\right)_{\eta,S} \frac{Dp}{Dt}}_{\text{compress}} + \frac{1}{\rho c_p}\left[-\nabla \cdot \underbrace{\left(\mathbf{q}^{mol} + \mathbf{q}^{rad}\right)}_{\text{heat flux}} + \underbrace{D_{ij}\sigma_{ij}^{mol}}_{\text{friction heat}} - \underbrace{\mathbf{I}_S^{mol} \cdot \nabla(h_s - h_w)}_{\text{mixing heat}}\right],$$

$$= \underbrace{\left(\frac{\partial T}{\partial p}\right)_{\eta,S} \frac{Dp}{Dt}}_{\text{compress}} - \frac{\nabla \cdot q^{all}}{\rho c_p} + \frac{\dot{q}}{\rho c_p},$$

$$\frac{DS}{Dt} = -\frac{1}{\rho}\nabla \cdot \underbrace{\mathbf{I}_S^{mol}}_{\text{salt flux}},$$

$$\rho = \underbrace{\rho(p, T, S)}_{\text{eqtn. of state}}.$$

Navier-Stokes+, Fundamental Continuum Ocean Eqtns, Following Müller (2006)

$$\frac{D\rho}{Dt} = -\rho \underbrace{\nabla\cdot\mathbf{u}}_{\text{divergence}},$$

$$D_{ij} = \frac{1}{2}(\nabla_i u_j + \nabla_j u_i)$$

$$\rho\frac{D\mathbf{u}}{Dt} = \nabla\cdot\underbrace{\left(-p\mathbf{I}+\sigma^{\mathrm{mol}}\right)}_{\text{stress tensor}} - \underbrace{2\rho\mathbf{\Omega}\times\mathbf{u}}_{\text{Coriolis}} - \underbrace{\rho\nabla(\phi)}_{\text{geopotential}},$$

$$\frac{DT}{Dt} = \underbrace{\left(\frac{\partial T}{\partial p}\right)_{\eta,S}\frac{Dp}{Dt}}_{\text{compress}} + \frac{1}{\rho c_p}\left[-\nabla\cdot\underbrace{\left(\mathbf{q}^{mol}+\mathbf{q}^{rad}\right)}_{\text{heat flux}} + \underbrace{D_{ij}\sigma_{ij}^{mol}}_{\text{friction heat}} - \underbrace{\mathbf{I}_S^{mol}\cdot\nabla(h_s-h_w)}_{\text{mixing heat}}\right],$$

$$= \underbrace{\left(\frac{\partial T}{\partial p}\right)_{\eta,S}\frac{Dp}{Dt}}_{\text{compress}} - \frac{\nabla\cdot q^{all}}{\rho c_p} + \frac{\dot{q}}{\rho c_p},$$

$$\frac{DS}{Dt} = -\frac{1}{\rho}\nabla\cdot\underbrace{\mathbf{I}_S^{mol}}_{\text{salt flux}},$$

$$\sigma_{ij}^{mol} = 2\mu D_{ij} - \frac{2}{3}\upsilon D_{kk}\delta_{ij}.$$

$$\rho = \underbrace{\rho(p,T,S)}_{\text{eqtn. of state}}.$$

$$\mathbf{q}^{mol} = -\rho\left(\kappa_T\nabla T - \kappa_{TS}\left[\nabla S - \gamma\nabla p\right]\right),$$

$$\mathbf{I}_s^{mol} = -\rho\left(\kappa_S\left[\nabla S - \gamma\nabla p\right] + \kappa_{ST}\nabla T\right).$$

But, hold on...

- These equations can only be used on an "ocean" less than 1 cubic meter in size for direct numerical simulations of a few seconds.
- Present computing: A "teragrid" we can afford: 1024x1024x1024x1024 gridpoints & timesteps
- Sound waves are killing us (CFL on 1400 m/s)!
  - Maybe we can filter them out?

Sound Waves

$$\frac{D\rho}{Dt} = -\rho \nabla \cdot \mathbf{u},$$

$$\left(\frac{Dp}{Dt}\right)_{S,\eta} = \left(\frac{\partial \rho}{\partial p}\right)_{S,\eta} \left(\frac{D\rho}{Dt}\right)_{S,\eta} = c^2 \left(\frac{D\rho}{Dt}\right)_{S,\eta}$$

$$\frac{Dp}{Dt} = -\rho c^2 \nabla \cdot \mathbf{u} + D_p^{\mathrm{mol}}.$$

$$\frac{D\mathbf{u}}{Dt} = \frac{1}{\rho} \nabla \cdot \left(-p\mathbf{I} + \sigma^{\mathrm{mol}}\right) - 2\boldsymbol{\Omega} \times \mathbf{u} - g\mathbf{k}$$

$$\boxed{\frac{\partial^2 p'}{\partial t^2} + c^2 \nabla^2 p' =} -2c^2 \overline{\rho} \boldsymbol{\Omega} \cdot \nabla \times \mathbf{u}' - c^2 \nabla \cdot \sigma^{\mathrm{mol}'} + D_p^{\mathrm{mol}}.$$

BFK. New Frontiers in Operational Oceanography, chapter Notions for the Motions of the Oceans, pages 27-73. GODAE OceanView, 2018.

Boussinesq (1897)

$$\rho = \rho_0 + \overline{\rho}(z) + \delta\rho(x, y, z, t),$$
$$b = g\left(\rho_0 - \delta\rho(x, y, z, t)\right)/\rho_0,$$
$$\overline{b} = g\left(\rho_0 - \overline{\rho}(z)\right)/\rho_0.$$

The Bossinesq Approx. Eqtns

$$0 \approx \nabla \cdot \mathbf{u},$$
$$\frac{D\mathbf{u}}{Dt} = \frac{1}{\rho_0}\nabla \cdot \left(-\pi\mathbf{I} + \sigma^{\mathrm{mol}}\right) - 2\mathbf{\Omega} \times \mathbf{u} + b\mathbf{k},$$
$$\frac{D\Theta}{Dt} \approx \frac{1}{\rho_0 C_p^0}\left[-\nabla \cdot \left(\mathbf{q}^{mol} + \mathbf{q}^{rad}\right) + D_{ij}\sigma_{ij}^{mol} - \mathbf{I}_S^{mol} \cdot \nabla(h_s - h_w)\right]$$
$$\frac{DS}{Dt} = -\frac{1}{\rho_0}\nabla \cdot \mathbf{I}_S^{mol},$$
$$b = g(\rho_0 + \overline{\rho}(z) - \rho(p - \pi, \Theta, S))/\rho_0 = b(z, \Theta, S).$$

Along with losing sound waves...

- We lose the ability to convert internal energy to mechanical (kinetic or potential). NO HEAT ENGINES, but a side advantage is decoupled thermal and mechanical energy budgets (reflective of the real ocean!)
- We lose the ability to directly simulate sea level rise (mass of ocean conservation is not the same as volume of ocean conservation)
- Could take an intermediate step—anelastic equations in pressure coordinates, as is done in atmosphere.

Can we simplify more?

$$\mathrm{Ro}_* \left[\partial_t \mathbf{v}_h + \mathbf{v}_h \cdot \nabla \mathbf{v}_h + \epsilon w \partial_z \mathbf{v}_h\right] + \underbrace{\left(1 + \frac{y\mathrm{Pl}_*}{\Delta y}\right) \mathbf{z} \times \mathbf{v}_h + \mathrm{M}_{R_*} \nabla_h \pi}_{\text{geostrophic}} = \frac{\mathrm{Ro}_*}{\mathrm{Re}_*} \nabla_i \sigma_{ih},$$

$$\mathrm{Fr}_*{}^2 \frac{\Delta z^2}{\Delta s^2} \left[\partial_t w + \mathbf{v}_h \cdot \nabla w + \epsilon w \partial_z \mathbf{v}_h\right] + \underbrace{\partial_z \pi - b}_{\text{hydrostatic}} = \frac{\mathrm{Fr}_*{}^2 \Delta z^2}{\mathrm{Re}_* \Delta s^2} \nabla_i \sigma_{iz},$$

$$\partial_t S + \mathbf{v}_h \cdot \nabla S + \epsilon w \partial_z S + w \partial_z \bar{S} = \frac{1}{\mathrm{Pe}_*} \nabla \cdot \mathbf{I}_S^{all},$$

$$\partial_t \Theta + \mathbf{v}_h \cdot \nabla \Theta + \epsilon w \partial_z \Theta + w \partial_z \bar{\Theta} = \frac{1}{\mathrm{Pe}_*} \nabla \cdot \mathbf{I}_\theta^{all},$$

$$\partial_t b + \mathbf{v}_h \cdot \nabla b + \epsilon w \partial_z b + w \partial_z \bar{b} = \frac{1}{\mathrm{Pe}_*} \nabla \cdot \left(\alpha \mathbf{I}_\theta^{all} - \beta \mathbf{I}_S^{all}\right),$$

$$\nabla \cdot \mathbf{v}_h + \epsilon \partial_z w = 0,$$

$$\mathrm{M}_{R_*} \equiv \max(1, \mathrm{Ro}_*), \qquad \epsilon \equiv \frac{\mathrm{Fr}_*{}^2}{\mathrm{Ro}_*} \mathrm{M}_{R_*} = \begin{cases} \mathrm{Fr}_*{}^2 & \mathrm{Ro}_* \geq 1, \\ \mathrm{Ro}_* \mathrm{Bu}_*{}^{-1} & \mathrm{Ro}_* < 1 \end{cases}$$

Boussinesq Equations
Following McWilliams (1985)

With dimensions based on model grid...

Hydrostatic & QG are just a step away...

BFK. New Frontiers in Operational Oceanography, chapter Notions for the Motions of the Oceans, pages 27-73. GODAE OceanView, 2018.

The Character of the Mesoscale

100 km

(NASA GSFC Gallery)

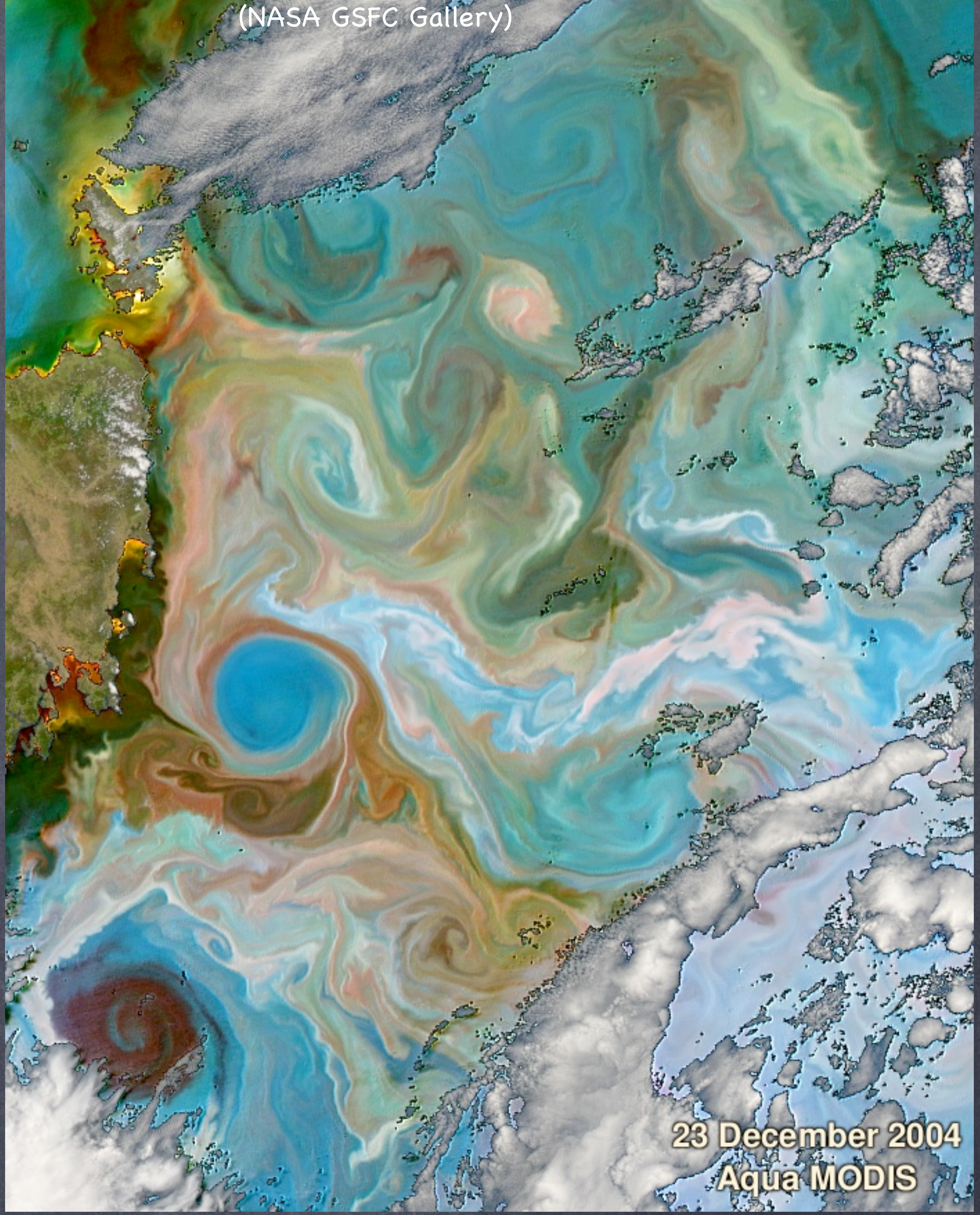

(Capet et al., 2008)

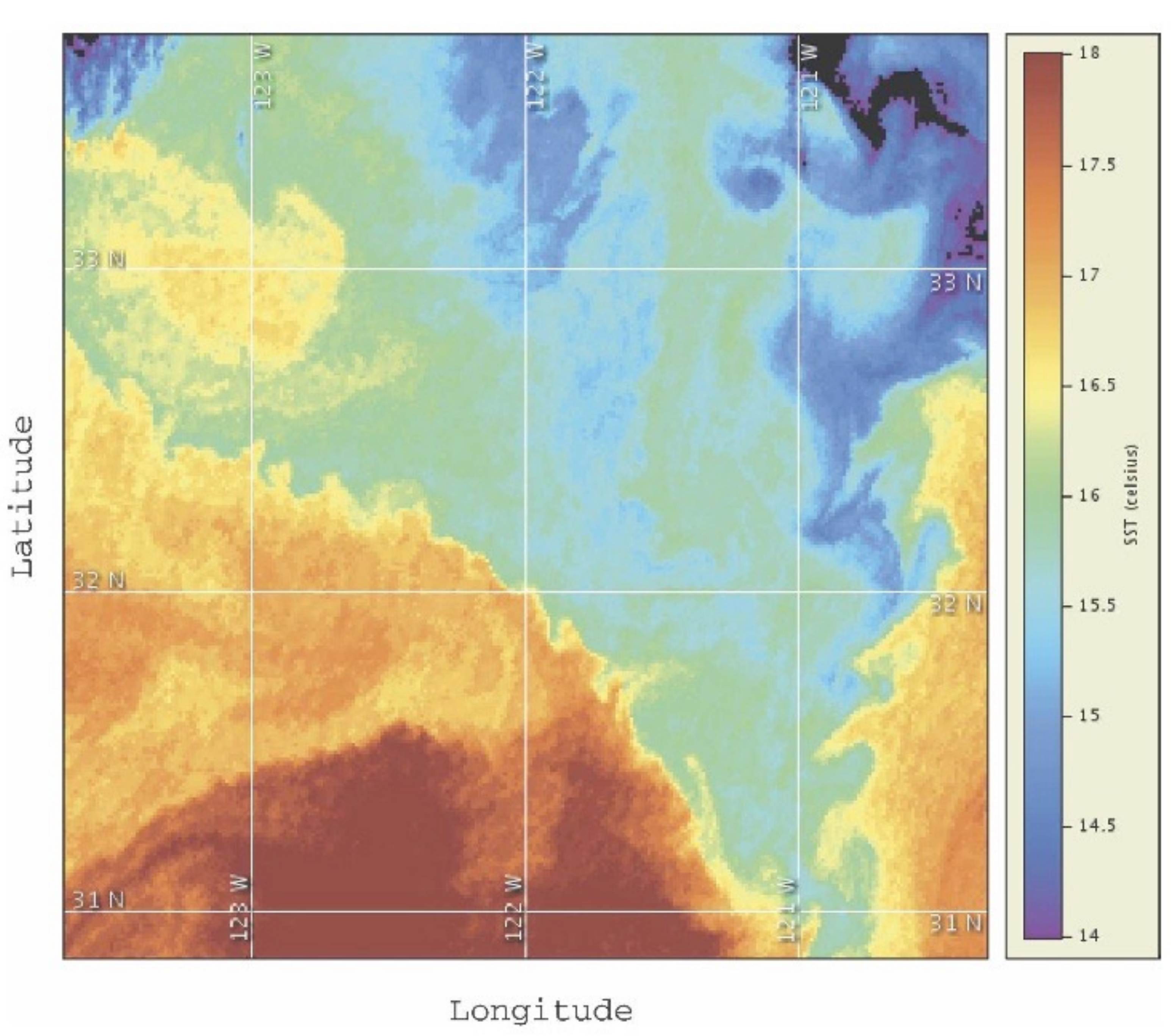

FIG. 16. Sea surface temperature measured at 1832 UTC 3 Jun 2006 off Point Conception in the California Current from CoastWatch (http://coastwatch.pfeg.noaa.gov). The fronts between recently upwelled water (i.e., 15°–16°C) and offshore water (≥17°C) show submesoscale instabilities with wavelengths around 30 km (right front) or 15 km (left front). Images for 1 day earlier and 4 days later show persistence of the instability events.

- Boundary Currents
- Eddies
- Ro=O(0.1)
- Ri=O(1000), Fr=O(0.01)
- Full Depth
- Eddies strain to produce Fronts
- 100km, months

Eddy processes mainly baroclinic & barotropic instability. Parameterizations of baroclinic instability (GM, Visbeck...).

The Character of the Mesoscale

100 km

(NASA GSFC Gallery)

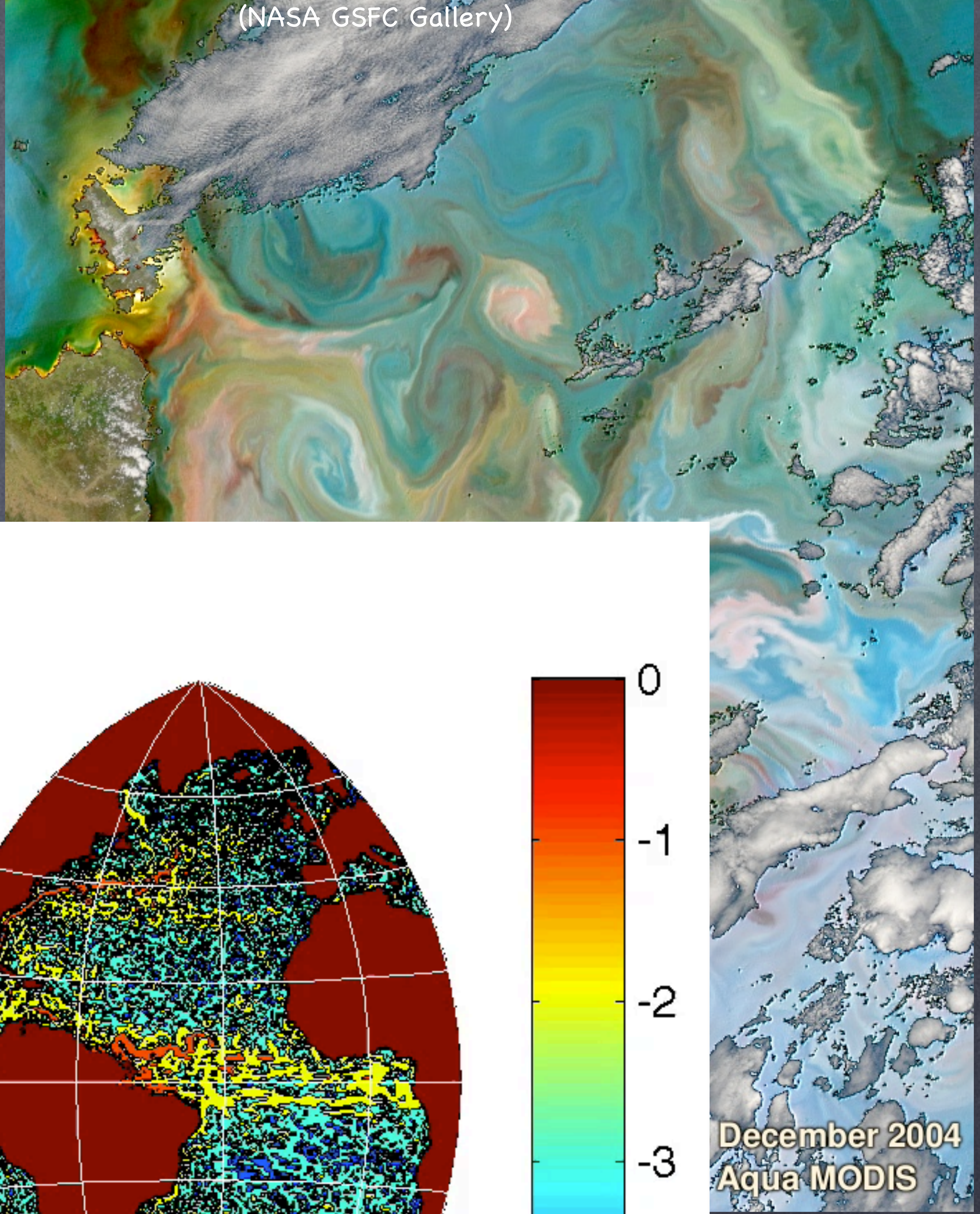

- Boundary Currents

(Capet et al., 2008)

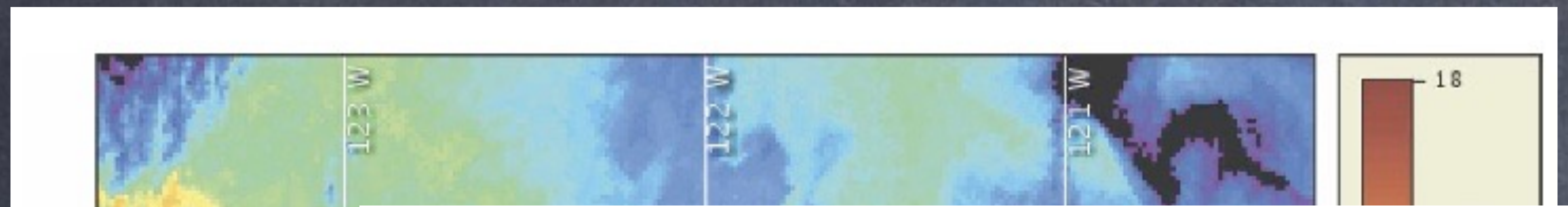

FIG. 16. Sea surface
California Current fro
upwelled water (i.e., 15
lengths around 30 km (
persistence of the insta

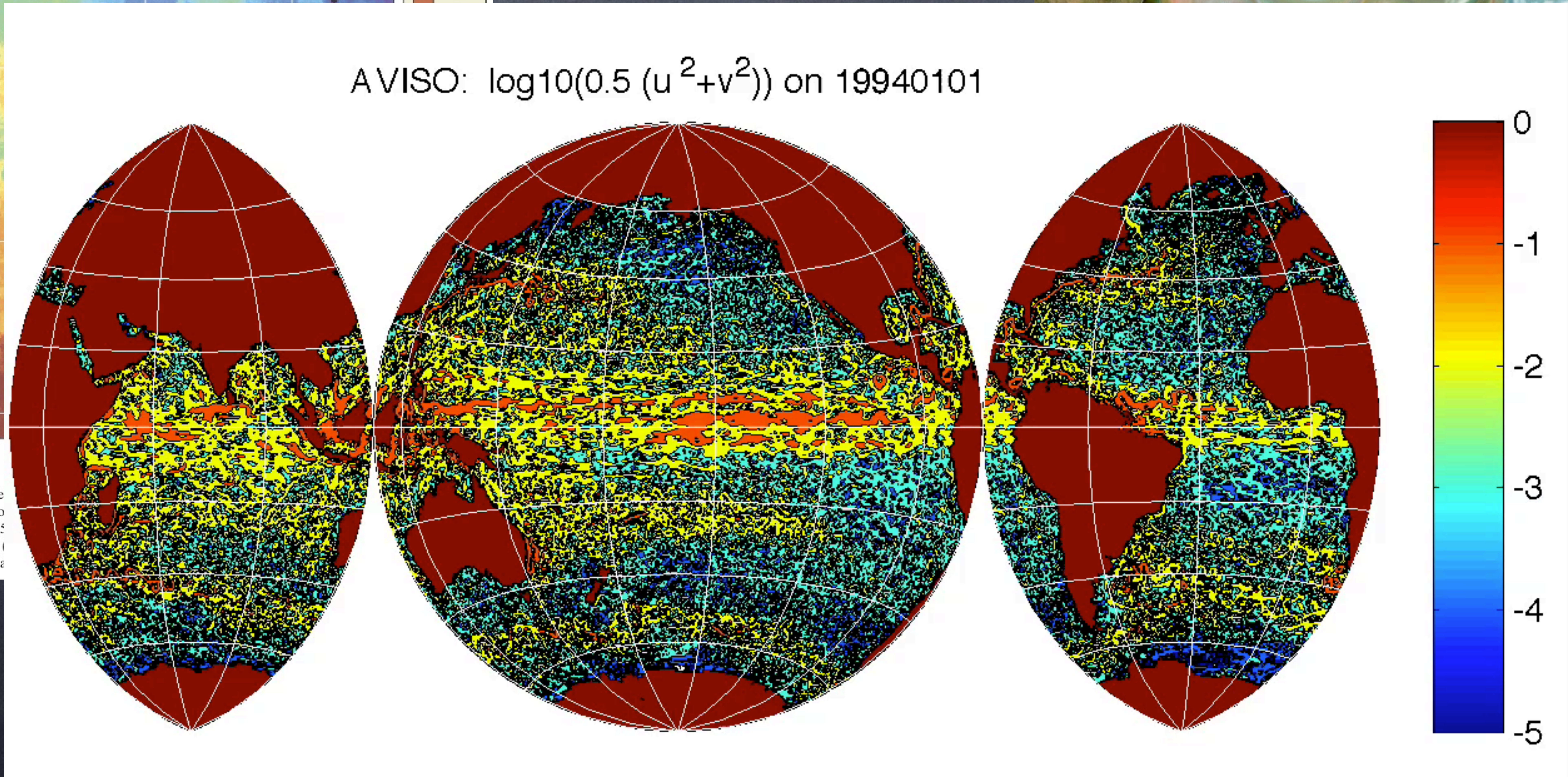

Th

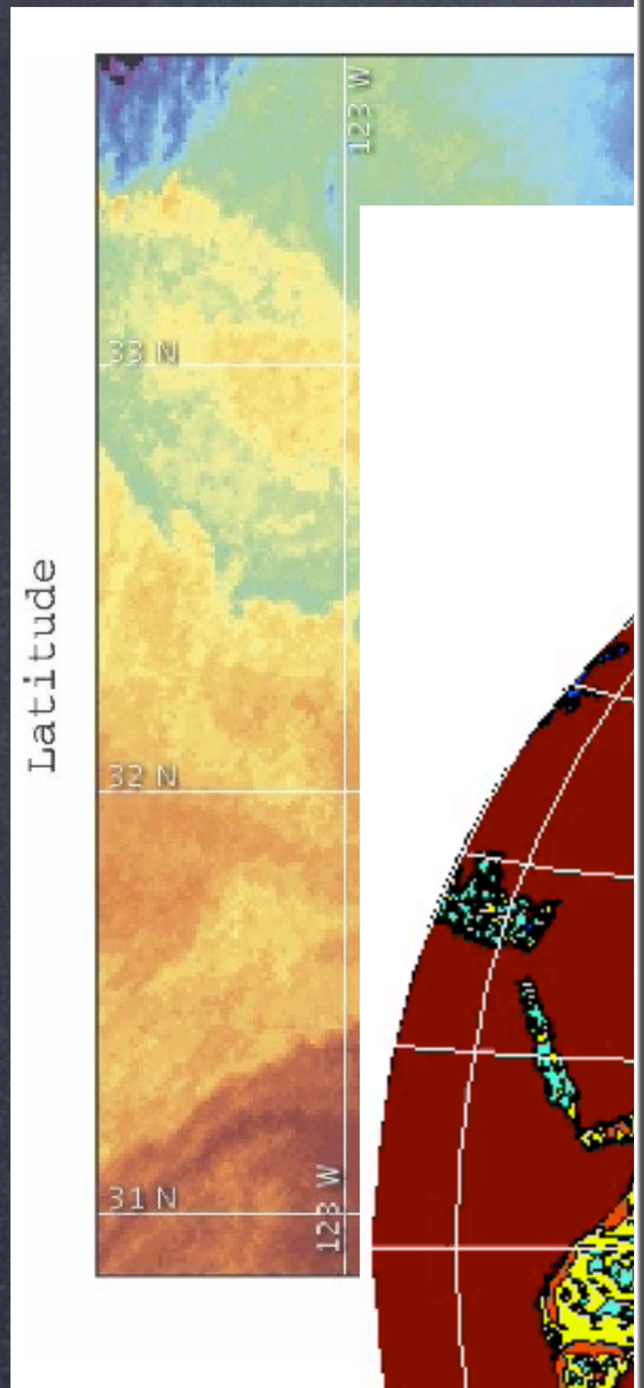

FIG. 16. Sea surface
California Current fro
upwelled water (i.e., 15
lengths around 30 km (
persistence of the insta

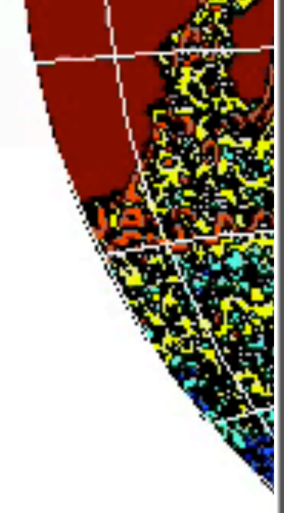

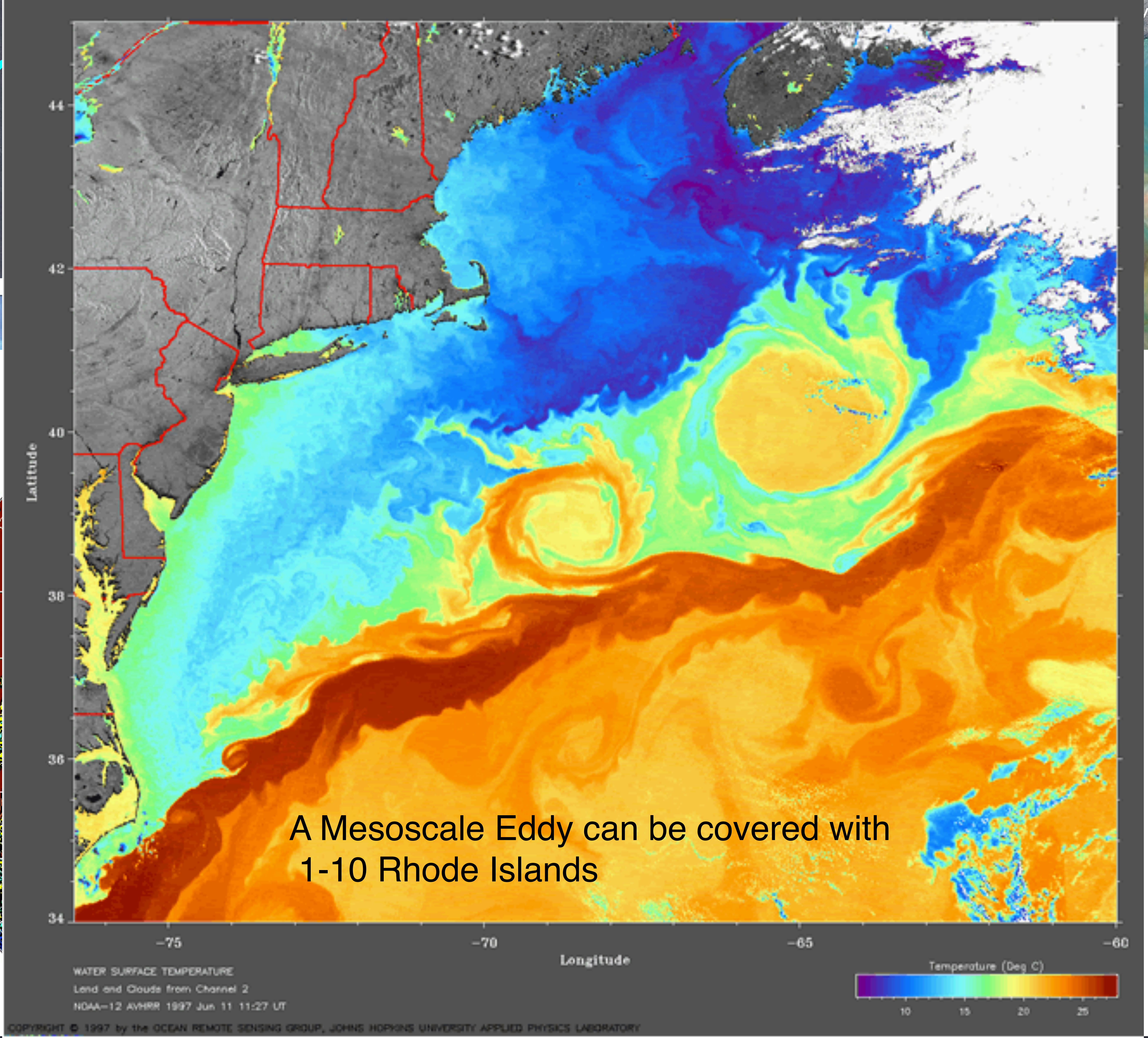

A Mesoscale Eddy can be covered with
1-10 Rhode Islands

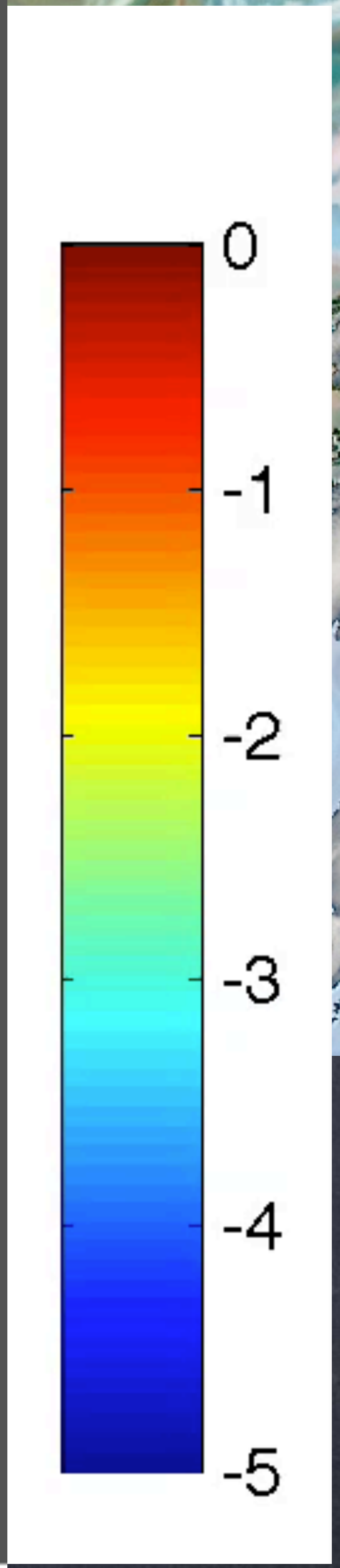

But, global models won't resolve these small processes for decades.

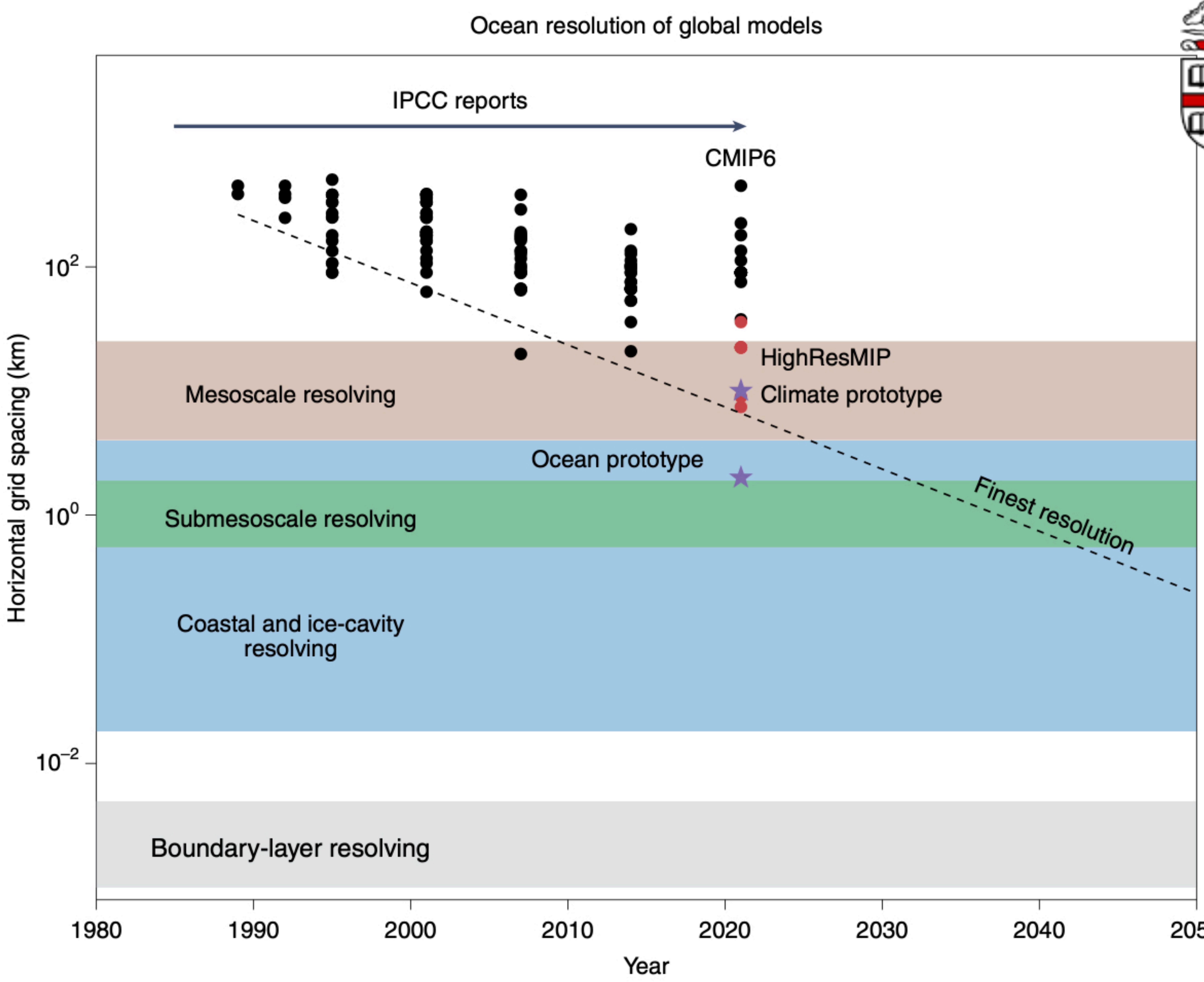

Fig. 2 | The evolution of global ocean model resolution by publication year. Shown are models from

Hewitt et al., *Nature Climate Change*, 2022

$$\mathrm{Ro}_*\left[\partial_t \mathbf{v}_h + \mathbf{v}_h\cdot\nabla\mathbf{v}_h + \epsilon w\partial_z\mathbf{v}_h\right] + \underbrace{\left(1+\frac{y\mathrm{Pl}_*}{\Delta y}\right)\mathbf{z}\times\mathbf{v}_h + \mathrm{M}_{R*}\nabla_h\pi}_{\text{geostrophic}} = \frac{\mathrm{Ro}_*}{\mathrm{Re}_*}\nabla_i\sigma_{ih},$$

$$\mathrm{Fr}_*{}^2\frac{\Delta z^2}{\Delta s^2}\left[\partial_t w + \mathbf{v}_h\cdot\nabla w + \epsilon w\partial_z\mathbf{v}_h\right] + \underbrace{\partial_z\pi - b}_{\text{hydrostatic}} = \frac{\mathrm{Fr}_*{}^2\Delta z^2}{\mathrm{Re}_*\Delta s^2}\nabla_i\sigma_{iz},$$

- Mesoscale:
- Ro=O(0.1)
- Ri=O(1000), Fr=O(0.01)

$$\partial_t S + \mathbf{v}_h\cdot\nabla S + \epsilon w\partial_z S + w\partial_z\bar{S} = \frac{1}{\mathrm{Pe}_*}\nabla\cdot\mathbf{I}_S^{all},$$

$$\partial_t\Theta + \mathbf{v}_h\cdot\nabla\Theta + \epsilon w\partial_z\Theta + w\partial_z\bar{\Theta} = \frac{1}{\mathrm{Pe}_*}\nabla\cdot\mathbf{I}_\theta^{all},$$

$$\partial_t b + \mathbf{v}_h\cdot\nabla b + \epsilon w\partial_z b + w\partial_z\bar{b} = \frac{1}{\mathrm{Pe}_*}\nabla\cdot\left(\alpha\mathbf{I}_\theta^{all} - \beta\mathbf{I}_S^{all}\right),$$

$$(\mathrm{Fr}^*)^{-2} = \frac{N^2H^2}{U^2} \sim \frac{N^2}{\partial^2 U/\partial z^2} = \mathrm{Ri}^*$$

$$\nabla\cdot\mathbf{v}_h + \epsilon\partial_z w = 0,$$

$$\mathrm{M}_{R*}\equiv\max(1,\mathrm{Ro}_*),\qquad \epsilon\equiv\frac{\mathrm{Fr}_*{}^2}{\mathrm{Ro}_*}\mathrm{M}_{R*} = \begin{cases}\mathrm{Fr}_*{}^2 & \mathrm{Ro}_*\geq 1,\\ \mathrm{Ro}_*\mathrm{Bu}_*{}^{-1} & \mathrm{Ro}_*<1\end{cases}$$

Boussinesq Equations
Following McWilliams (1985)

For Mesoscale, geostrophic & hydrostatic are good approximations.

Quasigeostrophy? No...

BFK. New Frontiers in Operational Oceanography, chapter Notions for the Motions of the Oceans, pages 27-73. GODAE OceanView, 2018.

The problems with quasigeostrophy…

- A great toy model, crucial in the early days of numerical weather and ocean prediction because *internal waves* are filtered out (i.e., big timesteps).

- However, QG also requires oversimplification of stratification (spatially uniform), which makes it unsuitable for climate.

- Finally, QG velocities are horizontally divergenceless, and…

Quasi-Geostrophic Equations

Continuously-stratified

The adiabatic quasi-geostrophic potential vorticity equation for a Boussinesq fluid on the β-plane, is

$$\frac{\mathrm{D}q}{\mathrm{D}t} = 0, \qquad q = \nabla^2\psi + f\beta y + \frac{\partial}{\partial z}\left(\frac{f_0^2}{N^2}\frac{\partial \psi}{\partial z}\right), \qquad \text{(QG.1)}$$

where ψ is the streamfunction. The horizontal velocities are given by $(u, v) = (-\partial\psi/\partial y, \partial\psi/\partial x)$. The boundary conditions at the top and bottom are given by the buoyancy equation,

$$\frac{\mathrm{D}b}{\mathrm{D}t} = 0, \qquad b = f_0\frac{\partial \psi}{\partial z}. \qquad \text{(QG.2)}$$

Two-level

The two-level or two-layer quasi-geostrophic equations are

$$\frac{\mathrm{D}q_i}{\mathrm{D}t} = 0, \qquad q_i = \nabla^2\psi_i + \beta y + \frac{k_d^2}{2}\left(\psi_j - \psi_i\right), \qquad \text{(QG.3)}$$

where $i = 1, 2$, denoting the top and bottom levels respectively, and $j = 3 - i$.

Quasigeostrophy? Not for submesoscales…

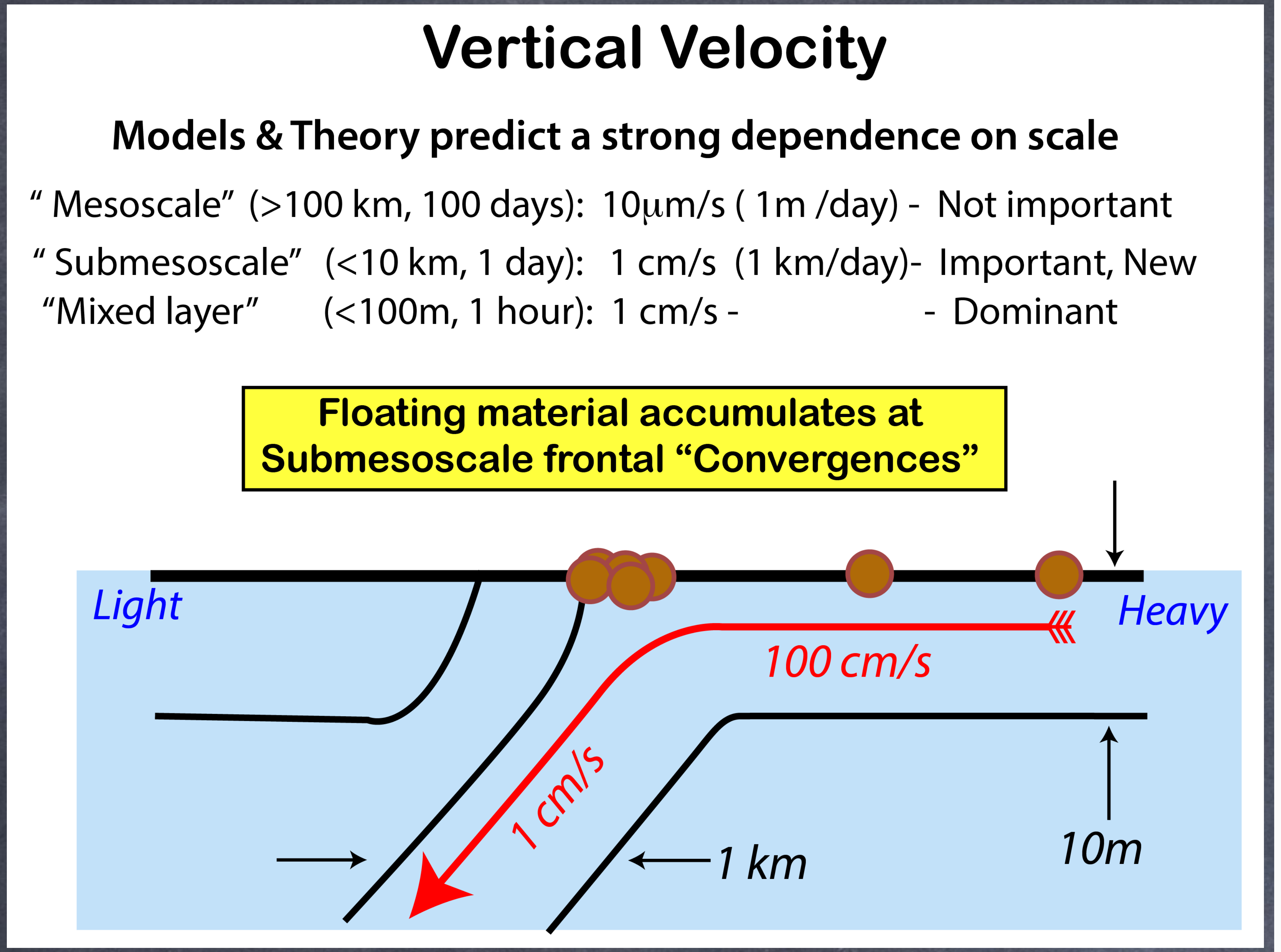

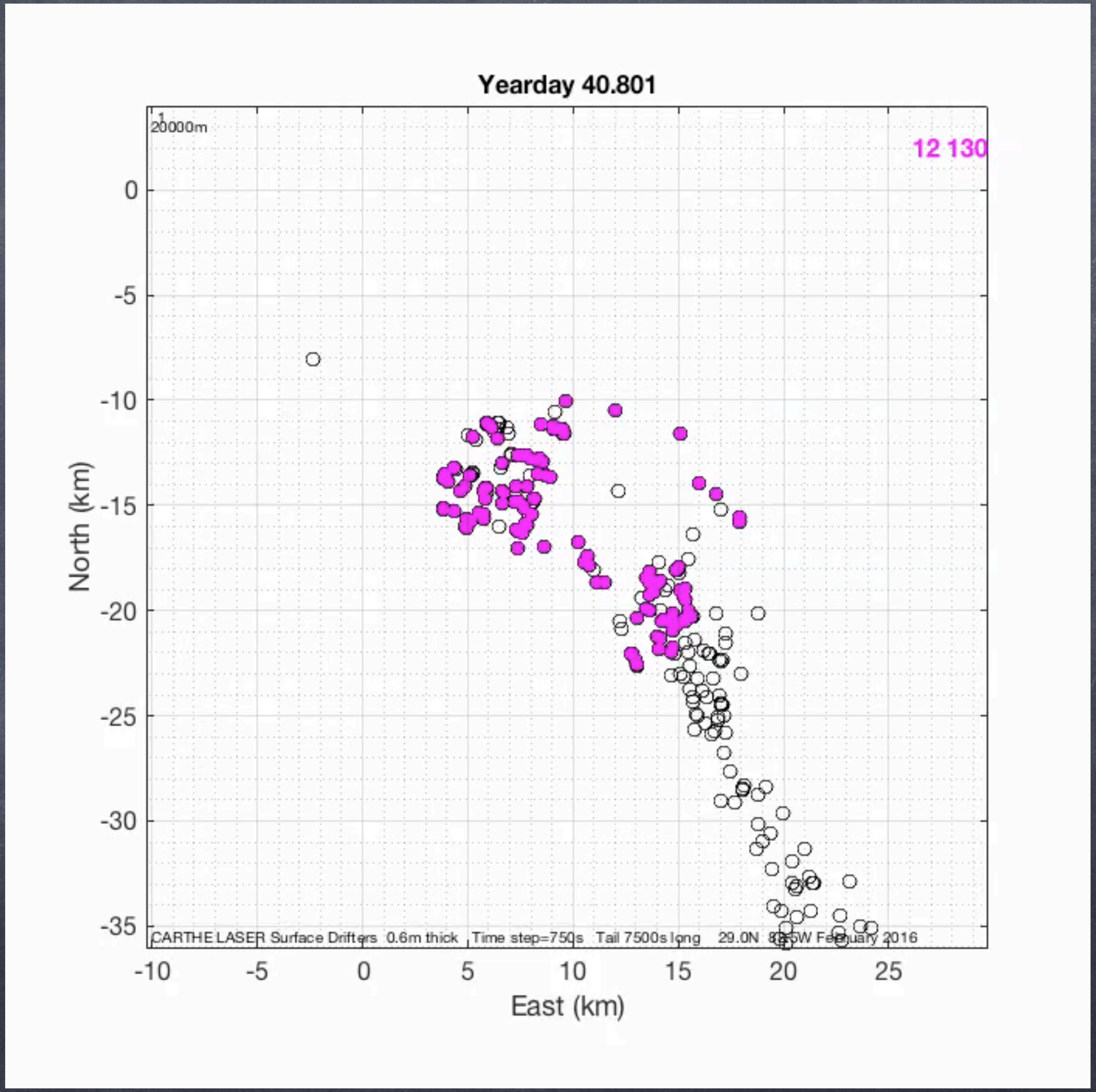

Movie & Slide Courtesy of Eric D'Asaro: See D'Asaro, E.A., Shcherbina, A.Y., Klymak, J.M., Molemaker, J., Novelli, G., Guigand, C.M., Haza, A.C., Haus, B.K., Ryan, E.H., Jacobs, G.A. and Huntley, H.S., 2018. Ocean convergence and the dispersion of flotsam. Proceedings of the National Academy of Sciences, 115(6), pp.1162-1167.

E. A. D'Asaro, D. F. Carlson, M. Chamecki, R. R. Harcourt, B. K. Haus, B. Fox-Kemper, M. J. Molemaker, A. C. Poje, and D. Yang. Advances in observing and understanding small-scale open ocean circulation during the Gulf of Mexico Research Initiative era. Frontiers in Marine Science, 7:349, May 2020.

Quasigeostrophy? Not for submesoscales…

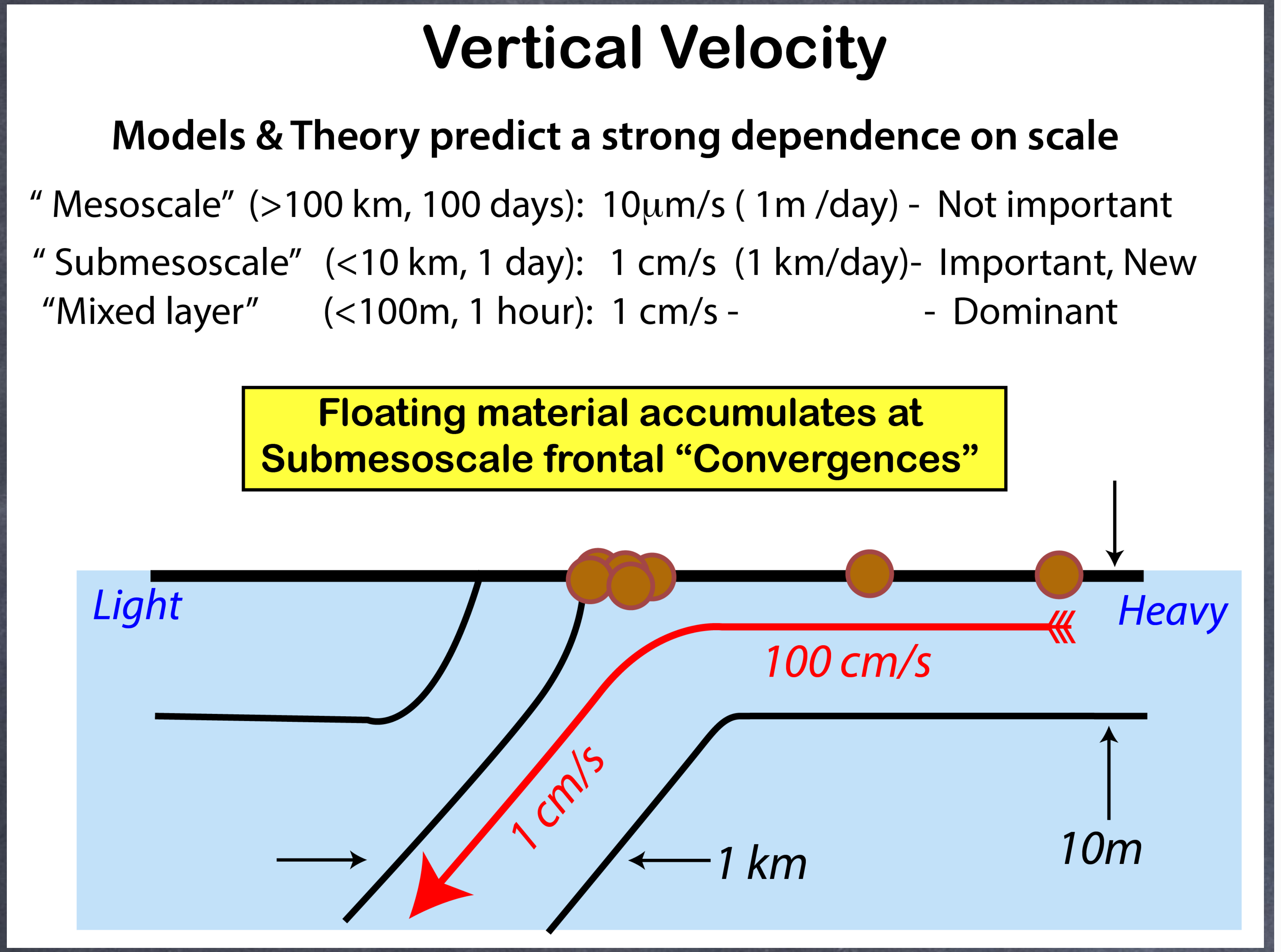

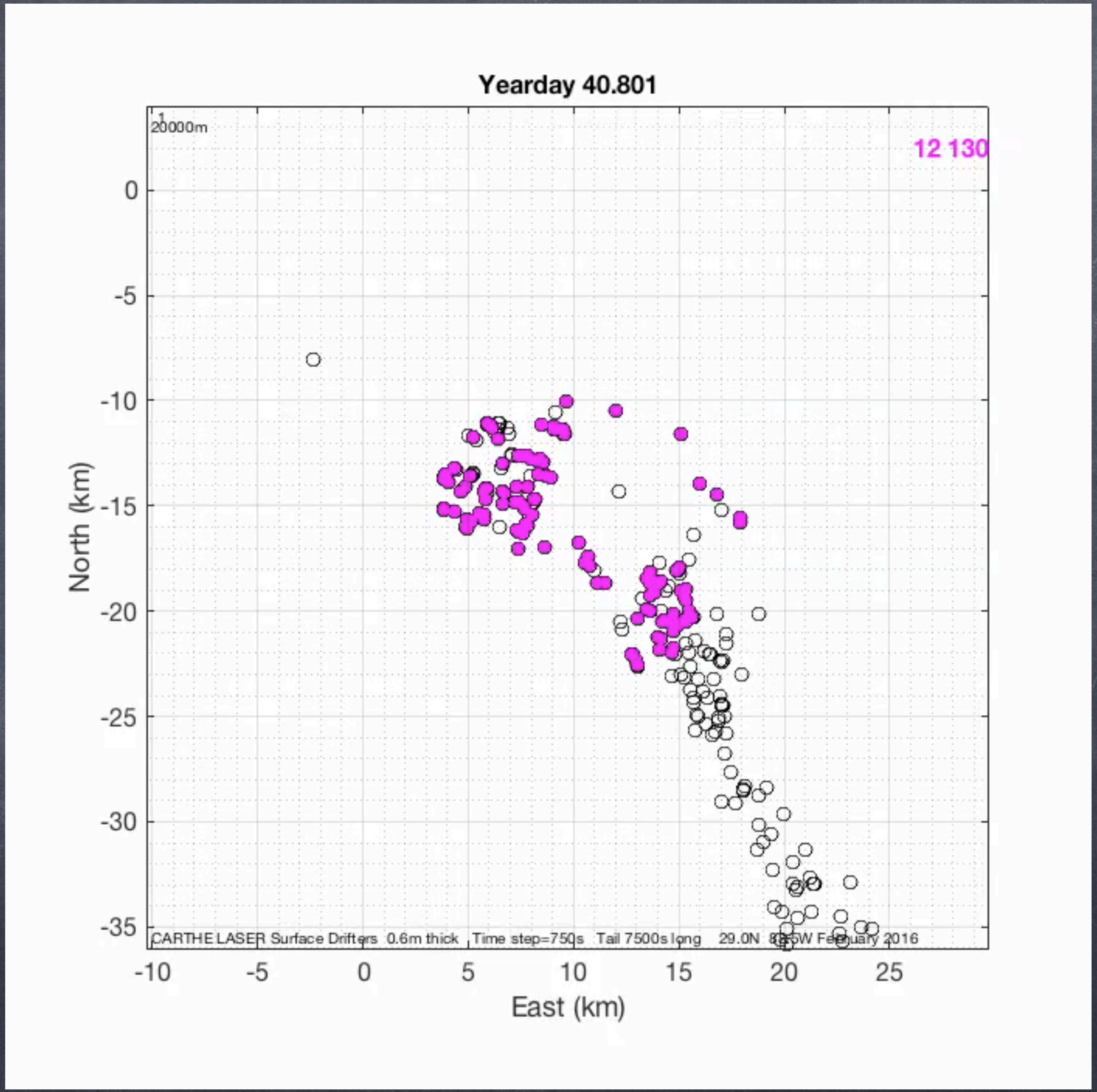

Movie & Slide Courtesy of Eric D'Asaro: See D'Asaro, E.A., Shcherbina, A.Y., Klymak, J.M., Molemaker, J., Novelli, G., Guigand, C.M., Haza, A.C., Haus, B.K., Ryan, E.H., Jacobs, G.A. and Huntley, H.S., 2018. Ocean convergence and the dispersion of flotsam. Proceedings of the National Academy of Sciences, 115(6), pp.1162-1167.

E. A. D'Asaro, D. F. Carlson, M. Chamecki, R. R. Harcourt, B. K. Haus, B. Fox-Kemper, M. J. Molemaker, A. C. Poje, and D. Yang. Advances in observing and understanding small-scale open ocean circulation during the Gulf of Mexico Research Initiative era. Frontiers in Marine Science, 7:349, May 2020.

E.g., submesoscale-sea ice interactions…

E.g., submesoscale-sea ice interactions…

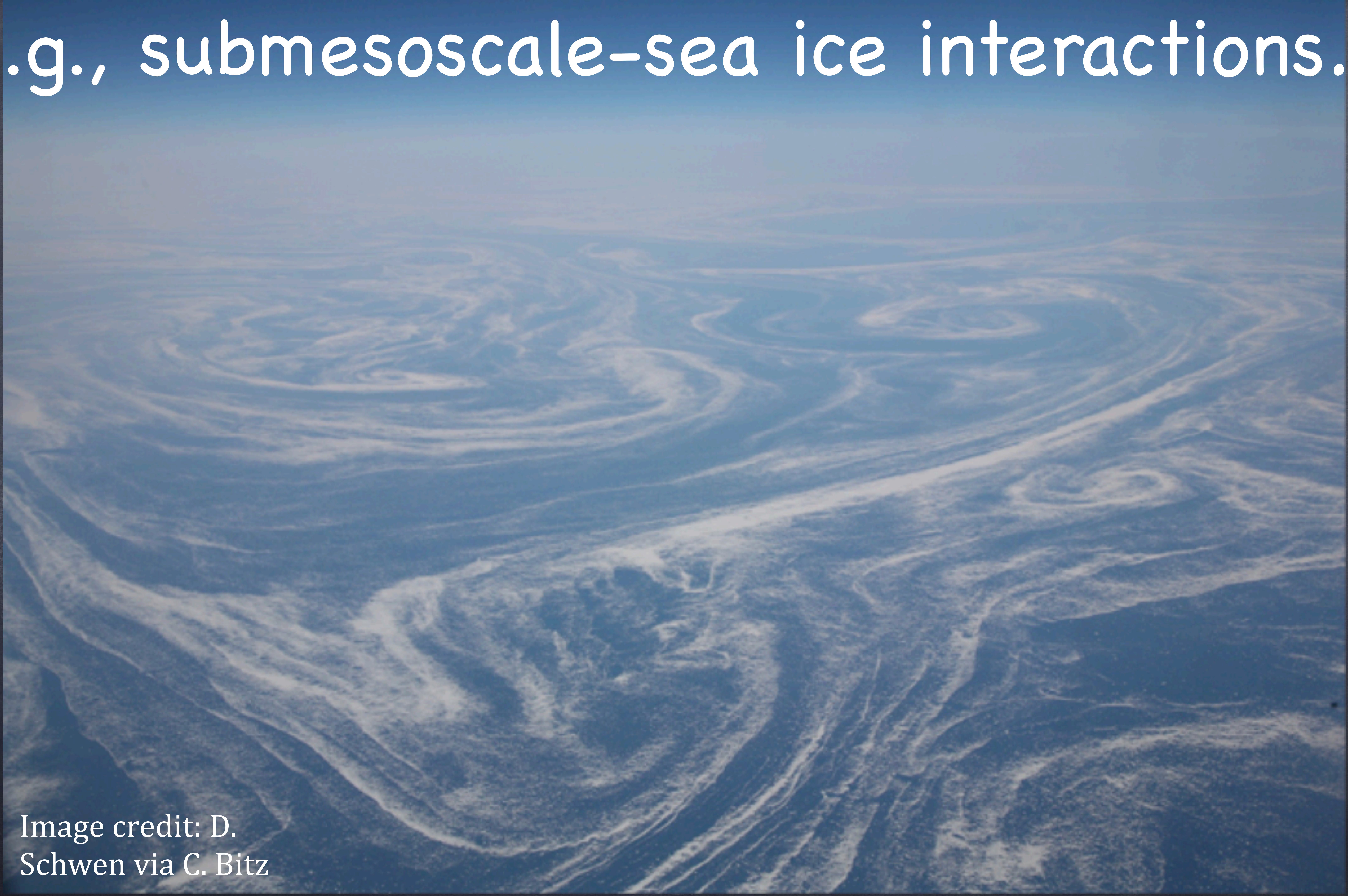

Character of the Submesoscale

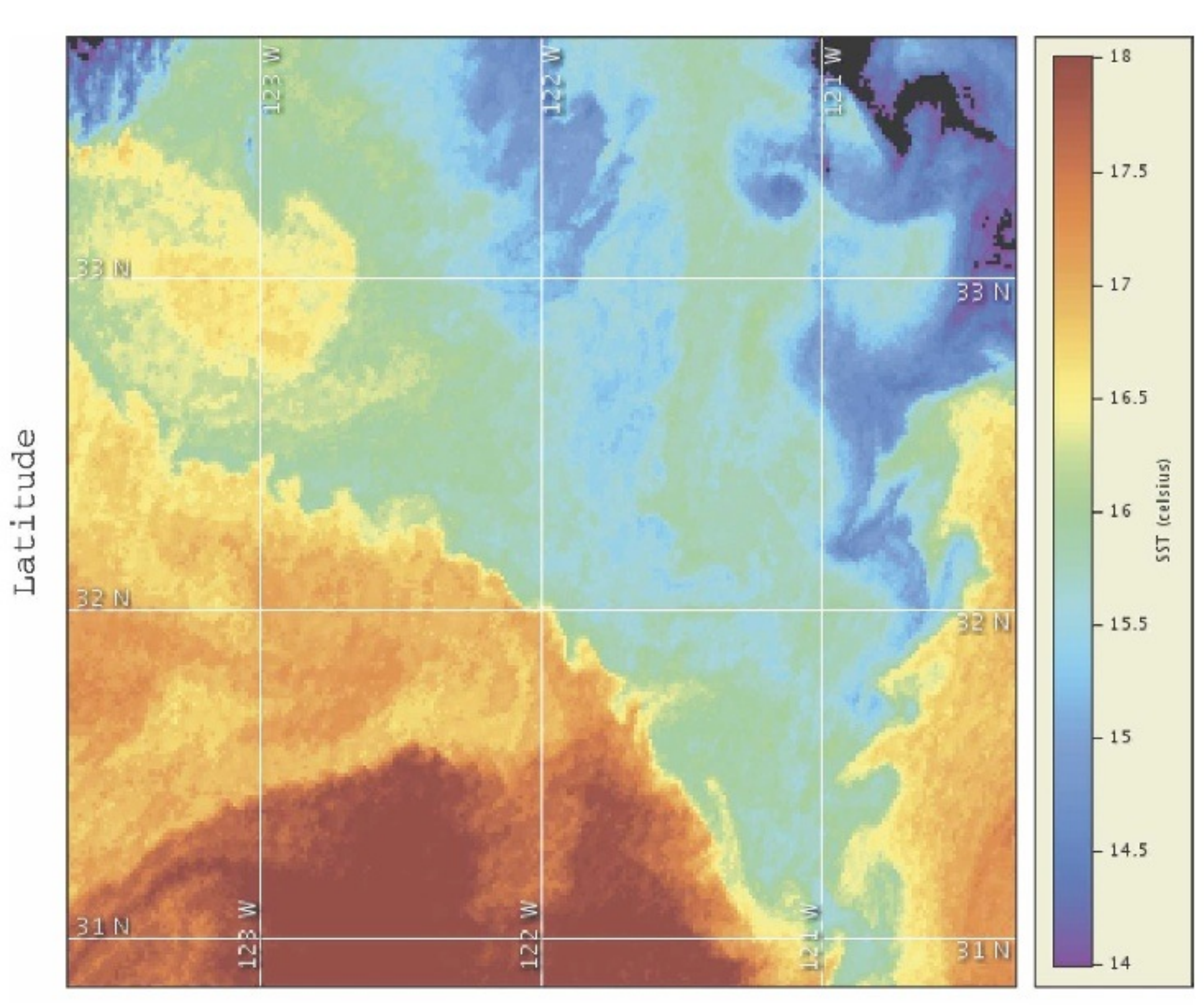

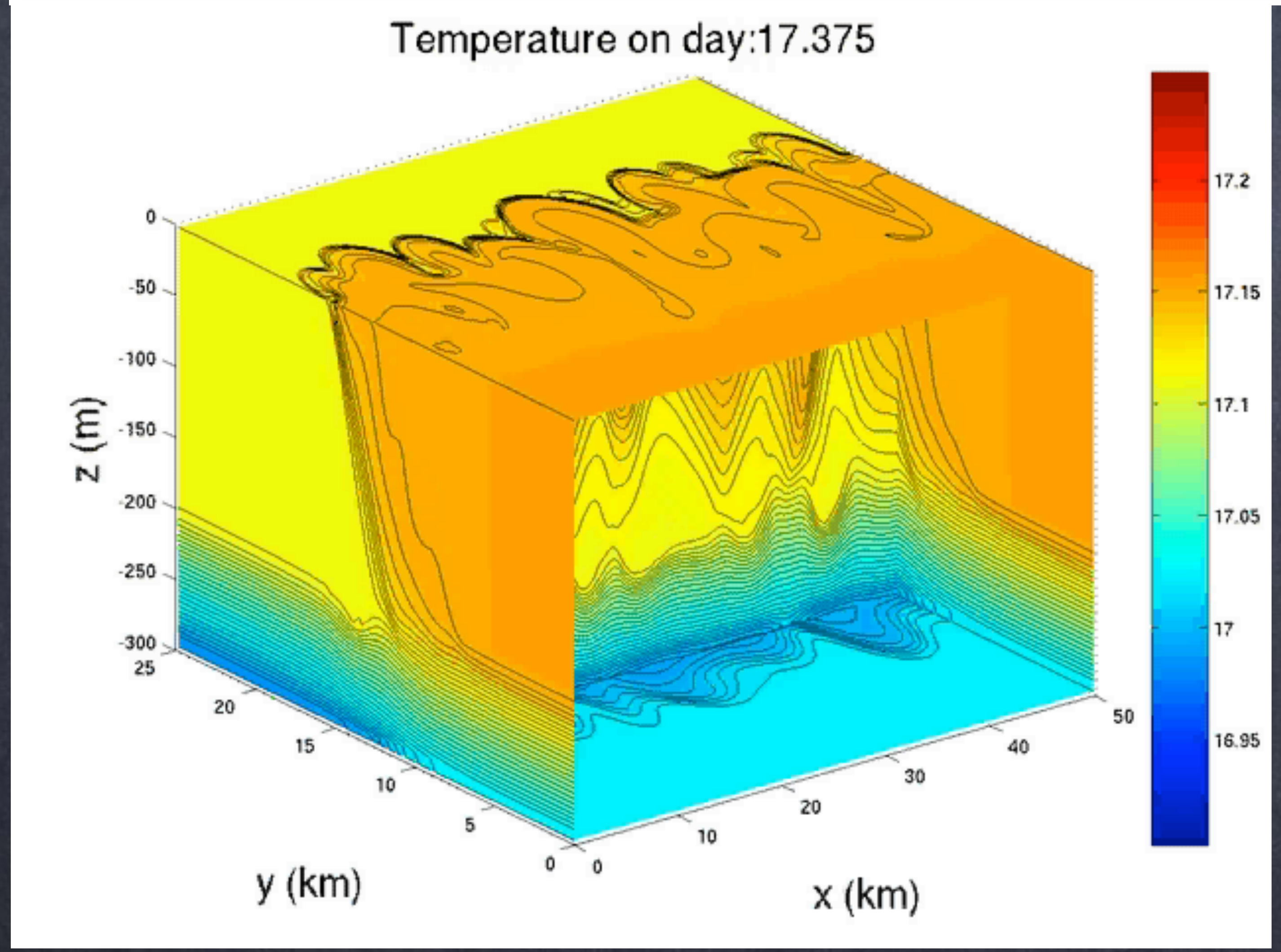

- Fronts
- Eddies
- Ro=O(1)
- Ri=O(1), Fr=O(1)
- near-surface (H=100m)
- 1-10km, days
- W/H~U/L
- hydrostatic
- Globally resolved in 2070-2100

← 10 km

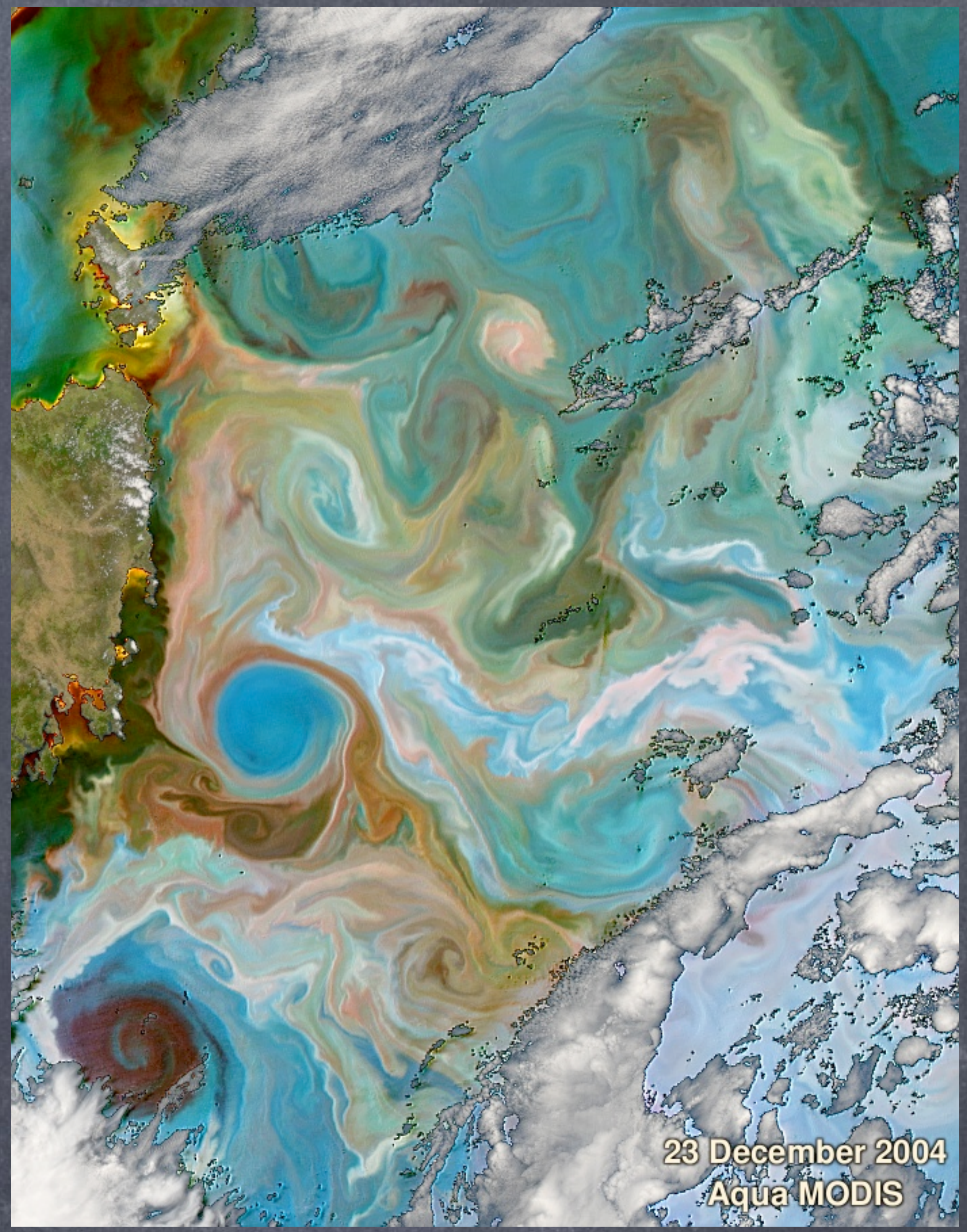

Eddy processes often baroclinic mixed layer instability

BFK, R. Ferrari, and R. W. Hallberg. Parameterization of mixed layer eddies. Part I: Theory and diagnosis. Journal of Physical Oceanography, 38(6):1145-1165, 2008

BFK, G. Danabasoglu, R. Ferrari, S. M. Griffies, R. W. Hallberg, M. M. Holland, M. E. Maltrud, S. Peacock, and B. L. Samuels. Parameterization of mixed layer eddies. III: Implementation and impact in global ocean climate simulations. Ocean Modelling, 39:61-78, 2011.

Character of the Submesoscale

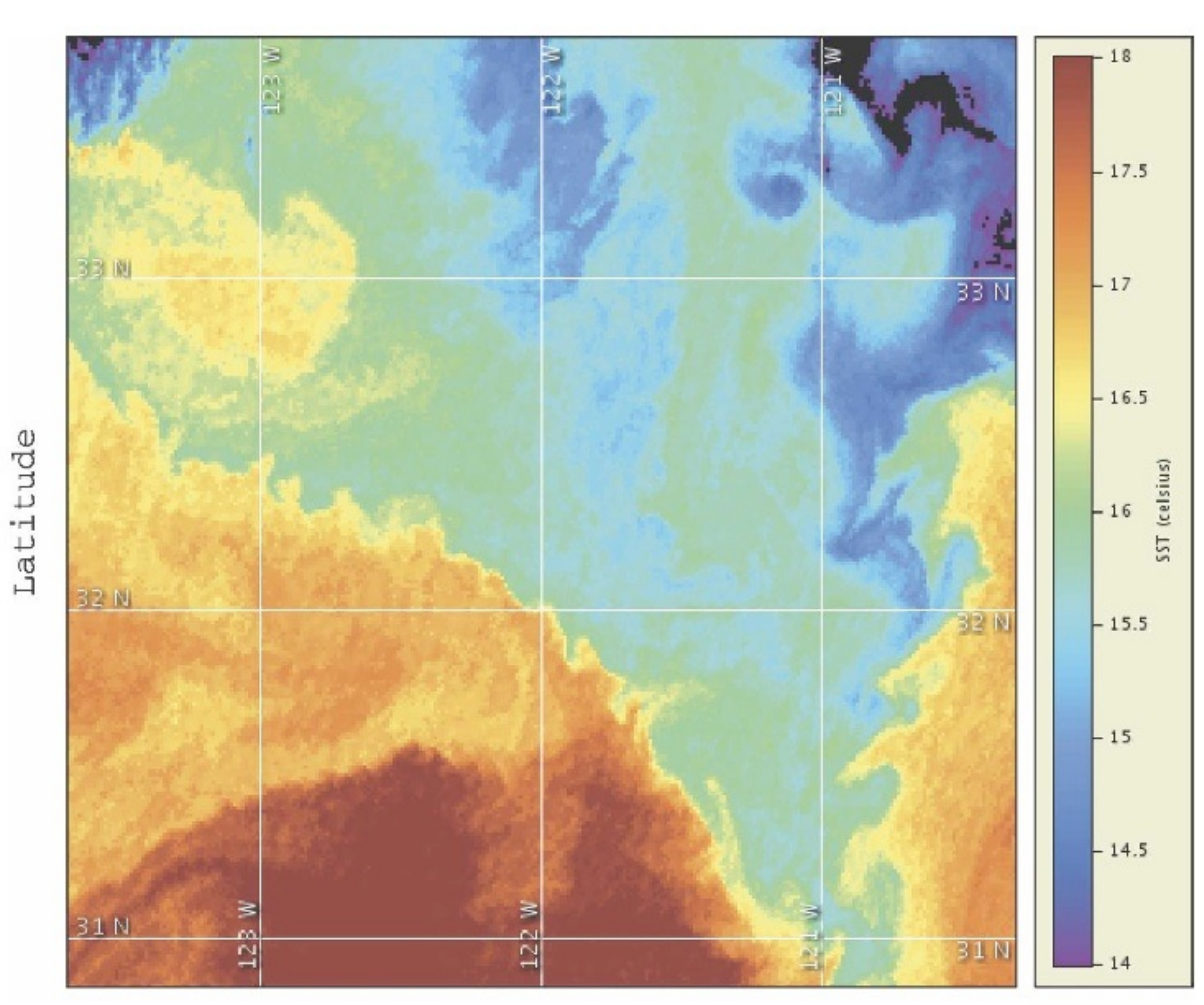

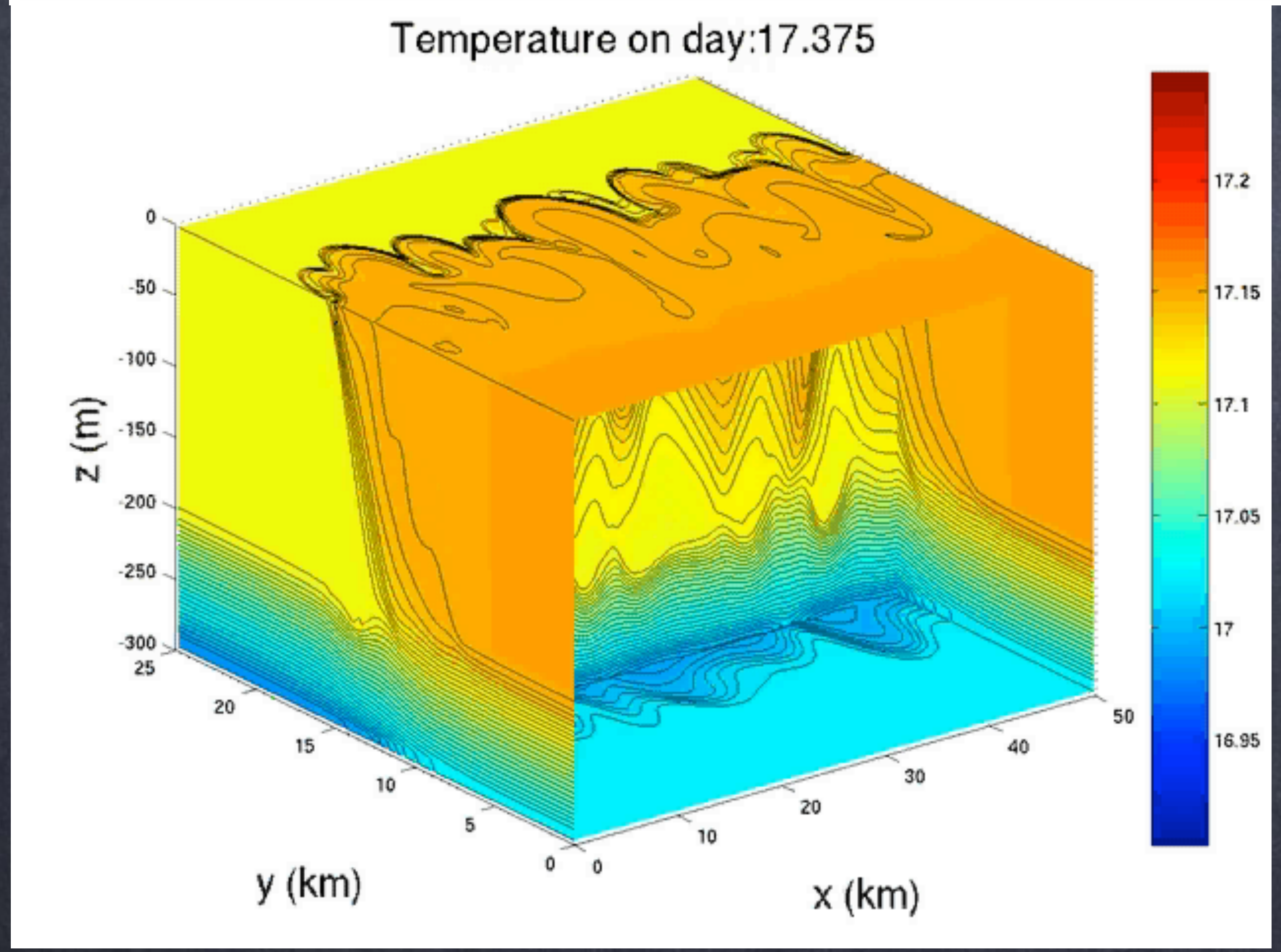

- Fronts
- Eddies
- Ro=O(1)
- Ri=O(1), Fr=O(1)
- near-surface (H=100m)
- 1-10km, days
- W/H~U/L
- hydrostatic
- Globally resolved in 2070-2100

← 10 km

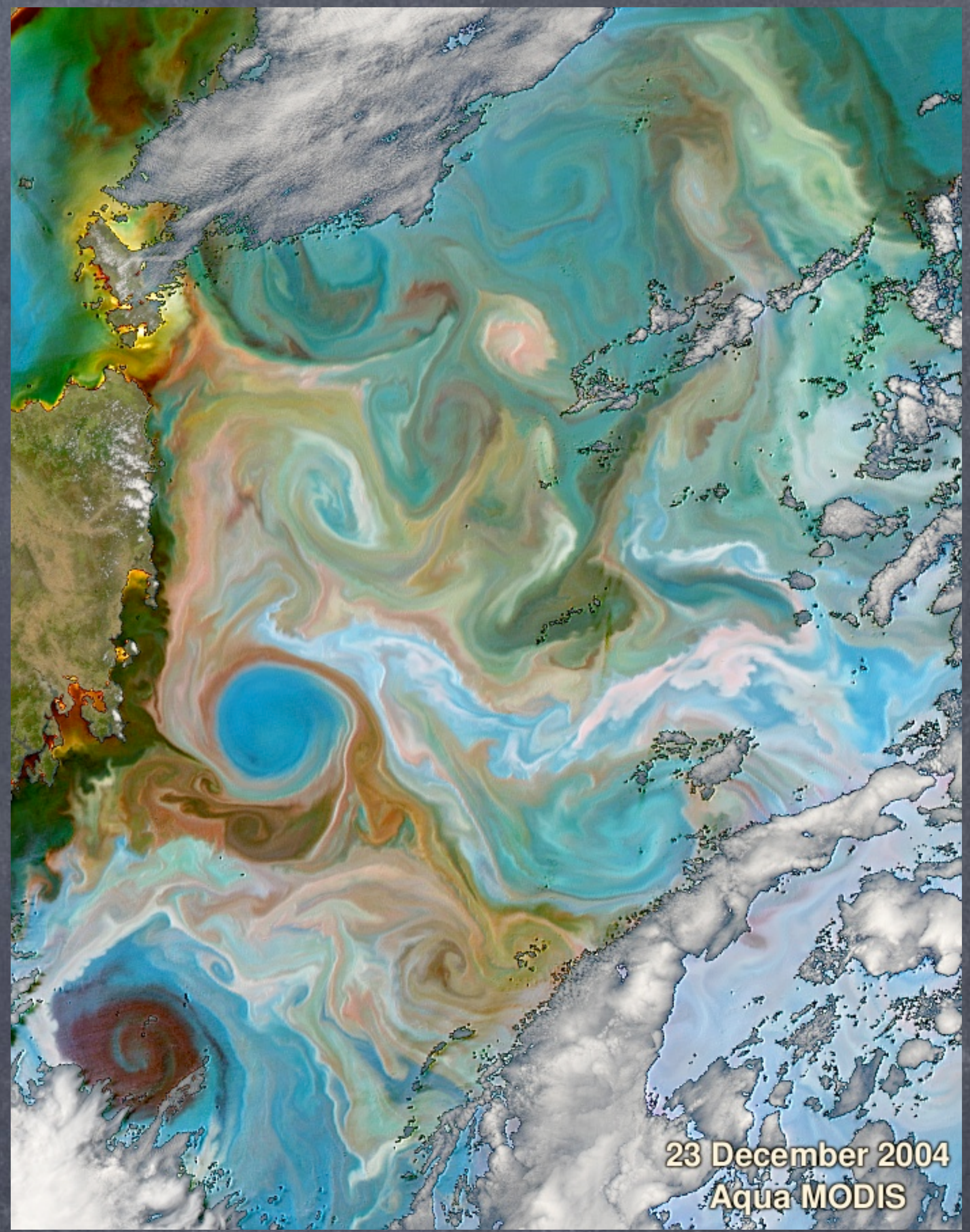

Eddy processes often baroclinic mixed layer instability

BFK, R. Ferrari, and R. W. Hallberg. Parameterization of mixed layer eddies. Part I: Theory and diagnosis. Journal of Physical Oceanography, 38(6):1145-1165, 2008

BFK, G. Danabasoglu, R. Ferrari, S. M. Griffies, R. W. Hallberg, M. M. Holland, M. E. Maltrud, S. Peacock, and B. L. Samuels. Parameterization of mixed layer eddies. III: Implementation and impact in global ocean climate simulations. Ocean Modelling, 39:61-78, 2011.

$$\mathrm{Ro}_* \left[\partial_t \mathbf{v}_h + \mathbf{v}_h \cdot \nabla \mathbf{v}_h + \epsilon w \partial_z \mathbf{v}_h\right] + \underbrace{\left(1 + \frac{y\mathrm{Pl}_*}{\Delta y}\right) \mathbf{z} \times \mathbf{v}_h + \mathrm{M}_{R_*} \nabla_h \pi}_{\text{geostrophic}} = \frac{\mathrm{Ro}_*}{\mathrm{Re}_*} \nabla_i \sigma_{ih},$$

$$\mathrm{Fr}_*{}^2 \frac{\Delta z^2}{\Delta s^2} \left[\partial_t w + \mathbf{v}_h \cdot \nabla w + \epsilon w \partial_z \mathbf{v}_h\right] + \underbrace{\partial_z \pi - b}_{\text{hydrostatic}} = \frac{\mathrm{Fr}_*{}^2 \Delta z^2}{\mathrm{Re}_* \Delta s^2} \nabla_i \sigma_{iz},$$

$$\partial_t S + \mathbf{v}_h \cdot \nabla S + \epsilon w \partial_z S + w \partial_z \bar{S} = \frac{1}{\mathrm{Pe}_*} \nabla \cdot \mathbf{I}_S^{all},$$

$$\partial_t \Theta + \mathbf{v}_h \cdot \nabla \Theta + \epsilon w \partial_z \Theta + w \partial_z \bar{\Theta} = \frac{1}{\mathrm{Pe}_*} \nabla \cdot \mathbf{I}_\theta^{all},$$

$$\partial_t b + \mathbf{v}_h \cdot \nabla b + \epsilon w \partial_z b + w \partial_z \bar{b} = \frac{1}{\mathrm{Pe}_*} \nabla \cdot \left(\alpha \mathbf{I}_\theta^{all} - \beta \mathbf{I}_S^{all}\right),$$

$$\nabla \cdot \mathbf{v}_h + \epsilon \partial_z w = 0,$$

$$\mathrm{M}_{R_*} \equiv \max(1, \mathrm{Ro}_*), \qquad \epsilon \equiv \frac{\mathrm{Fr}_*{}^2}{\mathrm{Ro}_*} \mathrm{M}_{R_*} = \begin{cases} \mathrm{Fr}_*{}^2 & \mathrm{Ro}_* \geq 1, \\ \mathrm{Ro}_* \mathrm{Bu}_*{}^{-1} & \mathrm{Ro}_* < 1 \end{cases}$$

Boussinesq Equations
Following McWilliams (1985)

Geostrophic is out for submeso...

What about hydrostatic?...

BFK. New Frontiers in Operational Oceanography, chapter Notions for the Motions of the Oceans, pages 27-73. GODAE OceanView, 2018.

At the submesoscale...

- Rossby, Richardson, Froude are all O(1), invalidating geostrophic balance & QG, hence the strong convergences.
- But, submesoscales are most active in the surface and bottom boundary layers—so it's just not deep enough to have O(1) aspect ratio.

$$\mathrm{Fr}_*{}^2 \frac{\Delta z^2}{\Delta s^2}\left[\partial_t w + \mathbf{v}_h \cdot \nabla w + \epsilon w \partial_z \mathbf{v}_h\right] + \underbrace{\partial_z \pi - b}_{\text{hydrostatic}} = \frac{\mathrm{Fr}_*{}^2 \Delta z^2}{\mathrm{Re}_* \Delta s^2} \nabla_i \sigma_{iz},$$

For example, the two classic hydrodynamic instabilities of the submesocale are this big... while boundary layers are only O(50m) deep.

Mixed Layer Instability Scale (km)

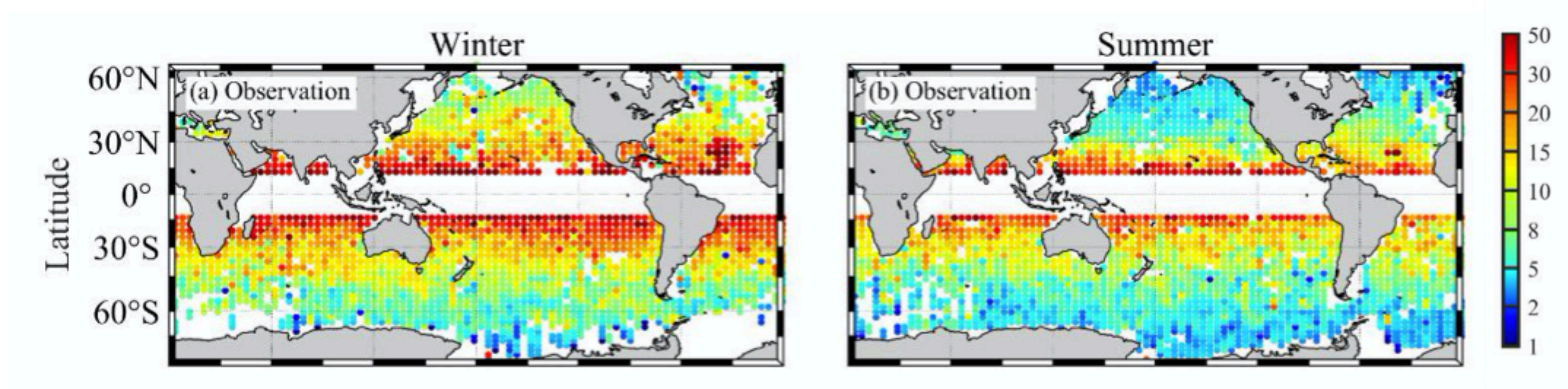

Symmetric Instability Scale (km)

February

August

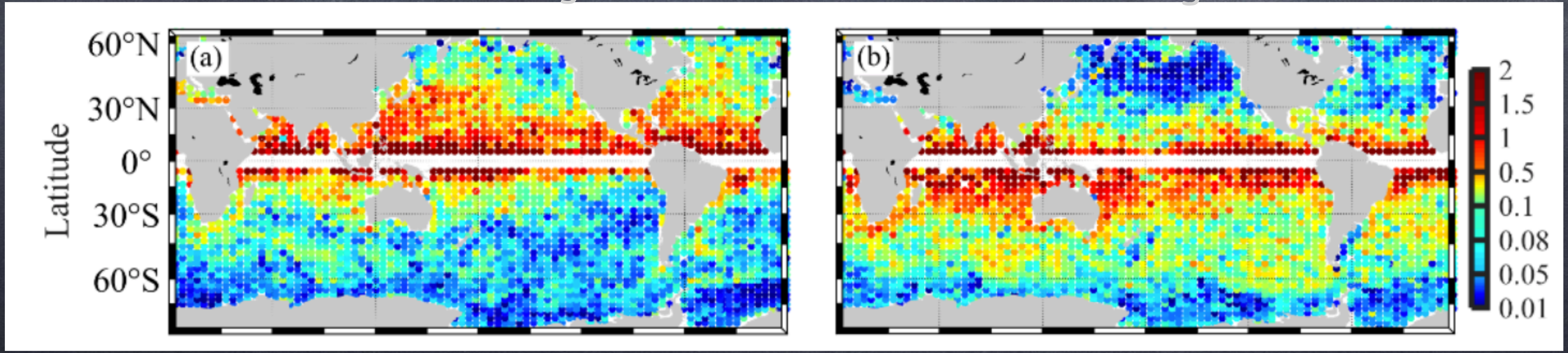

J. Dong, BFK, H. Zhang, and C. Dong. The scale of submesoscale baroclinic instability globally. JPO, 50(9):2649-2667, 2020. dx.doi.org/10.1175/JPO-D-20-0043.1
J. Dong, BFK, H. Zhang, and C. Dong. The Scale and Activity of Symmetric Instability Estimated from a Global Submesoscale-Permitting Ocean Model. JPO, 2021. dx.doi.org/10.1175/JPO-D-20-0159.1

$$\mathrm{Ro}_*\left[\partial_t \mathbf{v}_h + \mathbf{v}_h\cdot\nabla\mathbf{v}_h + \epsilon w\partial_z\mathbf{v}_h\right] + \underbrace{\left(1+\frac{y\mathrm{Pl}_*}{\Delta y}\right)\mathbf{z}\times\mathbf{v}_h + \mathrm{M}_{R_*}\nabla_h\pi}_{\text{geostrophic}} = \frac{\mathrm{Ro}_*}{\mathrm{Re}_*}\nabla_i\sigma_{ih},$$

$$\mathrm{Fr}_*{}^2\frac{\Delta z^2}{\Delta s^2}\left[\partial_t w + \mathbf{v}_h\cdot\nabla w + \epsilon w\partial_z\mathbf{v}_h\right] + \underbrace{\partial_z\pi - b}_{\text{hydrostatic}} = \frac{\mathrm{Fr}_*{}^2\Delta z^2}{\mathrm{Re}_*\Delta s^2}\nabla_i\sigma_{iz},$$

$$\partial_t S + \mathbf{v}_h\cdot\nabla S + \epsilon w\partial_z S + w\partial_z\bar{S} = \frac{1}{\mathrm{Pe}_*}\nabla\cdot\mathbf{I}_S^{all},$$

$$\partial_t\Theta + \mathbf{v}_h\cdot\nabla\Theta + \epsilon w\partial_z\Theta + w\partial_z\bar{\Theta} = \frac{1}{\mathrm{Pe}_*}\nabla\cdot\mathbf{I}_\theta^{all},$$

$$\partial_t b + \mathbf{v}_h\cdot\nabla b + \epsilon w\partial_z b + w\partial_z\bar{b} = \frac{1}{\mathrm{Pe}_*}\nabla\cdot\left(\alpha\mathbf{I}_\theta^{all} - \beta\mathbf{I}_S^{all}\right),$$

$$\nabla\cdot\mathbf{v}_h + \epsilon\partial_z w = 0,$$

$$\mathrm{M}_{R_*} \equiv \max(1,\mathrm{Ro}_*), \qquad \epsilon \equiv \frac{\mathrm{Fr}_*{}^2}{\mathrm{Ro}_*}\mathrm{M}_{R_*} = \begin{cases}\mathrm{Fr}_*{}^2 & \mathrm{Ro}_* \geq 1,\\ \mathrm{Ro}_*\mathrm{Bu}_*{}^{-1} & \mathrm{Ro}_* < 1\end{cases}$$

Boussinesq Equations
Following McWilliams (1985)

Geostrophic is out for submeso...
Hydrostatic is OK!

BFK. New Frontiers in Operational Oceanography, chapter Notions for the Motions of the Oceans, pages 27-73. GODAE OceanView, 2018.

The Character of the Langmuir Scale

- Near-surface
- Langmuir Cells & Langmuir Turb.
- Ro>>1
- Ri<1: Nonhydro
- 1-100m (H=L)
- 10s to 1hr
- w, u=O(10cm/s)
- Stokes drift
- Eqtns:Craik-Leibovich
- Params: McWilliams & Sullivan, 2000, Van Roekel et al. 2012
- Resolved routinely in 2170

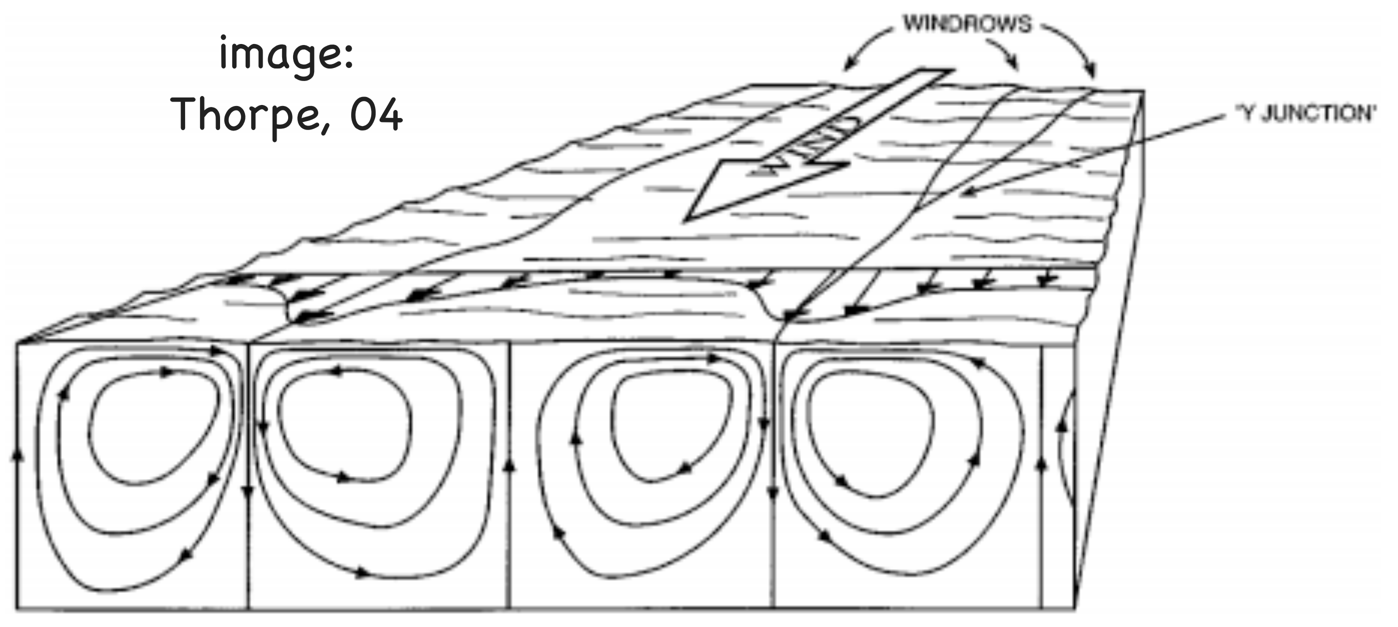

Figure 1 Sketch showing the pattern of mean flow in idealized Langmuir circulation. The windrows may be 2 m to 300 m apart, and the cell form is roughly square (as shown). In practice the flow is turbulent, especially near the water surface, and the windrows (Figure 2) amalgamate and meander in space and time. Bands of bubbles or buoyant algae may form within the downward-going (or downwelling) flow (see Figure 3).

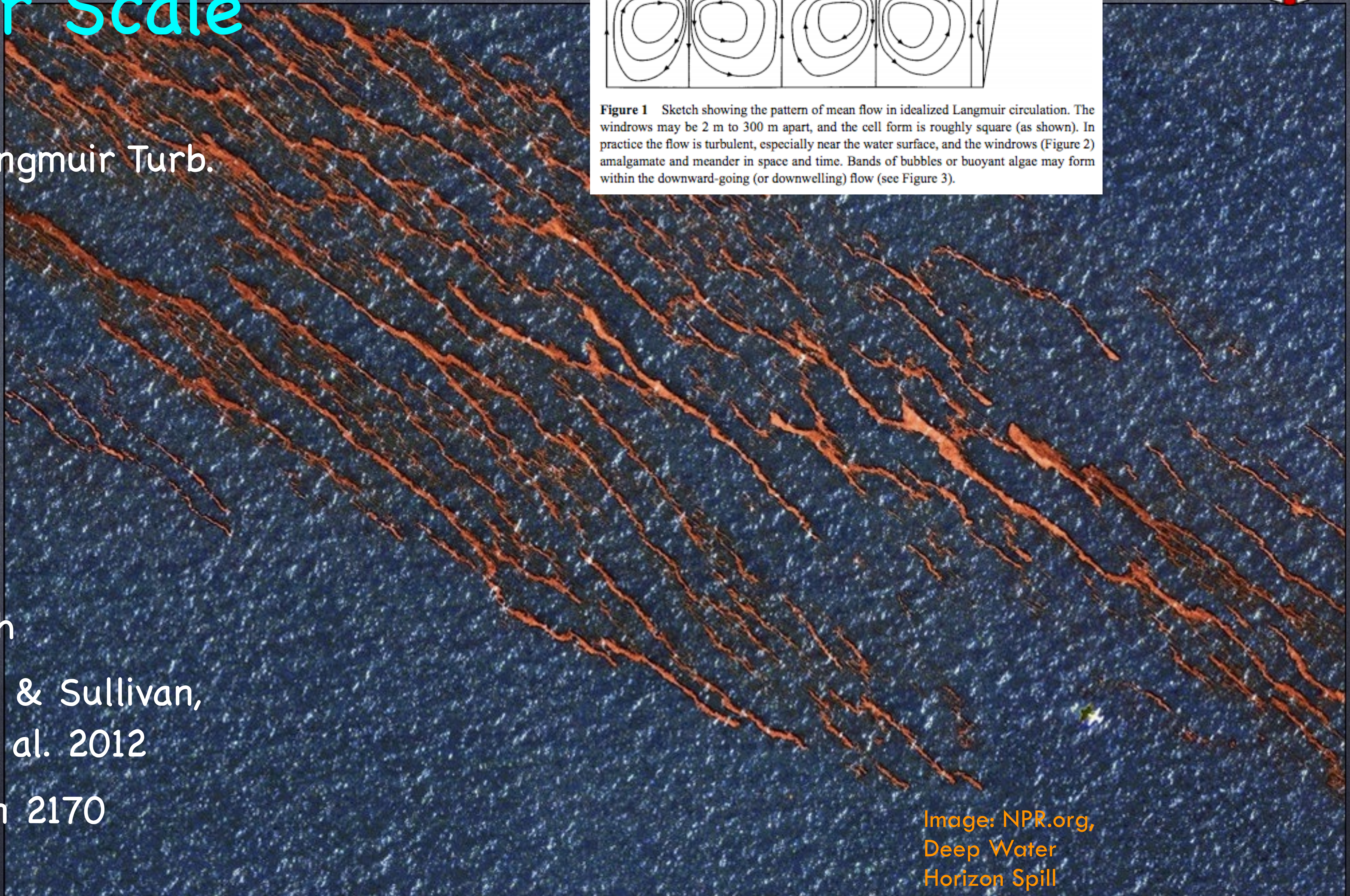

Image: NPR.org, Deep Water Horizon Spill

OK...

Tell us something new!

- The Wave-Averaged Boussinesq equations (or Craik-Leibovich eqtns.) have been used for Langmuir turbulence sims for about 20 years.
- But, they are capable of much more!
- This is, in essence, our first parameterization of unresolved effects—waves

Surface Waves are...

Fast, small, approx. irrotational solutions of the Boussinesq Equations

Have a Stokes drift depending on sea state (wave age, winds)

A. Webb and B. Fox-Kemper. Wave spectral moments and Stokes drift estimation. Ocean Modelling, 40(3-4):273-288, 2011.

A. Webb and B. Fox-Kemper. Impacts of wave spreading and multidirectional waves on estimating Stokes drift. Ocean Modelling, 96(1):49-64, 2015.

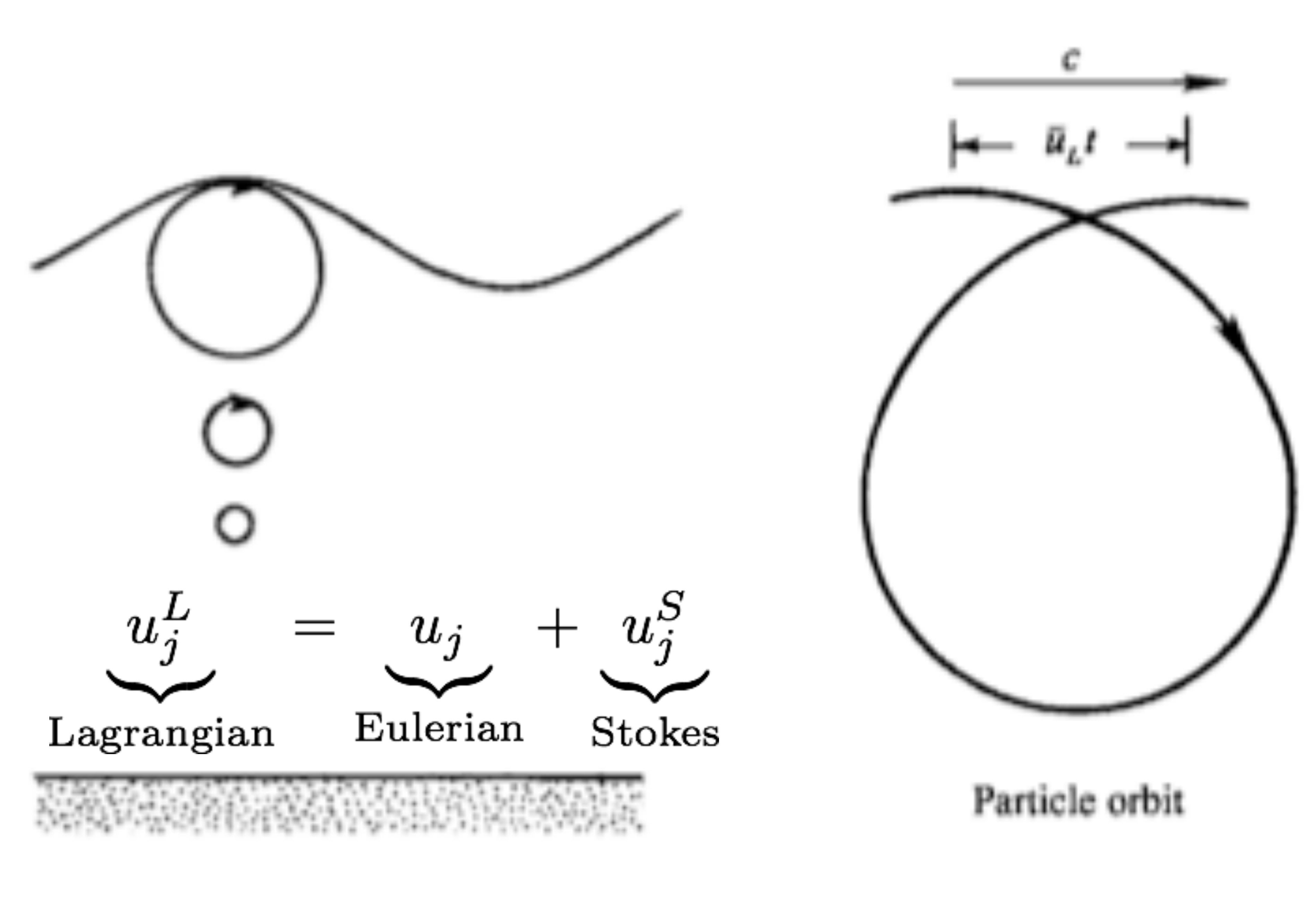

Surface Waves are...

Fast, small, approx. irrotational solutions of the Boussinesq Equations

Have a Stokes drift depending on sea state (wave age, winds)

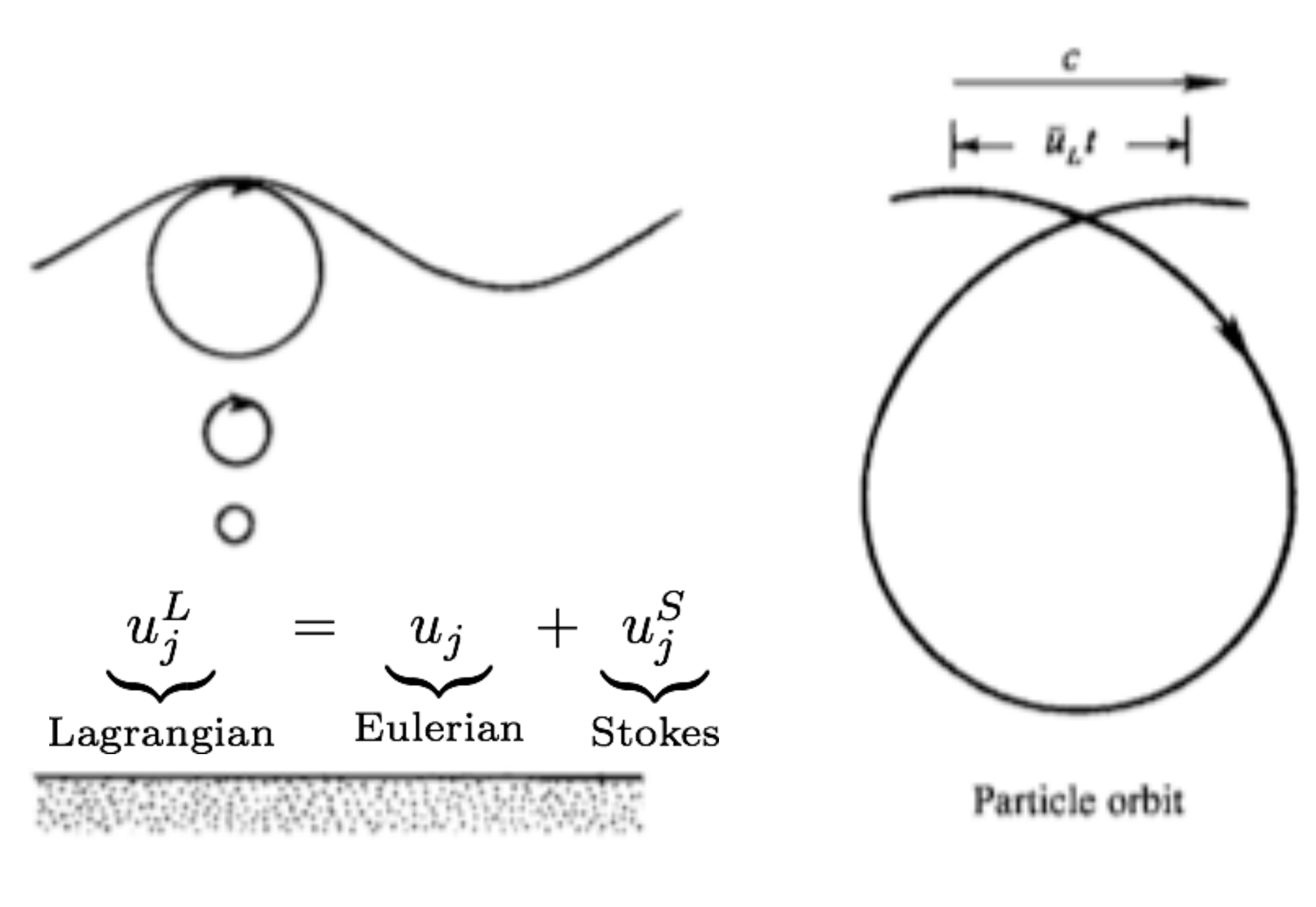

A. Webb and B. Fox-Kemper. Wave spectral moments and Stokes drift estimation. Ocean Modelling, 40(3-4):273-288, 2011.

A. Webb and B. Fox-Kemper. Impacts of wave spreading and multidirectional waves on estimating Stokes drift. Ocean Modelling, 96(1):49-64, 2015.

Surface Waves are...

Fast, small, approx. irrotational solutions of the Boussinesq Equations

Have a Stokes drift depending on sea state (wave age, winds)

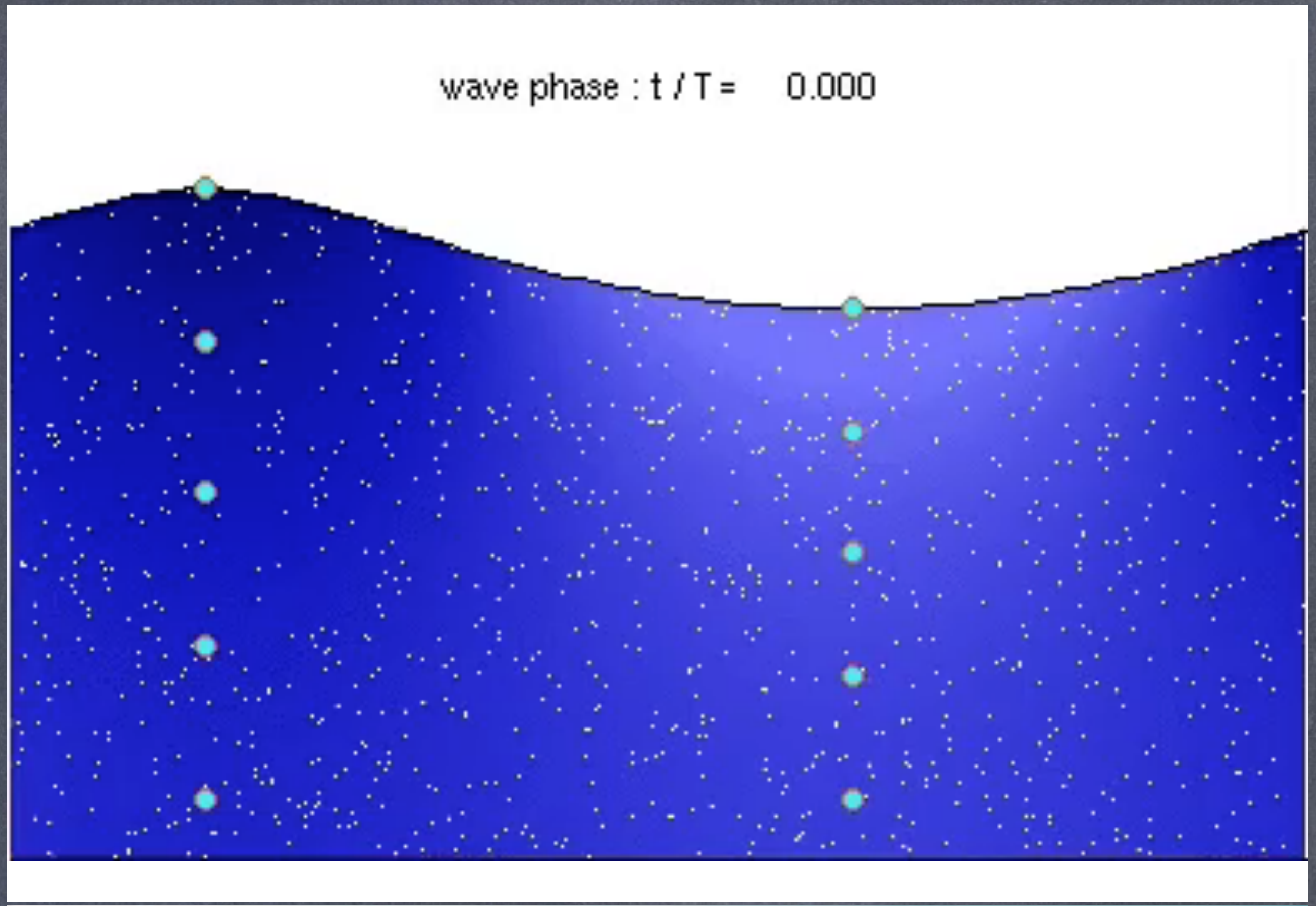

A. Webb and B. Fox-Kemper. Wave spectral moments and Stokes drift estimation. Ocean Modelling, 40(3-4):273-288, 2011.

A. Webb and B. Fox-Kemper. Impacts of wave spreading and multidirectional waves on estimating Stokes drift. Ocean Modelling, 96(1):49-64, 2015.

3 Effects Dominate open ocean
"Wave-Averaged Equations":
(Craik, Leibovich, McWilliams et al. 1997, Lane et al. 2007)
All rely only on Stokes drift of waves & vorticity in flow;
easier to model than radiation stresses

1: Stokes Advection: parcels, tracers, momentum move with Lagrangian, not Eulerian flow

2: Stokes Coriolis: water parcels experience Coriolis force during this motion

3: Stokes Shear Force

N. Suzuki and BFK. Understanding Stokes forces in the wave-averaged equations. Journal of Geophysical Research-Oceans, 121:1-18, 2016.

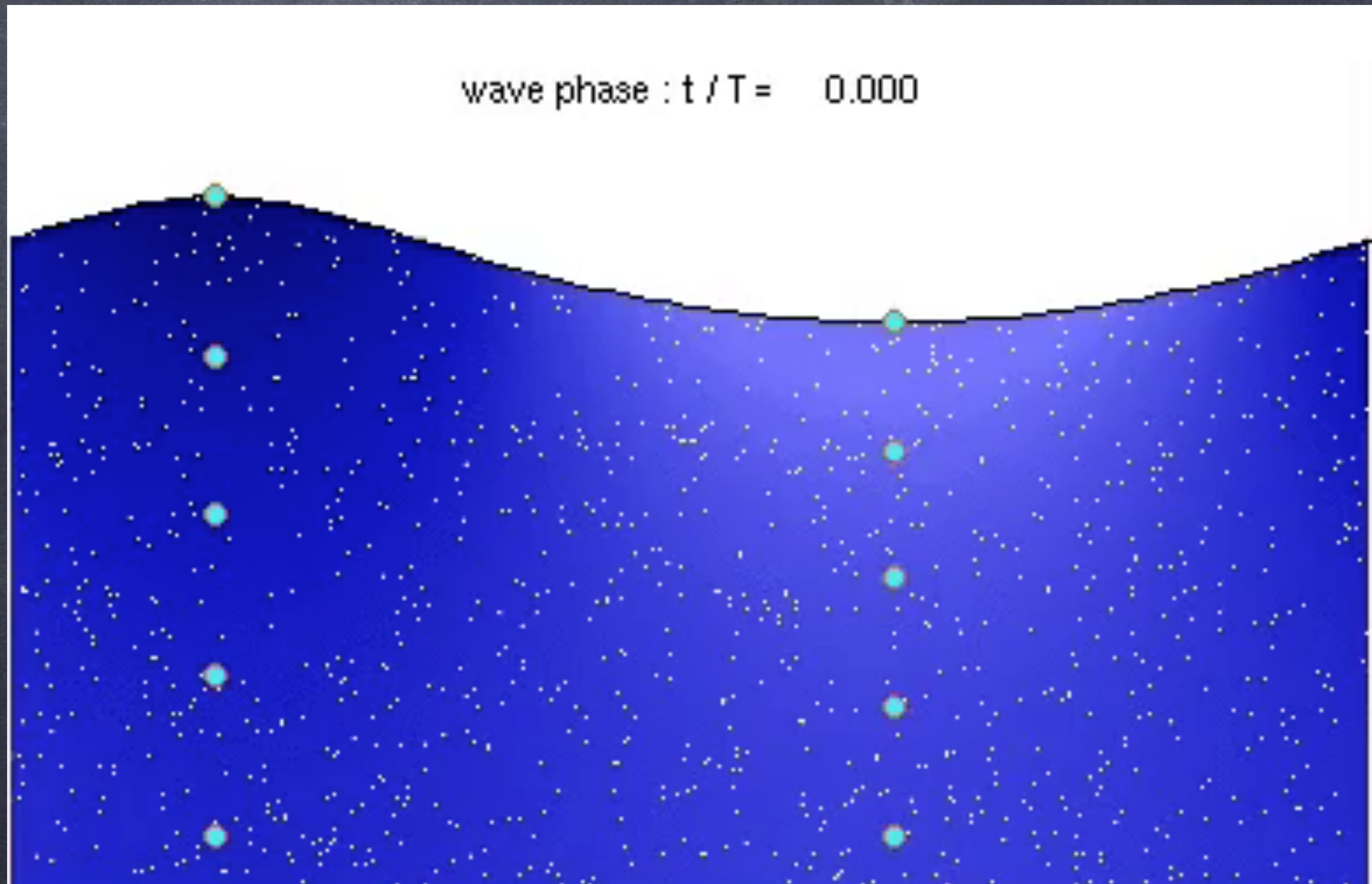

3 Effects Dominate open ocean "Wave-Averaged Equations":

(Craik, Leibovich, McWilliams et al. 1997, Lane et al. 2007)

All rely only on Stokes drift of waves & vorticity in flow;

easier to model than radiation stresses

1: Stokes Advection: parcels, tracers, momentum move with Lagrangian, not Eulerian flow

2: Stokes Coriolis: water parcels experience Coriolis force during this motion

3: Stokes Shear Force

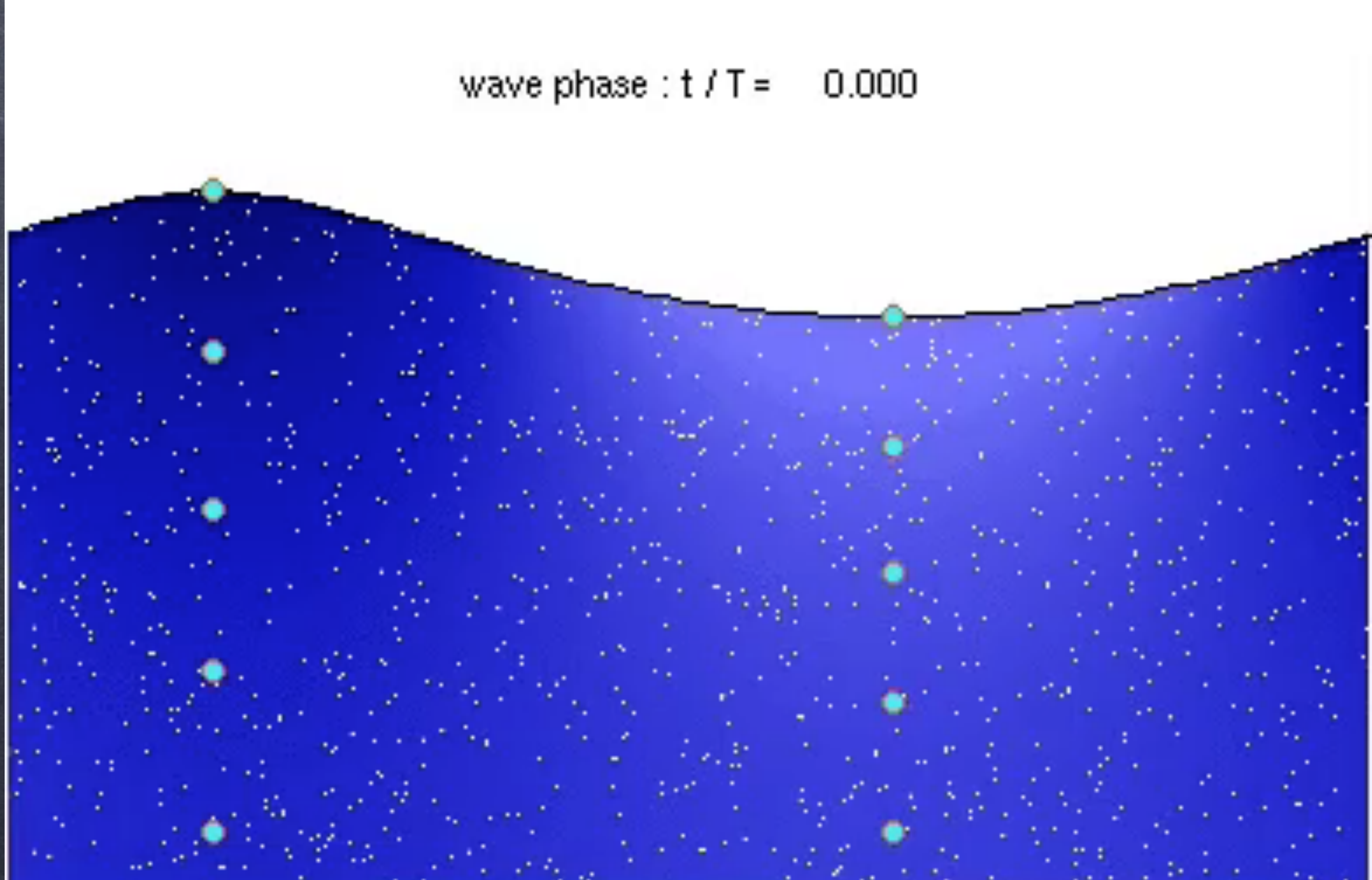

N. Suzuki and BFK. Understanding Stokes forces in the wave-averaged equations. Journal of Geophysical Research-Oceans, 121:1-18, 2016.

Wave-Averaged Equations following

Lane et al. (07), McWilliams & F-K (13)
and Suzuki & F-K (16)

$$\underbrace{v_j^L}_{\text{Lagrangian}} = \underbrace{v_j}_{\text{Eulerian}} + \underbrace{v_j^S}_{\text{Stokes}}$$

Coupling Depends on Stokes drift—WAVE effects in YELLOW

Boundary conditions, plus:

(Lagrangian) geostrophic

$$Ro\left[v_{i,t} + v_j^L v_{i,j}\right] + \frac{M_{Ro}}{Ri} w v_{i,z} + \boxed{\epsilon_{izj} v_j^L = -M_{Ro}\pi_{,i}} + \frac{Ro}{Re} v_{i,jj}$$

$$\frac{\alpha^2}{Ri}\left[w_{,t} + v_j^L w_{,j} + \frac{M_{Ro}}{RoRi} w w_{,z}\right] = \underbrace{\boxed{-\pi_{,z} + b}}_{\text{hydrostatic}} - \varepsilon v_j^L v_{j,z}^s + \frac{\alpha^2}{ReRi} w_{,jj}$$

$$b_t + v_j^L b_{,j} + \frac{M_{Ro}}{RoRi} w b_z = \frac{1}{Pe} b_{,jj}$$

$$v_{j,j} + \frac{M_{Ro}}{RoRi} w_z = 0$$

$$\boxed{\varepsilon = \frac{V^s H}{f L H_s}}$$

$$Re = \frac{UL}{\nu} \quad Ro = \frac{U}{fL} \quad Ri = \frac{N^2}{(U_{,z})^2} \quad \alpha = H/L \quad M_{Ro} \equiv \max(1, Ro)$$

J. C. McWilliams and BFK. Oceanic wave-balanced surface fronts and filaments. Journal of Fluid Mechanics, 730:464-490, 2013.

N. Suzuki and BFK. Understanding Stokes forces in the wave-averaged equations. JGR-Oceans, 121:1-18, 2016.

20km x 20km x 150m domain

15 Day Simulation

This is a 300 teragrid simulation to span both submesoscale & Langmuir scale

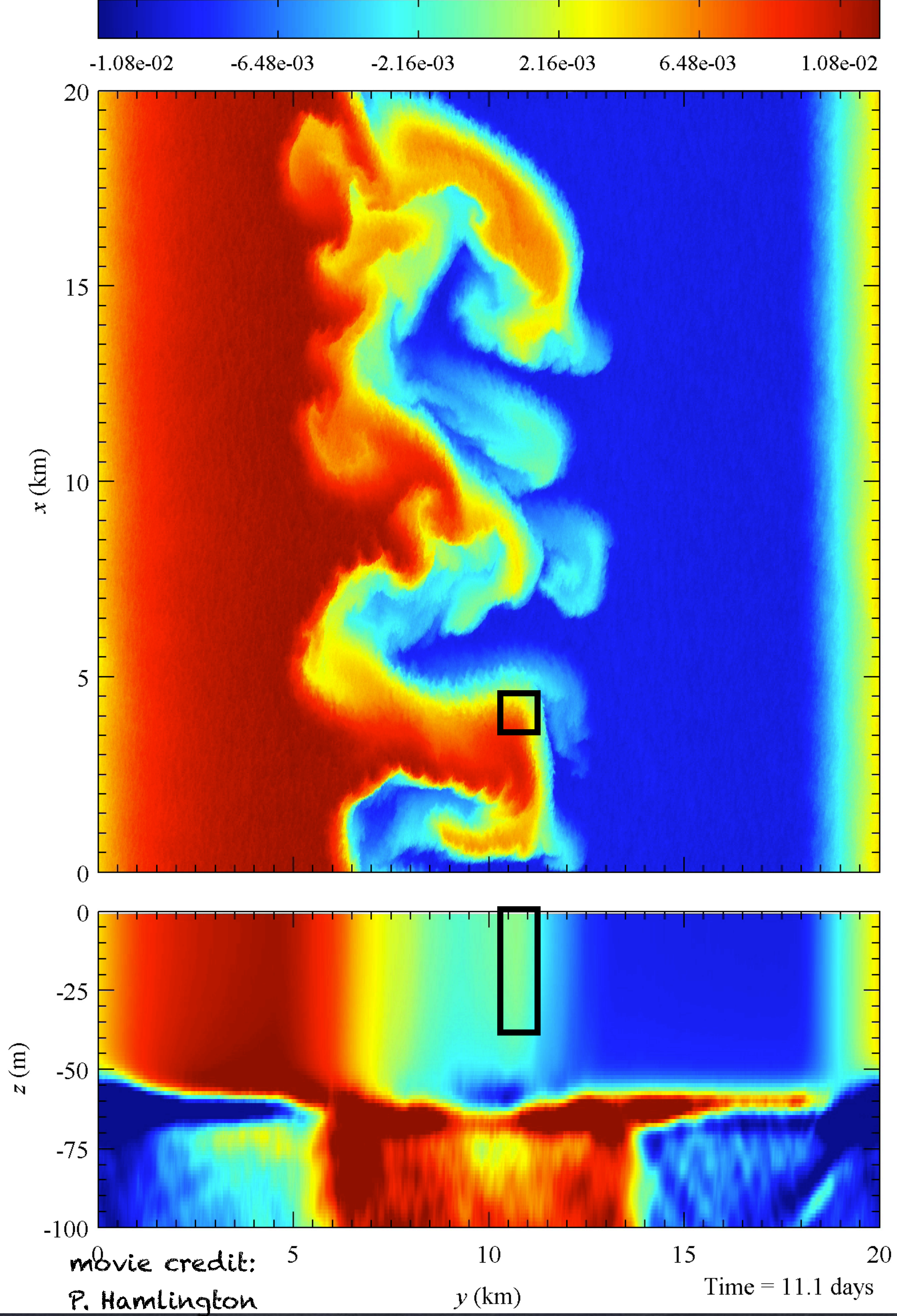

P. E. Hamlington, L. P. Van Roekel, BFK, K. Julien, and G. P. Chini. Langmuir-submesoscale interactions: Descriptive analysis of multiscale frontal spin-down simulations. Journal of Physical Oceanography, 44(9):2249-2272, September 2014.

20km x 20km x 150m domain

15 Day Simulation

This is a 300 teragrid simulation to span both submesoscale & Langmuir scale

P. E. Hamlington, L. P. Van Roekel, BFK, K. Julien, and G. P. Chini. Langmuir-submesoscale interactions: Descriptive analysis of multiscale frontal spin-down simulations. Journal of Physical Oceanography, 44(9):2249-2272, September 2014.

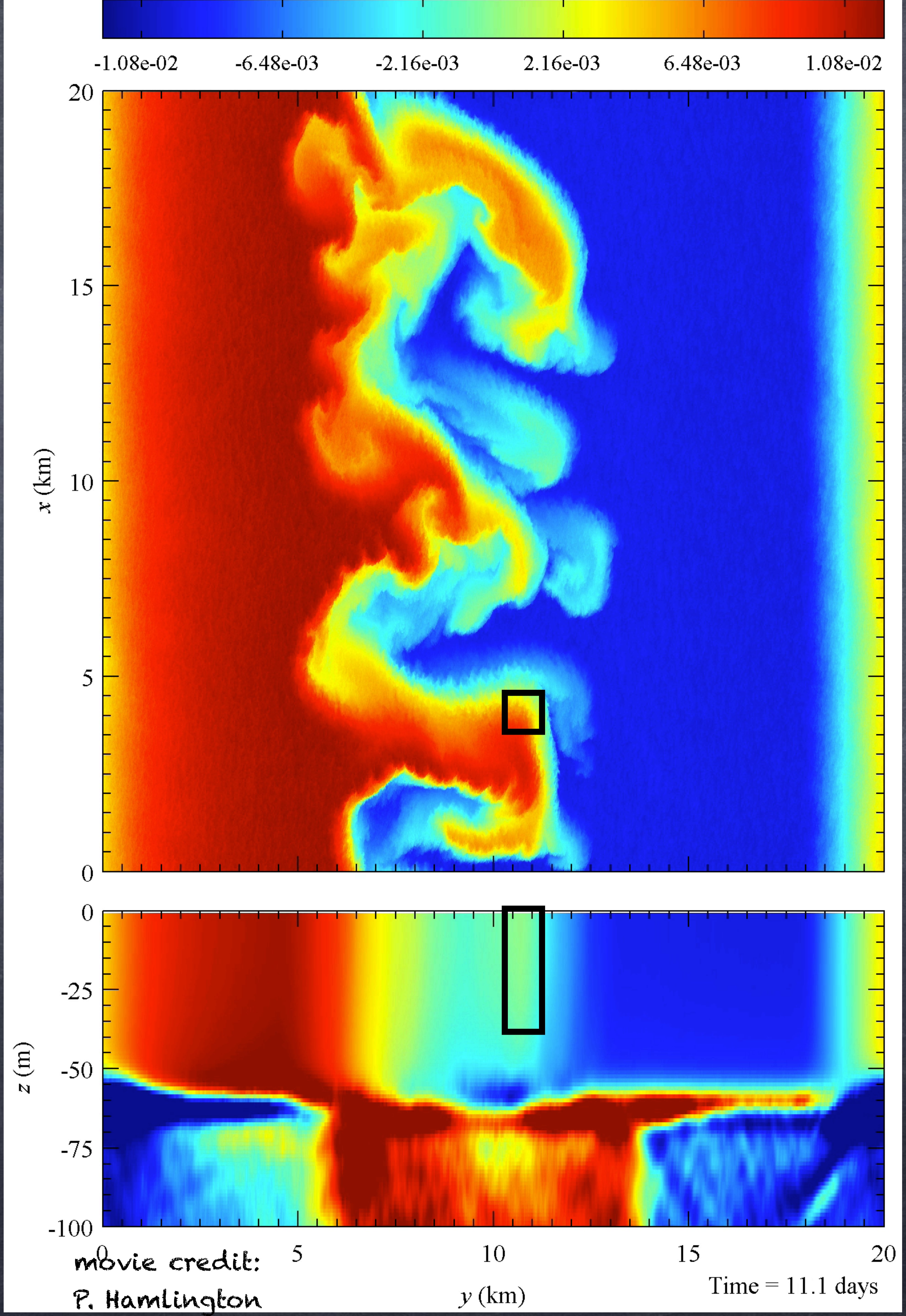

Wave-Averaged Equations following

Lane et al. (07), McWilliams & F-K (13)
and Suzuki & F-K (16)

$$\underbrace{v_j^L}_{\text{Lagrangian}} = \underbrace{v_j}_{\text{Eulerian}} + \underbrace{v_j^S}_{\text{Stokes}}$$

Coupling Depends on Stokes drift—WAVE effects in YELLOW

Boundary conditions, plus:

(Lagrangian) geostrophic

$$Ro\left[v_{i,t} + v_j^L v_{i,j}\right] + \frac{M_{Ro}}{Ri} w v_{i,z} + \boxed{\epsilon_{izj} v_j^L = -M_{Ro}\pi_{,i}} + \frac{Ro}{Re} v_{i,jj}$$

$$\frac{\alpha^2}{Ri}\left[w_{,t} + v_j^L w_{,j} + \frac{M_{Ro}}{RoRi} w w_{,z}\right] = \boxed{-\pi_{,z} + b} - \varepsilon v_j^L v_{j,z}^s + \frac{\alpha^2}{ReRi} w_{,jj}$$

hydrostatic

$$b_t + v_j^L b_{,j} + \frac{M_{Ro}}{RoRi} w b_z = \frac{1}{Pe} b_{,jj}$$

$$v_{j,j} + \frac{M_{Ro}}{RoRi} w_z = 0$$

$$\boxed{\varepsilon = \frac{V^s H}{f L H_s}}$$

$$Re = \frac{UL}{\nu} \quad Ro = \frac{U}{fL} \quad Ri = \frac{N^2}{(U_{,z})^2} \quad \alpha = H/L \quad M_{Ro} \equiv \max(1, Ro)$$

J. C. McWilliams and BFK. Oceanic wave-balanced surface fronts and filaments. Journal of Fluid Mechanics, 730:464-490, 2013.

N. Suzuki and BFK. Understanding Stokes forces in the wave-averaged equations. JGR-Oceans, December 2015. Submitted.

3 Wave Effects, 1: Lagrangian Advection:

Particles, tracers, momentum flow with Lagrangian, not Eulerian flow

$$Ro\left[v_{i,t}+v_j^L v_{i,j}\right]+\frac{M_{Ro}}{Ri}wv_{i,z}+\epsilon_{izj}v_j^L=-M_{Ro}\pi_{,i}+\frac{Ro}{Re}v_{i,jj}$$

$$\frac{\alpha^2}{Ri}\left[w_{,t}+v_j^L w_{,j}+\frac{M_{Ro}}{RoRi}ww_{,z}\right]=-\pi_{,z}+b-\varepsilon v_j^L v_{j,z}^s+\frac{\alpha^2}{ReRi}w_{,jj}$$

$$b_t+v_j^L b_{,j}+\frac{M_{Ro}}{RoRi}wb_z=\frac{1}{Pe}b_{,jj}$$

Adding a Stokes advection term converts total to Lagrangian advection

$$\underbrace{v_j^L}_{\text{Lagrangian}}=\underbrace{v_j}_{\text{Eulerian}}+\underbrace{v_j^S}_{\text{Stokes}}$$

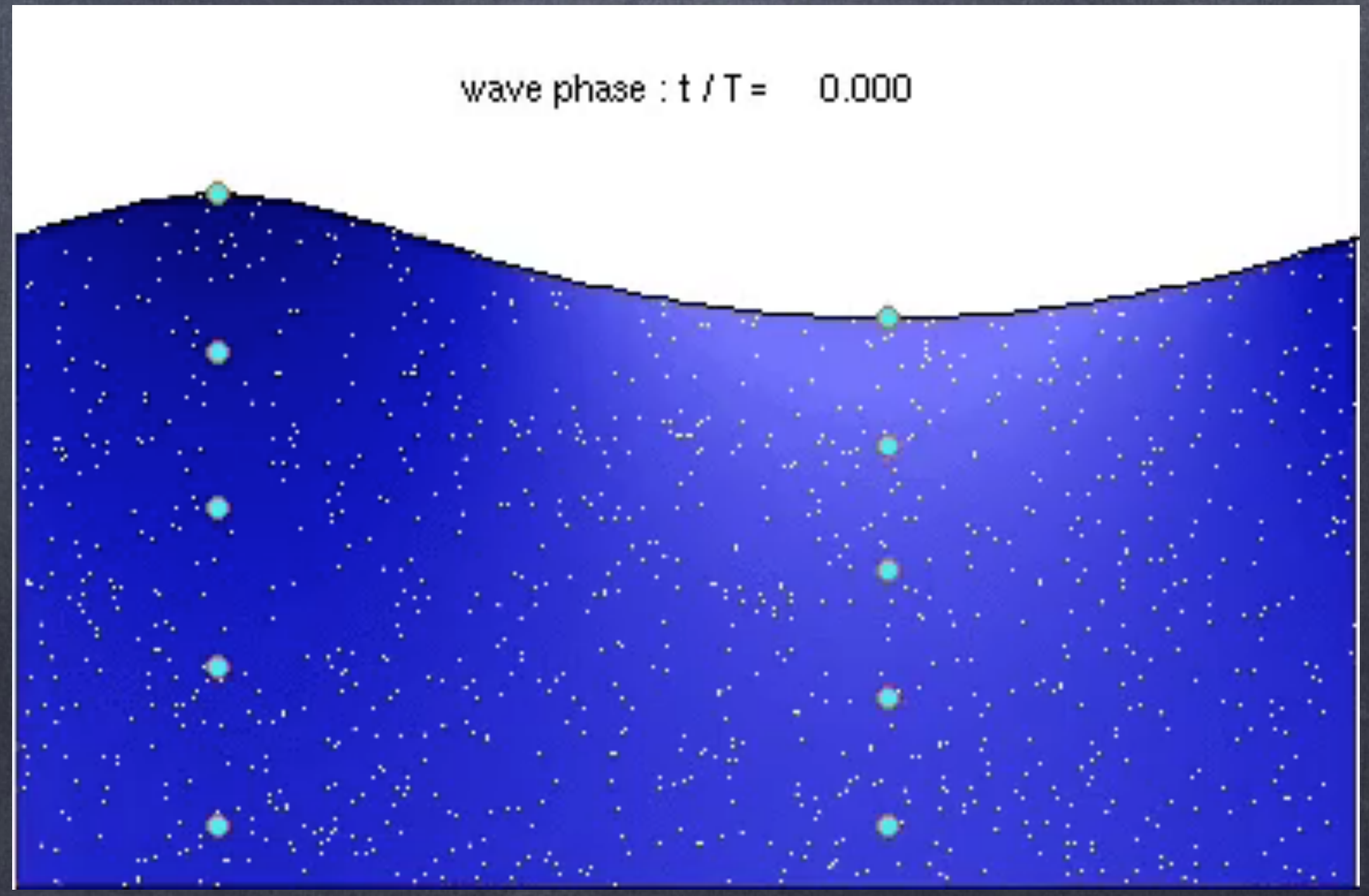

N. Suzuki and BFK. Understanding Stokes forces in the wave-averaged equations. JGR-Oceans, December 2015. Submitted.

3 Wave Effects, 1: Lagrangian Advection:

Particles, tracers, momentum flow with Lagrangian, not Eulerian flow

$$Ro\left[v_{i,t} + v_j^L v_{i,j}\right] + \frac{M_{Ro}}{Ri} w v_{i,z} + \epsilon_{izj} v_j^L = -M_{Ro}\pi_{,i} + \frac{Ro}{Re} v_{i,jj}$$

$$\frac{\alpha^2}{Ri}\left[w_{,t} + v_j^L w_{,j} + \frac{M_{Ro}}{RoRi} w w_{,z}\right] = -\pi_{,z} + b - \varepsilon v_j^L v_{j,z}^s + \frac{\alpha^2}{ReRi} w_{,jj}$$

$$b_t + v_j^L b_{,j} + \frac{M_{Ro}}{RoRi} w b_z = \frac{1}{Pe} b_{,jj}$$

Adding a Stokes advection term converts total to Lagrangian advection

$$\underbrace{v_j^L}_{\text{Lagrangian}} = \underbrace{v_j}_{\text{Eulerian}} + \underbrace{v_j^S}_{\text{Stokes}}$$

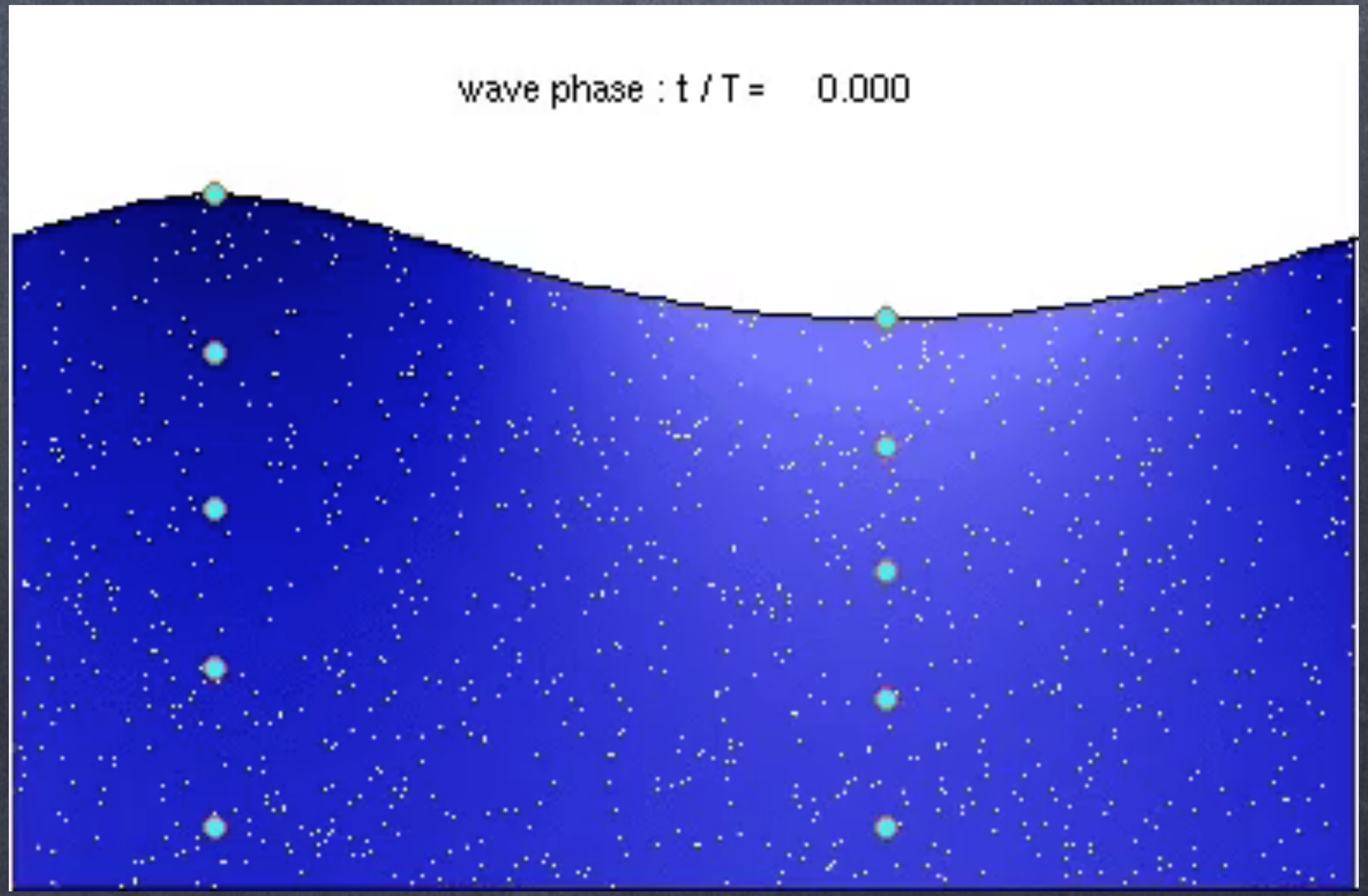

N. Suzuki and BFK. Understanding Stokes forces in the wave-averaged equations. JGR-Oceans, December 2015. Submitted.

3 Wave Effects, 2: Lagrangian Coriolis:

Particles, tracers, momentum flow with Lagrangian, not Eulerian flow—Experience Coriolis force during this motion

$$Ro\left[v_{i,t} + v_j^L v_{i,j}\right] + \frac{M_{Ro}}{Ri} w v_{i,z} + \boxed{\epsilon_{izj} v_j^L} = -M_{Ro}\pi_{,i} + \frac{Ro}{Re} v_{i,jj}$$

$$\frac{\alpha^2}{Ri}\left[w_{,t} + v_j^L w_{,j} + \frac{M_{Ro}}{RoRi} w w_{,z}\right] = -\pi_{,z} + b - \varepsilon v_j^L v_{j,z}^s + \frac{\alpha^2}{ReRi} w_{,jj}$$

$$b_t + v_j^L b_{,j} + \frac{M_{Ro}}{RoRi} w b_z = \frac{1}{Pe} b_{,jj}$$

Adding a Stokes Coriolis term converts total to Lagrangian

$$\underbrace{v_j^L}_{\text{Lagrangian}} = \underbrace{v_j}_{\text{Eulerian}} + \underbrace{v_j^S}_{\text{Stokes}}$$

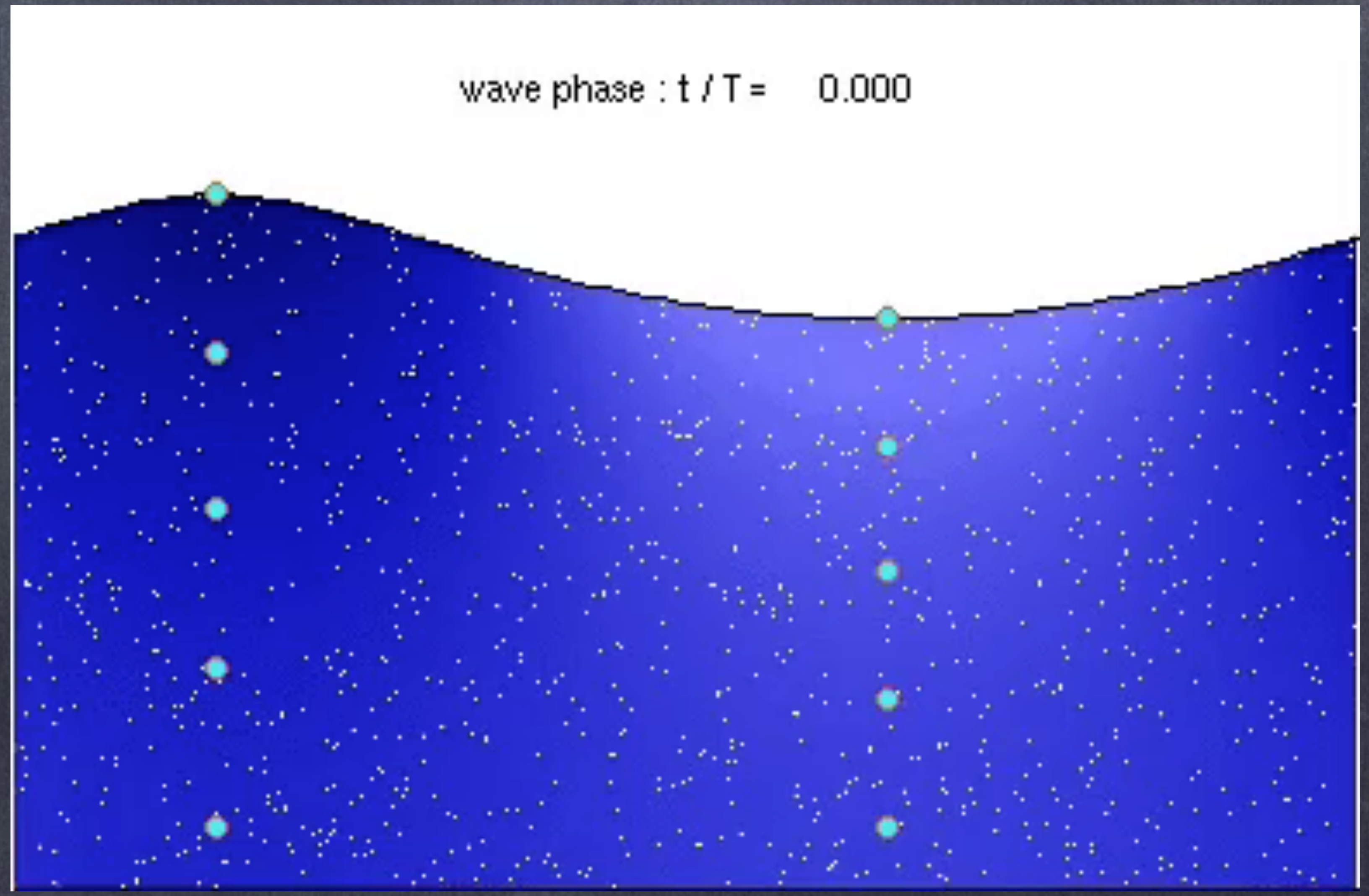

N. Suzuki and BFK. Understanding Stokes forces in the wave-averaged equations. JGR-Oceans, December 2015. Submitted.

3 Wave Effects, 2: Lagrangian Coriolis:

Particles, tracers, momentum flow with Lagrangian, not Eulerian flow—Experience Coriolis force during this motion

$$Ro\left[v_{i,t} + v_j^L v_{i,j}\right] + \frac{M_{Ro}}{Ri} w v_{i,z} + \boxed{\epsilon_{izj} v_j^L} = -M_{Ro}\pi_{,i} + \frac{Ro}{Re} v_{i,jj}$$

$$\frac{\alpha^2}{Ri}\left[w_{,t} + v_j^L w_{,j} + \frac{M_{Ro}}{RoRi} w w_{,z}\right] = -\pi_{,z} + b - \varepsilon v_j^L v^s_{j,z} + \frac{\alpha^2}{ReRi} w_{,jj}$$

$$b_t + v_j^L b_{,j} + \frac{M_{Ro}}{RoRi} w b_z = \frac{1}{Pe} b_{,jj}$$

Adding a Stokes Coriolis term converts total to Lagrangian

$$\underbrace{v_j^L}_{\text{Lagrangian}} = \underbrace{v_j}_{\text{Eulerian}} + \underbrace{v_j^S}_{\text{Stokes}}$$

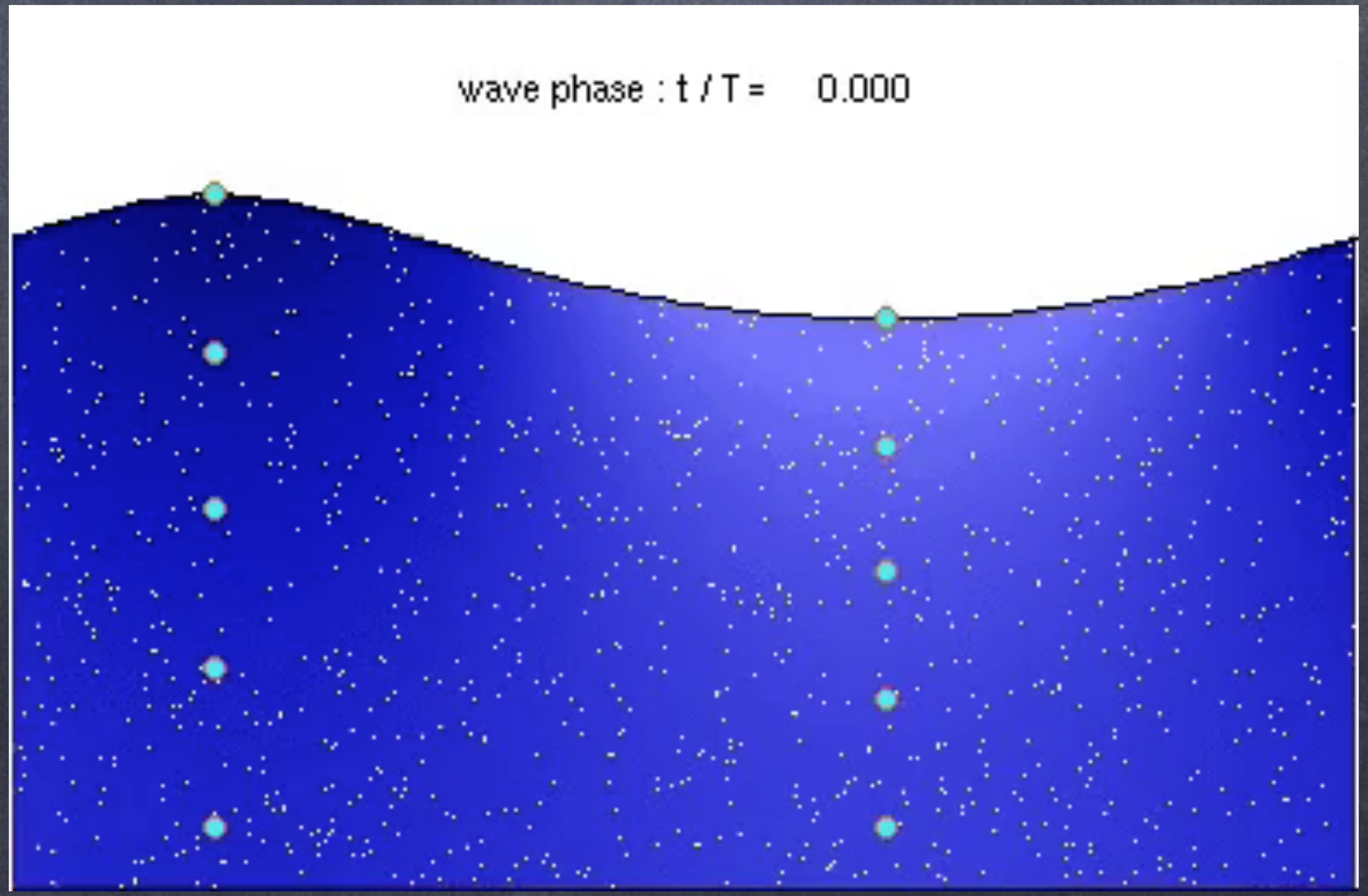

N. Suzuki and BFK. Understanding Stokes forces in the wave-averaged equations. JGR-Oceans, December 2015. Submitted.

image:
Thorpe, 04

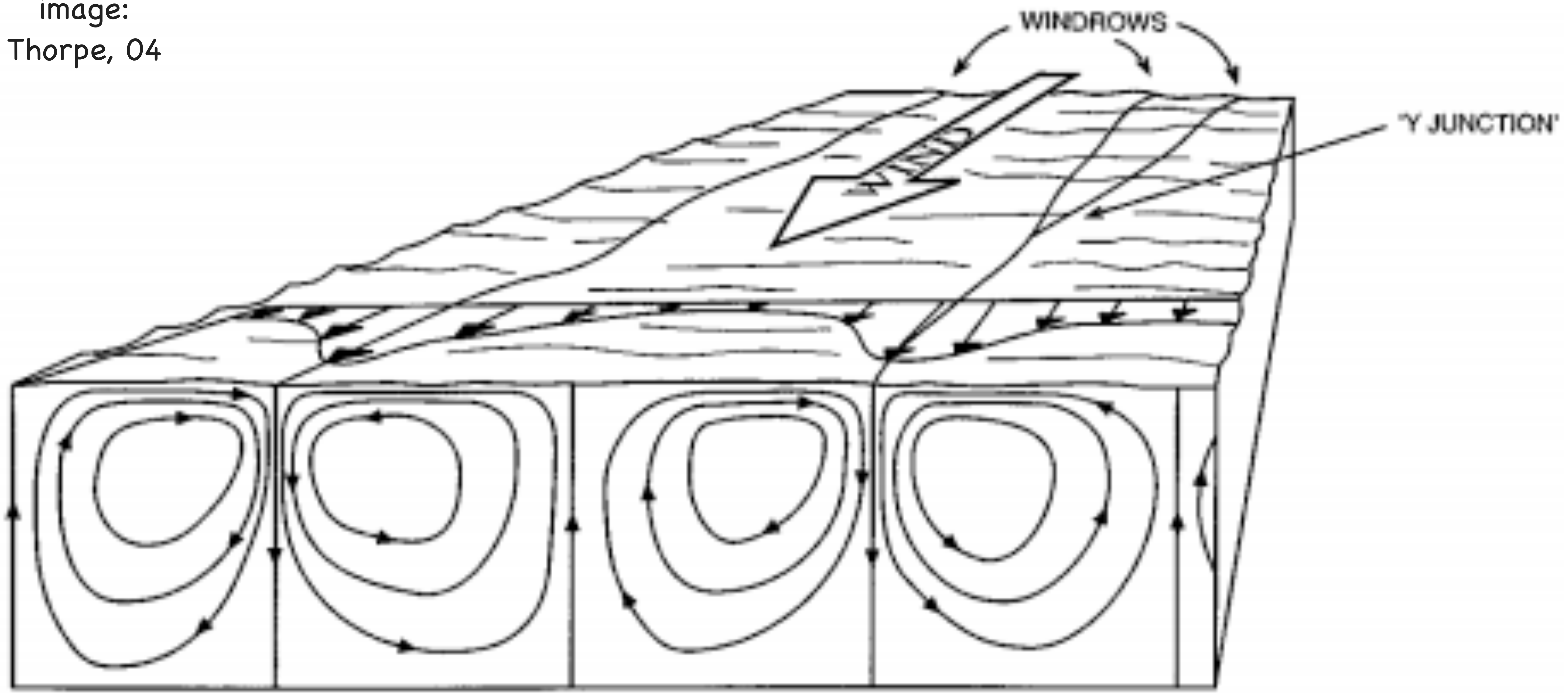

Figure 1 Sketch showing the pattern of mean flow in idealized Langmuir circulation. The windrows may be 2 m to 300 m apart, and the cell form is roughly square (as shown). In practice the flow is turbulent, especially near the water surface, and the windrows (Figure 2) amalgamate and meander in space and time. Bands of bubbles or buoyant algae may form within the downward-going (or downwelling) flow (see Figure 3).

$$\frac{\alpha^2}{Ri}\left[w_{,t} + v_j^L w_{,j} + \frac{M_{Ro}}{RoRi} w w_{,z}\right] = -\pi_{,z} + b - \varepsilon v_j^L v_{j,z}^s + \frac{\alpha^2}{ReRi} w_{,jj}$$

N. Suzuki and BFK. Understanding Stokes forces in the wave-averaged equations. Journal of Geophysical Research-Oceans, 121:1-18, 2016.

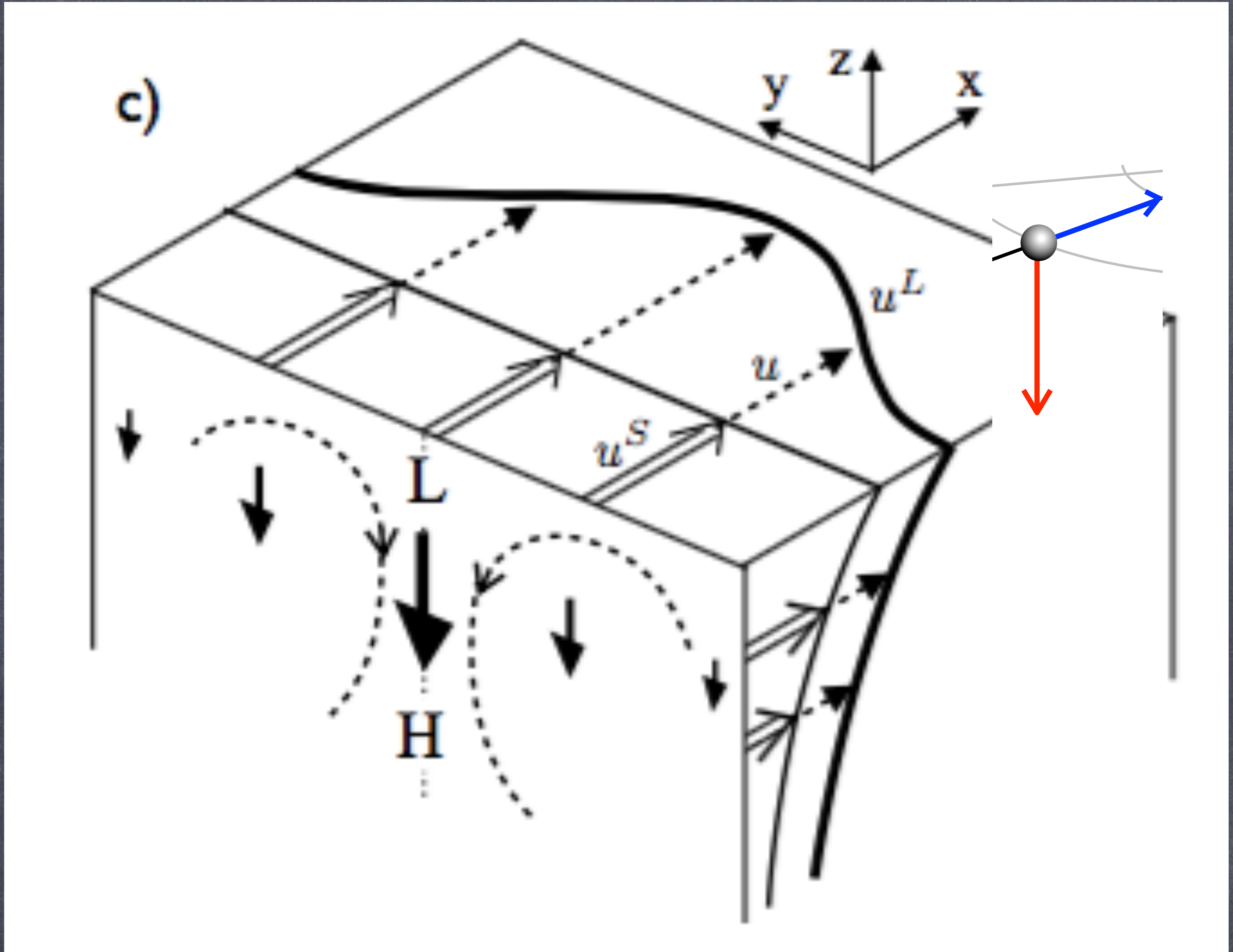

$$\frac{\alpha^2}{Ri}\left[w_{,t} + v_j^L w_{,j} + \frac{M_{Ro}}{RoRi} w w_{,z}\right] = -\pi_{,z} + b - \varepsilon v_j^L v_{j,z}^s + \frac{\alpha^2}{ReRi} w_{,jj}$$

N. Suzuki and BFK. Understanding Stokes forces in the wave-averaged equations. Journal of Geophysical Research-Oceans, 121:1-18, 2016.

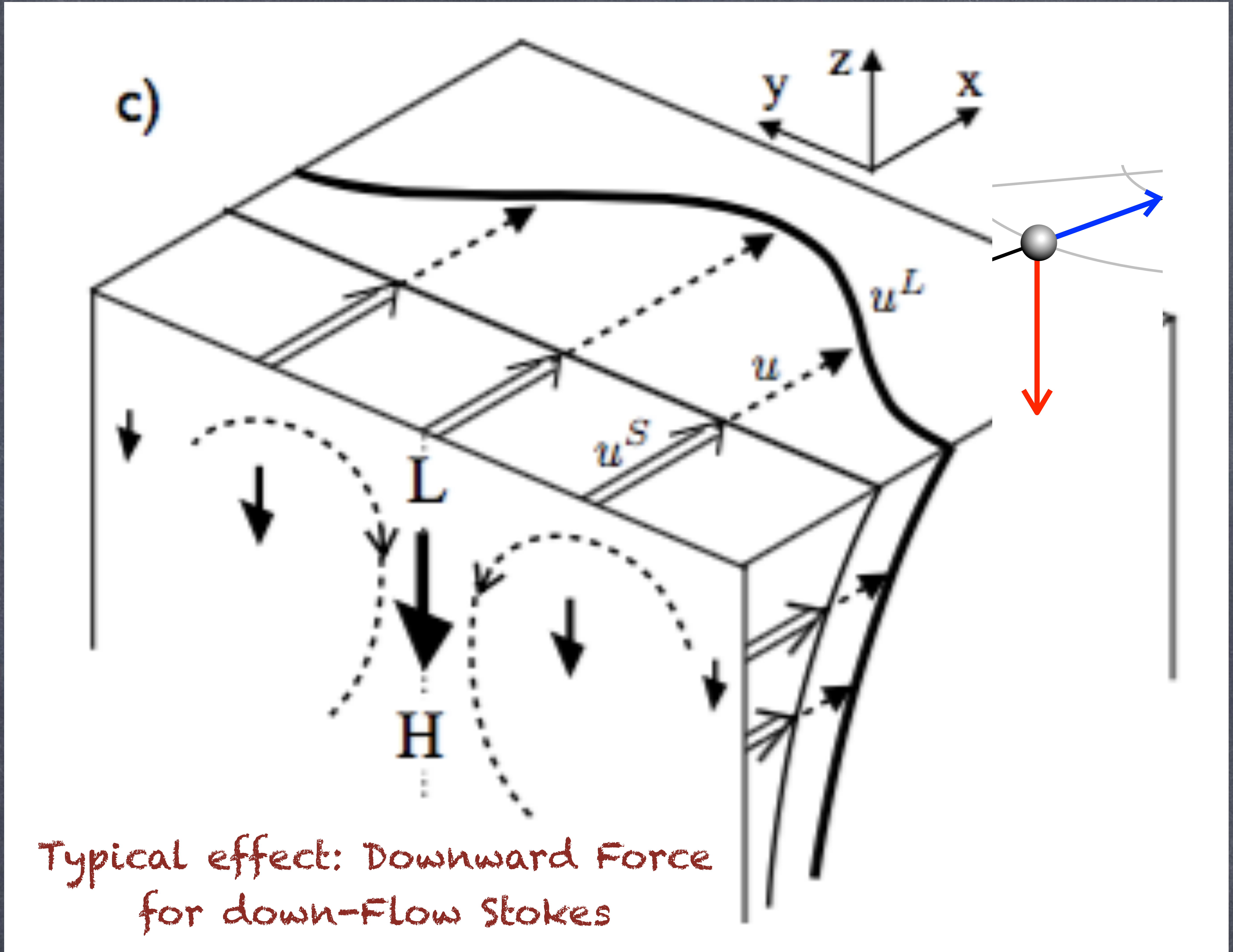

$$\frac{\alpha^2}{Ri}\left[w_{,t}+v_j^L w_{,j}+\frac{M_{Ro}}{RoRi}ww_{,z}\right]=-\pi_{,z}+b-\varepsilon v_j^L v_{j,z}^s+\frac{\alpha^2}{ReRi}w_{,jj}$$

N. Suzuki and BFK. Understanding Stokes forces in the wave-averaged equations. Journal of Geophysical Research-Oceans, 121:1-18, 2016.

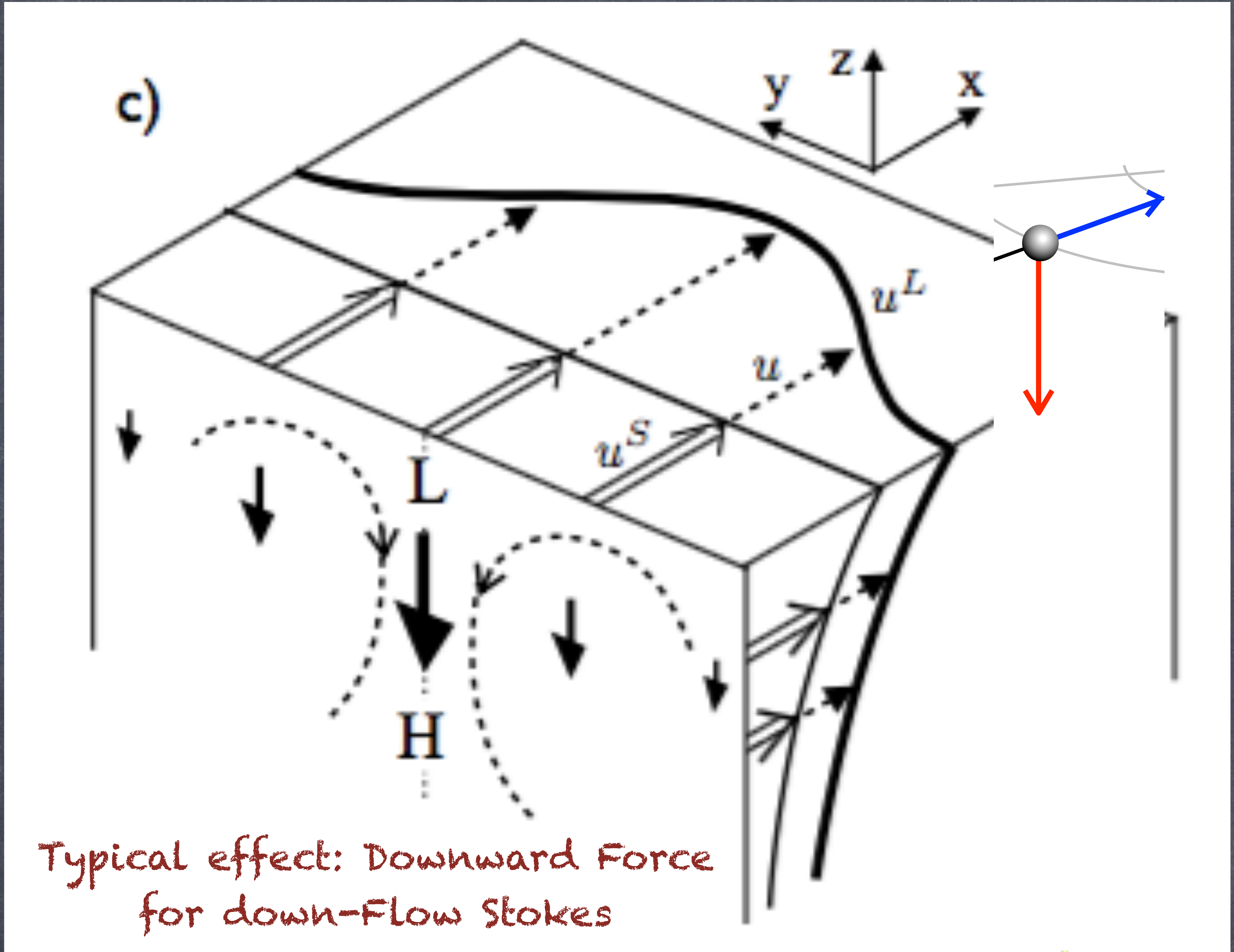

"wavy hydrostatic" if $\epsilon \gg 1$

$$\frac{\alpha^2}{Ri}\left[w_{,t} + v_j^L w_{,j} + \frac{M_{Ro}}{RoRi} w w_{,z}\right] = \boxed{-\pi_{,z} + b - \varepsilon v_j^L v^s_{j,z}} + \frac{\alpha^2}{ReRi} w_{,jj}$$

N. Suzuki and BFK. Understanding Stokes forces in the wave-averaged equations. Journal of Geophysical Research-Oceans, 121:1-18, 2016.

$\cancel{Ri < 1 \Rightarrow SI}$

Wavy Submesoscale Instability Different: Symmetric Instability

★ $fQ<0 \Rightarrow SI$

Ri = 0.5

Stokes Forces Stabilize SI

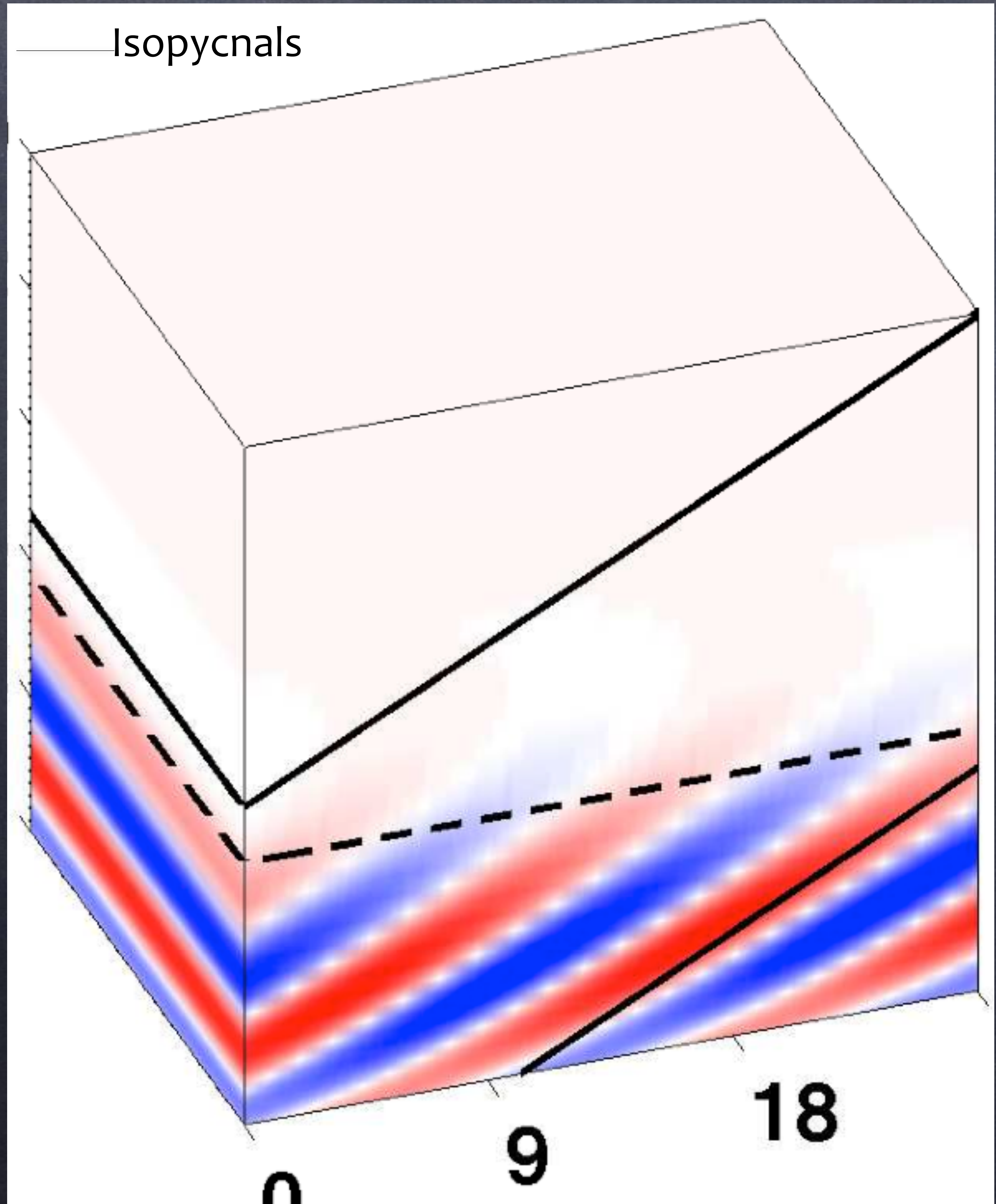

Cross front velocity for the fastest growing mode

S. Haney, BFK, K. Julien, and A. Webb. Symmetric and geostrophic instabilities in the wave-forced ocean mixed layer. JPO 45:3033-3056, 2015.

Ri = 2

Stokes Forces Destabilize SI

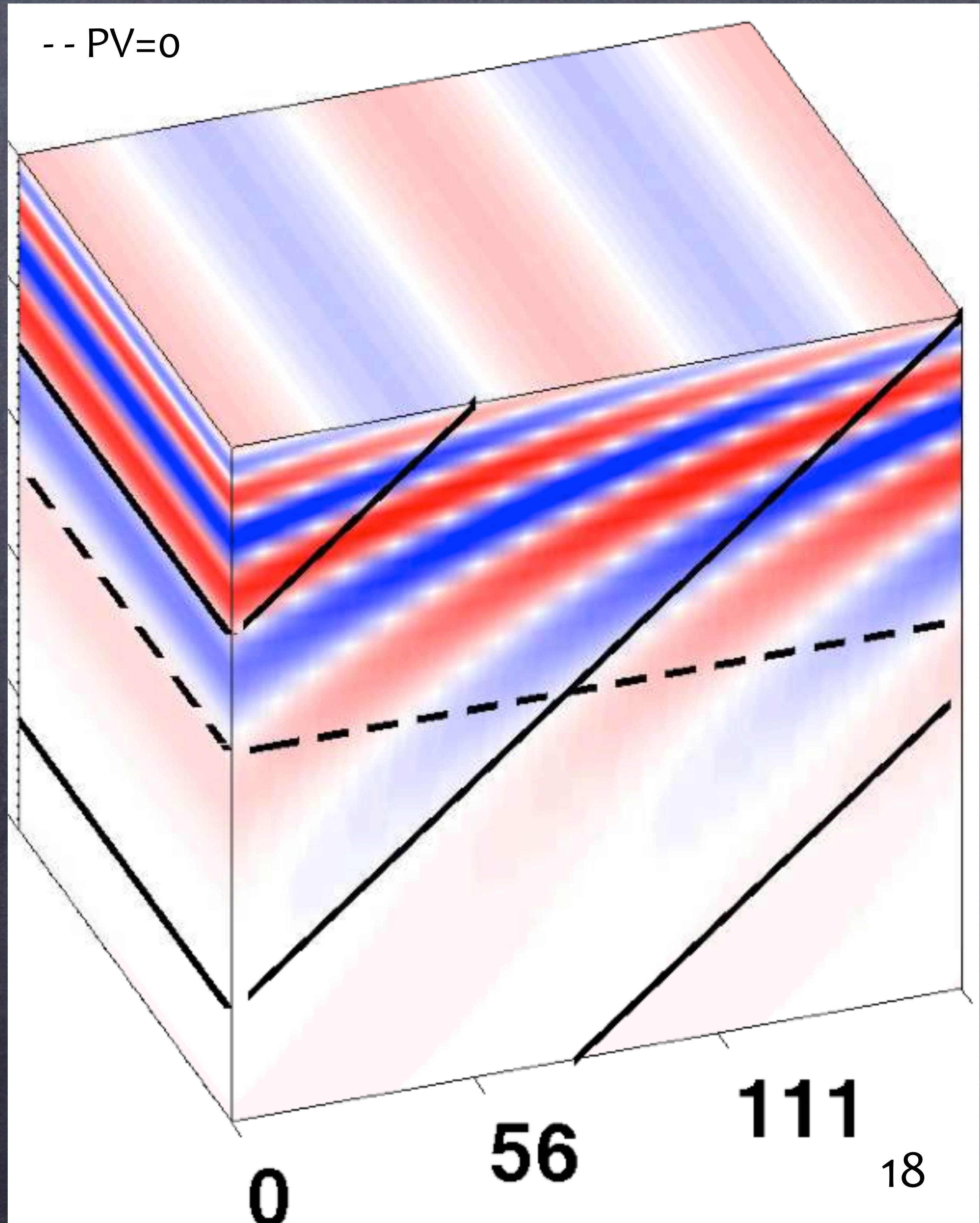

Do Stokes force directly affect larger scales?

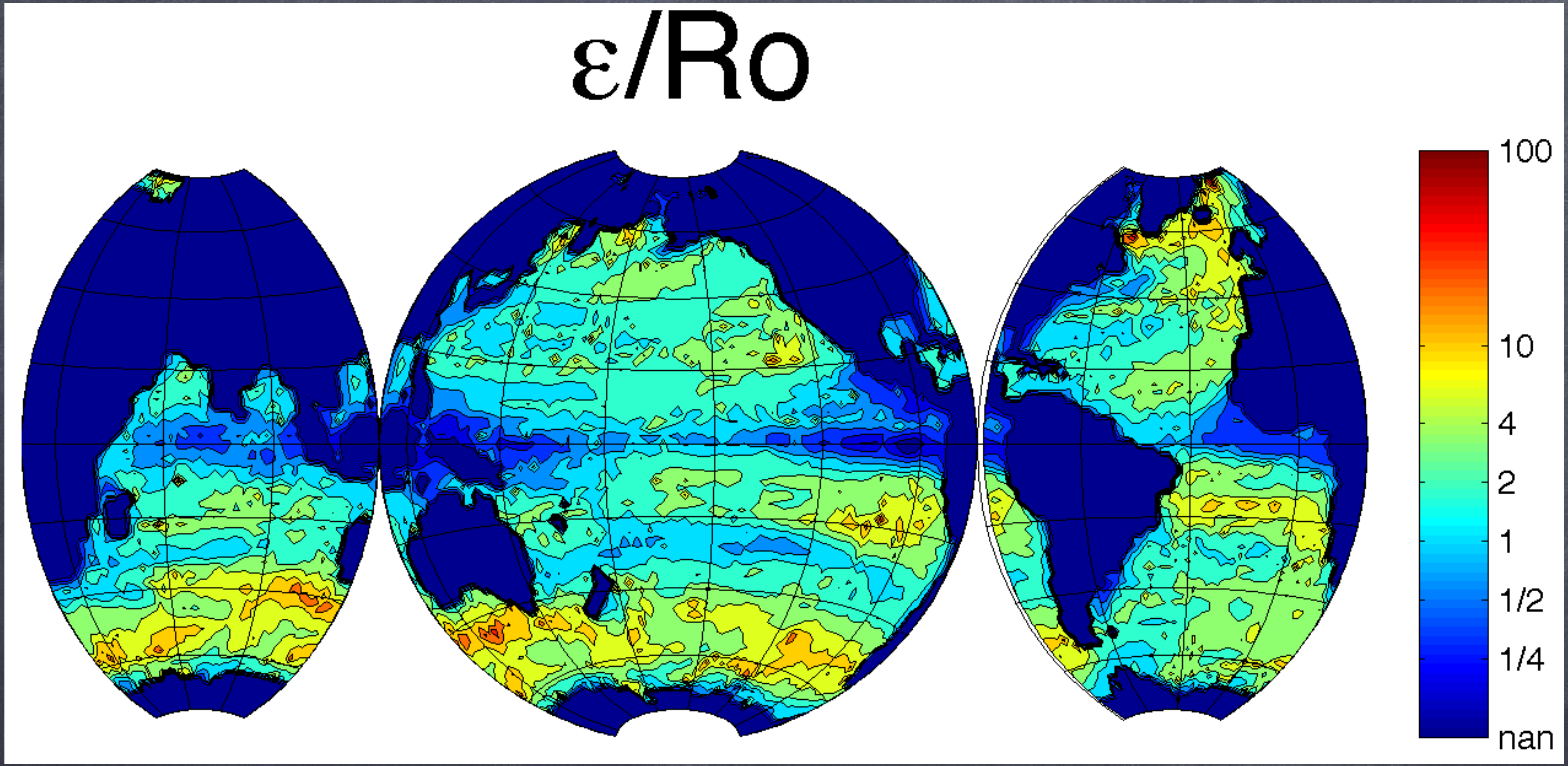

$$\varepsilon = \frac{V^s H}{f L H_s} \qquad Ro = \frac{U}{fL}$$

J. C. McWilliams and BFK. Oceanic wave-balanced surface fronts and filaments. Journal of Fluid Mechanics, 730:464-490, 2013.

Do Stokes force directly affect larger scales?

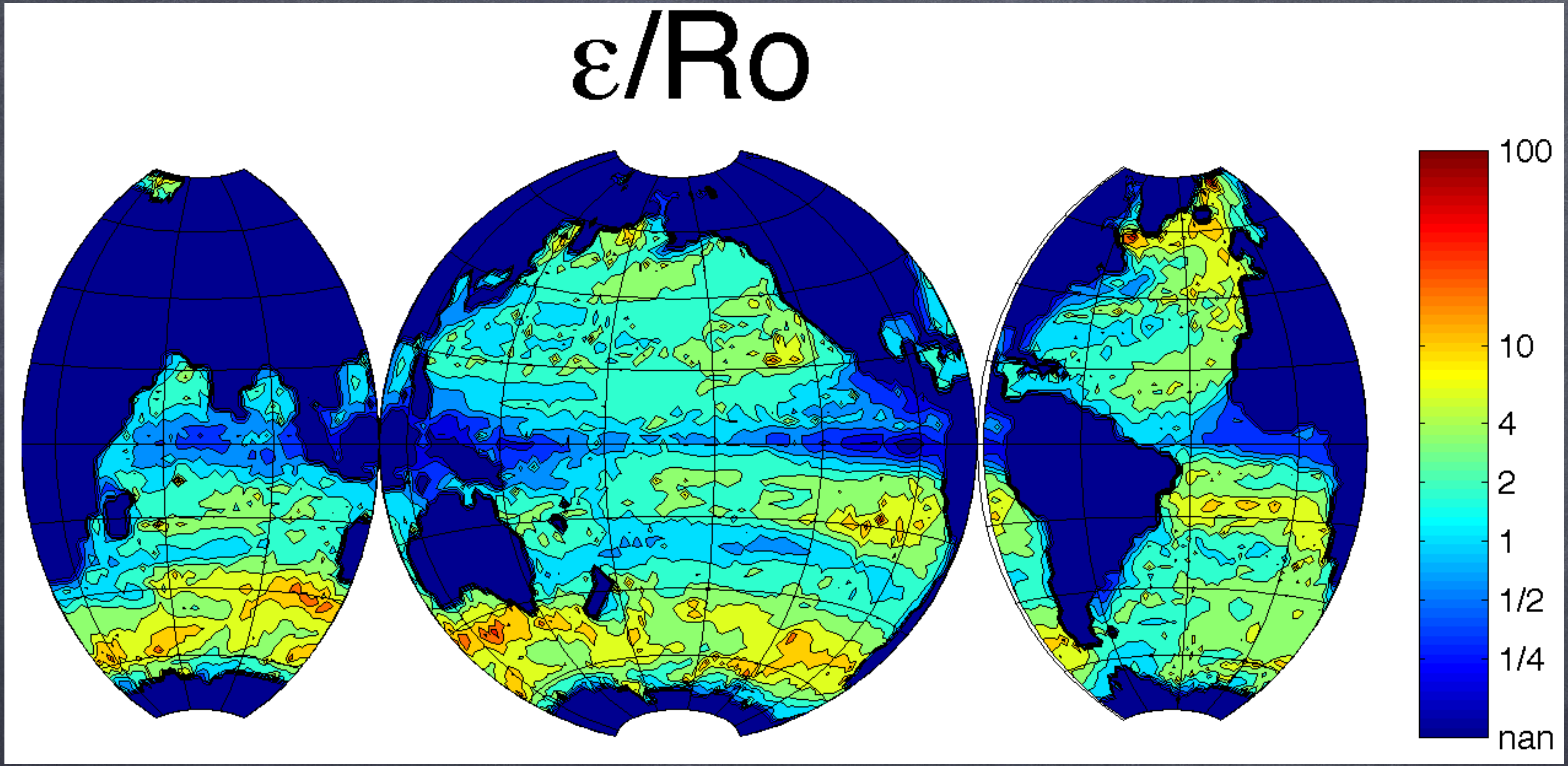

"wavy hydrostatic" if

$$\epsilon \gg 1$$

$$\varepsilon = \frac{V^s H}{f L H_s}$$

$$Ro = \frac{U}{fL}$$

J. C. McWilliams and BFK. Oceanic wave-balanced surface fronts and filaments. Journal of Fluid Mechanics, 730:464-490, 2013.

Are Fronts and Filaments different with Stokes shear force?

$$\frac{\alpha^2}{Ri}\left[w_{,t} + v_j^L w_{,j} + \frac{M_{Ro}}{RoRi} w w_{,z}\right] = -\pi_{,z} + b - \varepsilon v_j^L v^s_{j,z} + \frac{\alpha^2}{ReRi} w_{,jj}$$

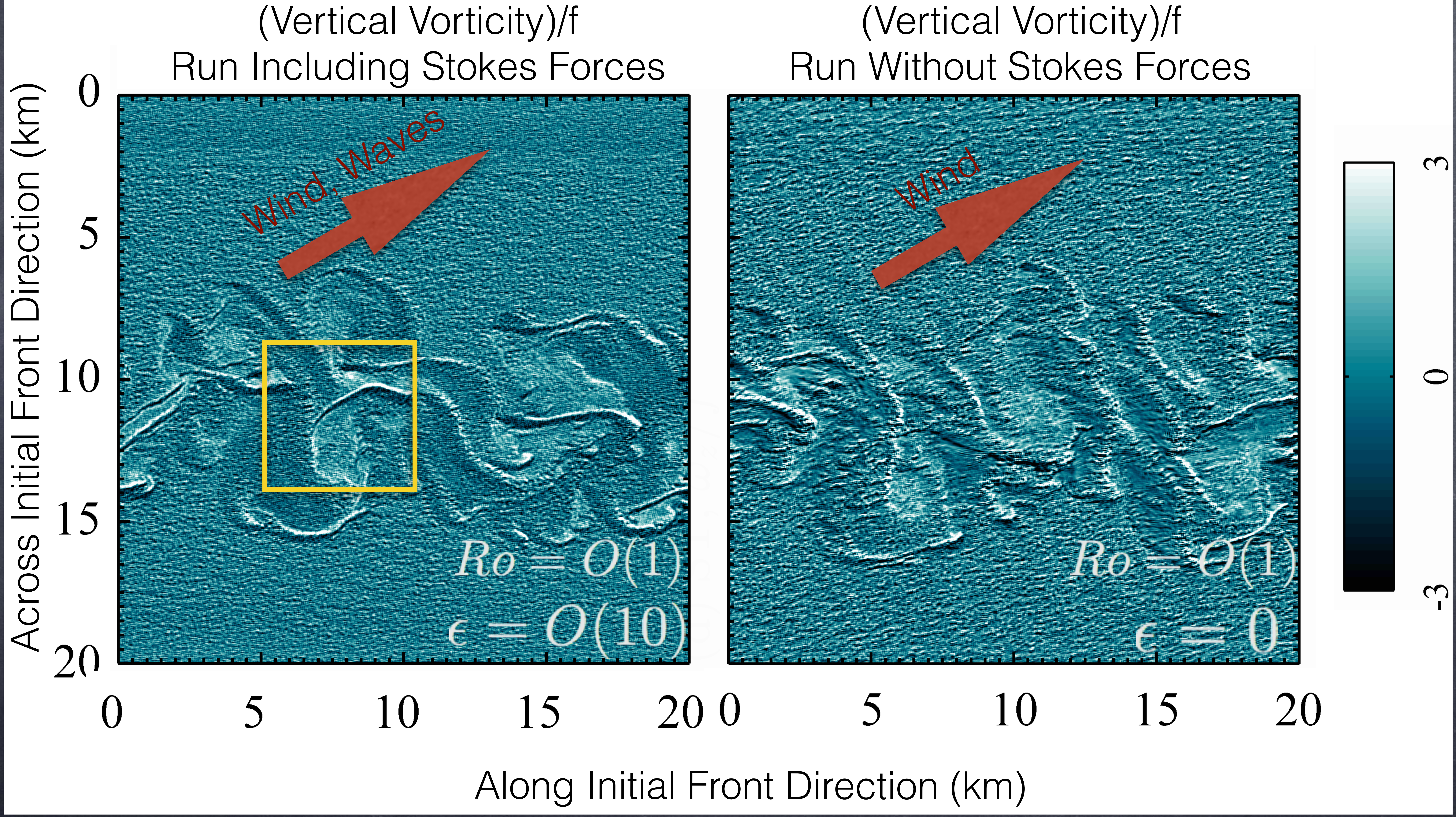

N. Suzuki, BFK, P. E. Hamlington, and L. P. Van Roekel. Surface waves affect frontogenesis. Journal of Geophysical Research-Oceans, 121:1-28, 2016.

N. Suzuki and BFK. Understanding Stokes forces in the wave-averaged equations. Journal of Geophysical Research-Oceans, 121:1-18, 2016.

J. C. McWilliams and BFK. Oceanic wave-balanced surface fronts and filaments. Journal of Fluid Mechanics, 730:464-490, 2013.

Are Fronts and Filaments different with Stokes shear force?

$$\frac{\alpha^2}{Ri}\left[w_{,t}+v_j^L w_{,j}+\frac{M_{Ro}}{RoRi}ww_{,z}\right]=-\pi_{,z}+b-\varepsilon v_j^L v_{j,z}^s+\frac{\alpha^2}{ReRi}w_{,jj}$$

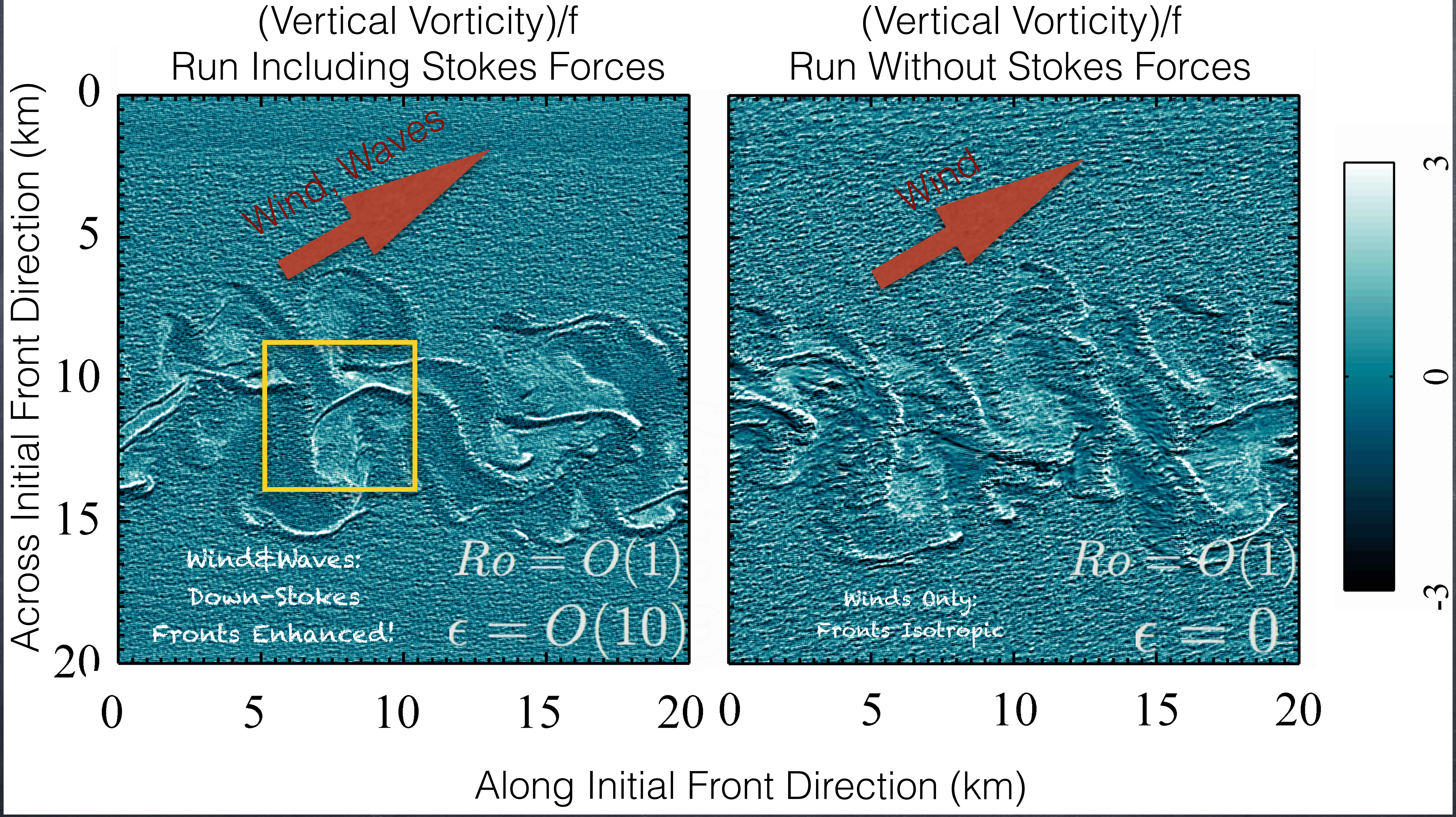

N. Suzuki, BFK, P. E. Hamlington, and L. P. Van Roekel. Surface waves affect frontogenesis. Journal of Geophysical Research-Oceans, 121:1-28, 2016.

N. Suzuki and BFK. Understanding Stokes forces in the wave-averaged equations. Journal of Geophysical Research-Oceans, 121:1-18, 2016.

J. C. McWilliams and BFK. Oceanic wave-balanced surface fronts and filaments. Journal of Fluid Mechanics, 730:464-490, 2013.

Diverse types of interaction: Stronger Langmuir (small) Turbulence

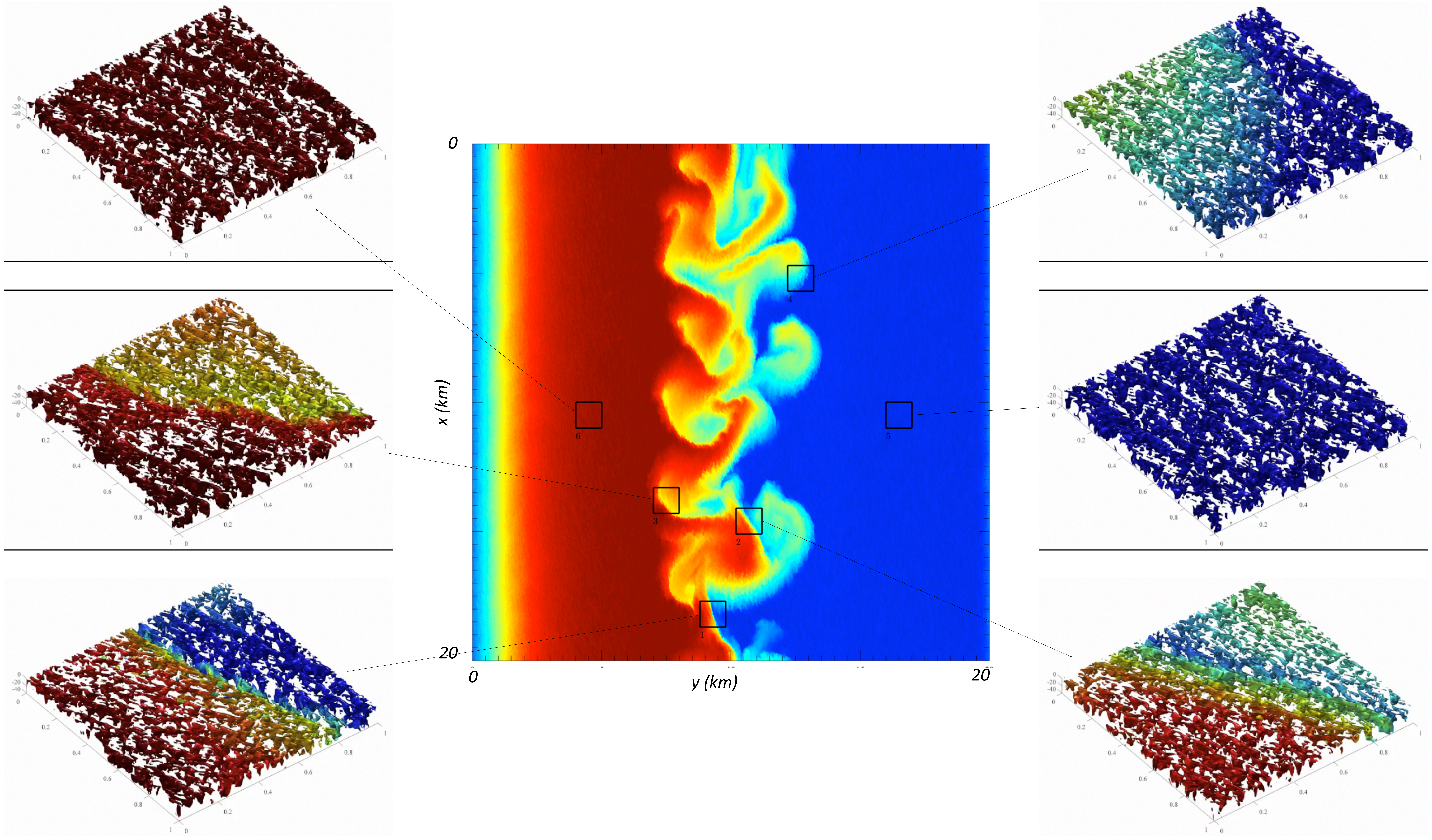

P. E. Hamlington, L. P. Van Roekel, BFK, K. Julien, and G. P. Chini. Langmuir-submesoscale interactions: Descriptive analysis of multiscale frontal spin-down simulations. Journal of Physical Oceanography, 44(9):2249-2272, September 2014.

Diverse types of interaction: Stronger Langmuir (small) Turbulence

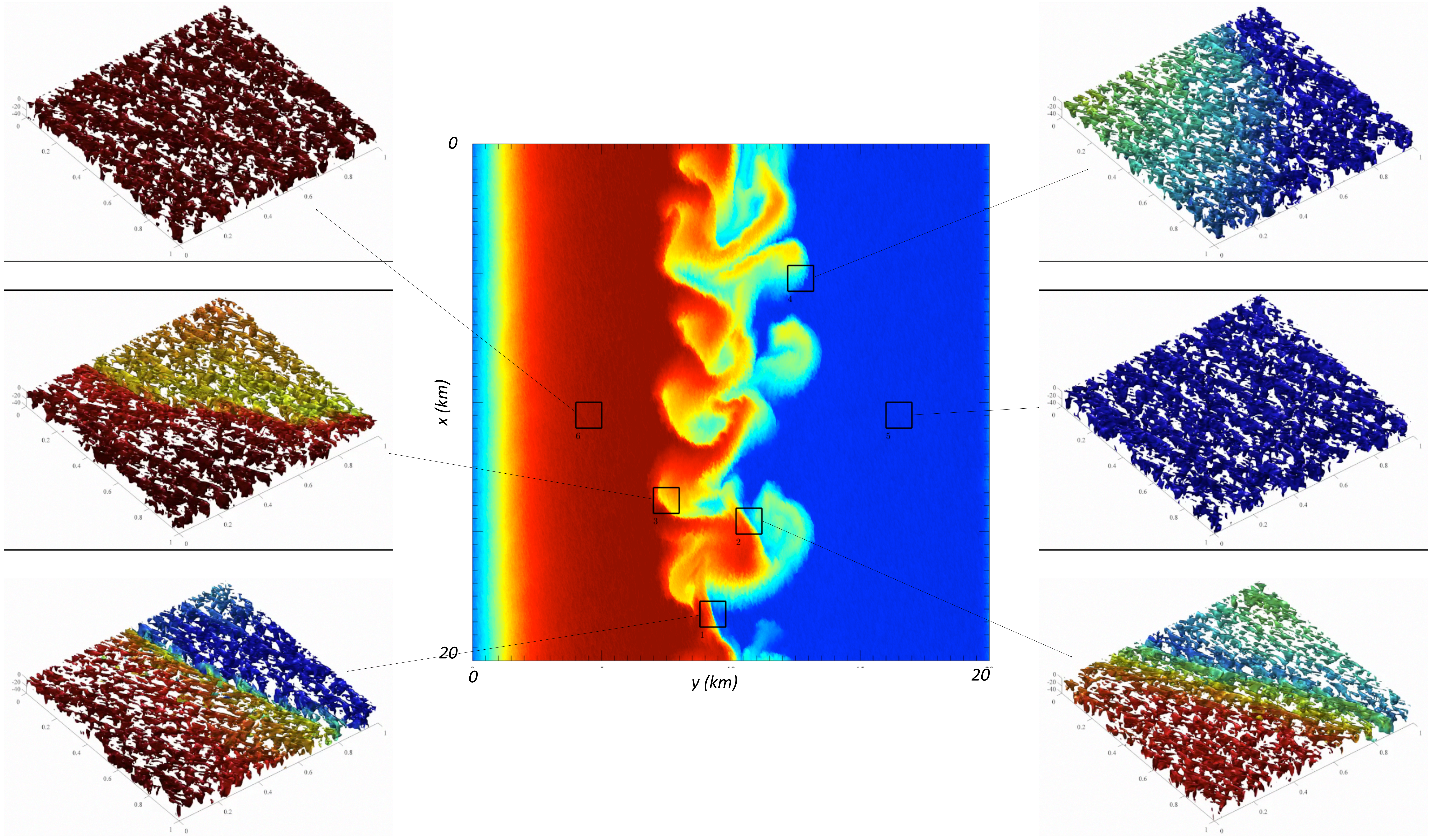

P. E. Hamlington, L. P. Van Roekel, BFK, K. Julien, and G. P. Chini. Langmuir-submesoscale interactions: Descriptive analysis of multiscale frontal spin-down simulations. Journal of Physical Oceanography, 44(9):2249-2272, September 2014.

20km x 20km x 150m domain
10 Day Simulation

Colors=Temp.
Surfaces on Large w

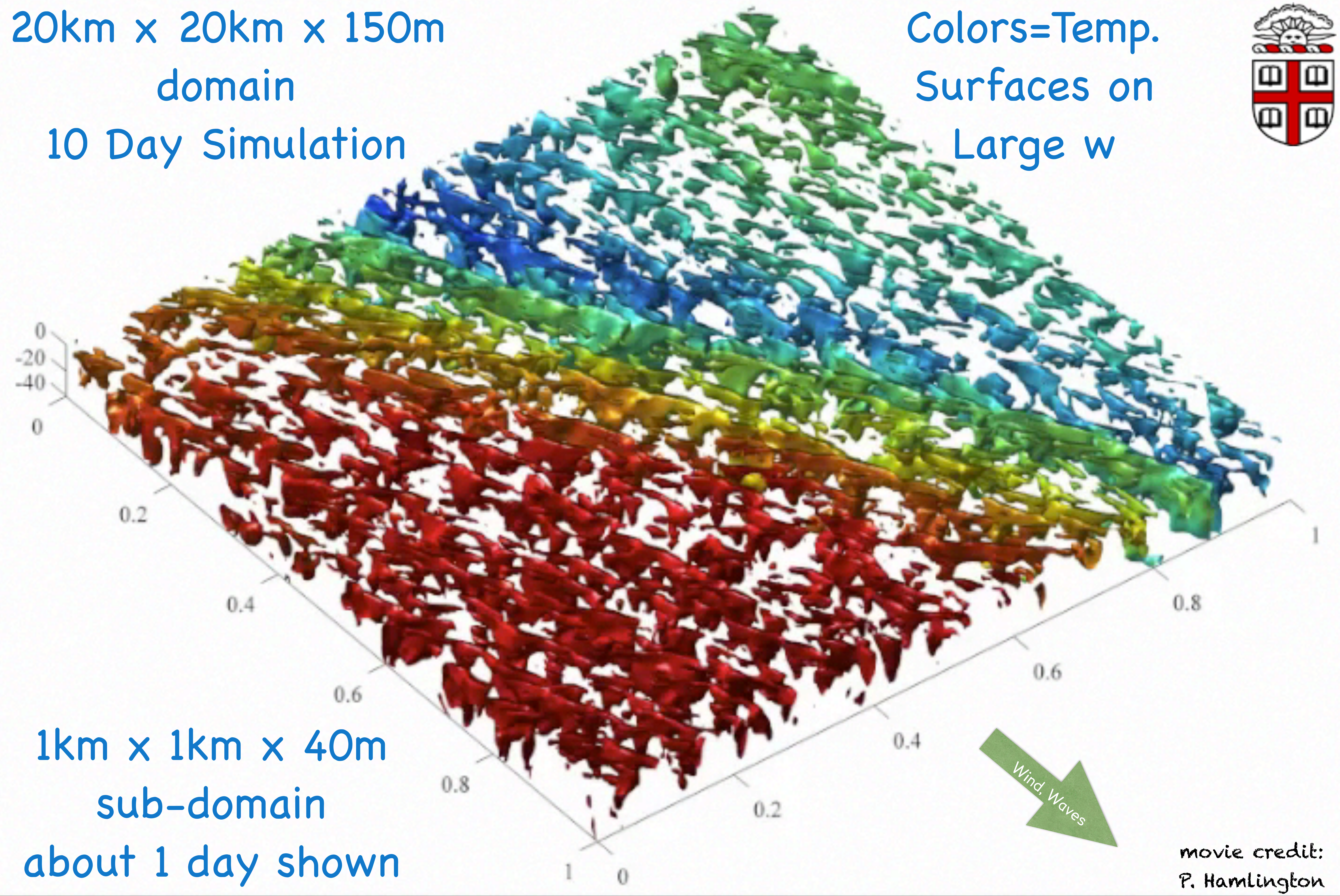

1km x 1km x 40m sub-domain
about 1 day shown

movie credit:
P. Hamlington

P. E. Hamlington, L. P. Van Roekel, BFK, K. Julien, and G. P. Chini. Langmuir-submesoscale interactions: Descriptive analysis of multiscale frontal spin-down simulations. Journal of Physical Oceanography, 44(9):2249-2272, September 2014.

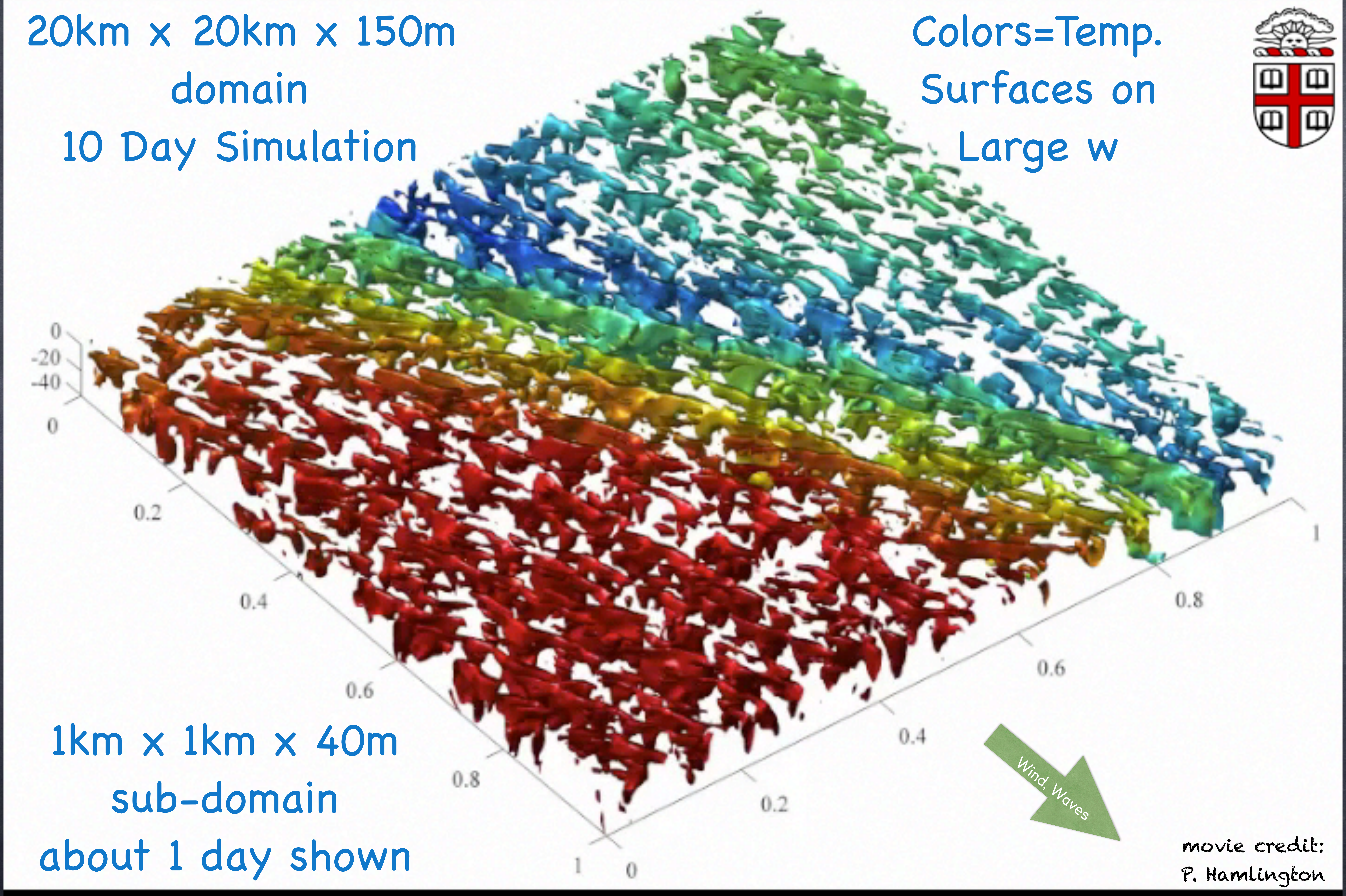

P. E. Hamlington, L. P. Van Roekel, BFK, K. Julien, and G. P. Chini. Langmuir-submesoscale interactions: Descriptive analysis of multiscale frontal spin-down simulations. Journal of Physical Oceanography, 44(9):2249-2272, September 2014.

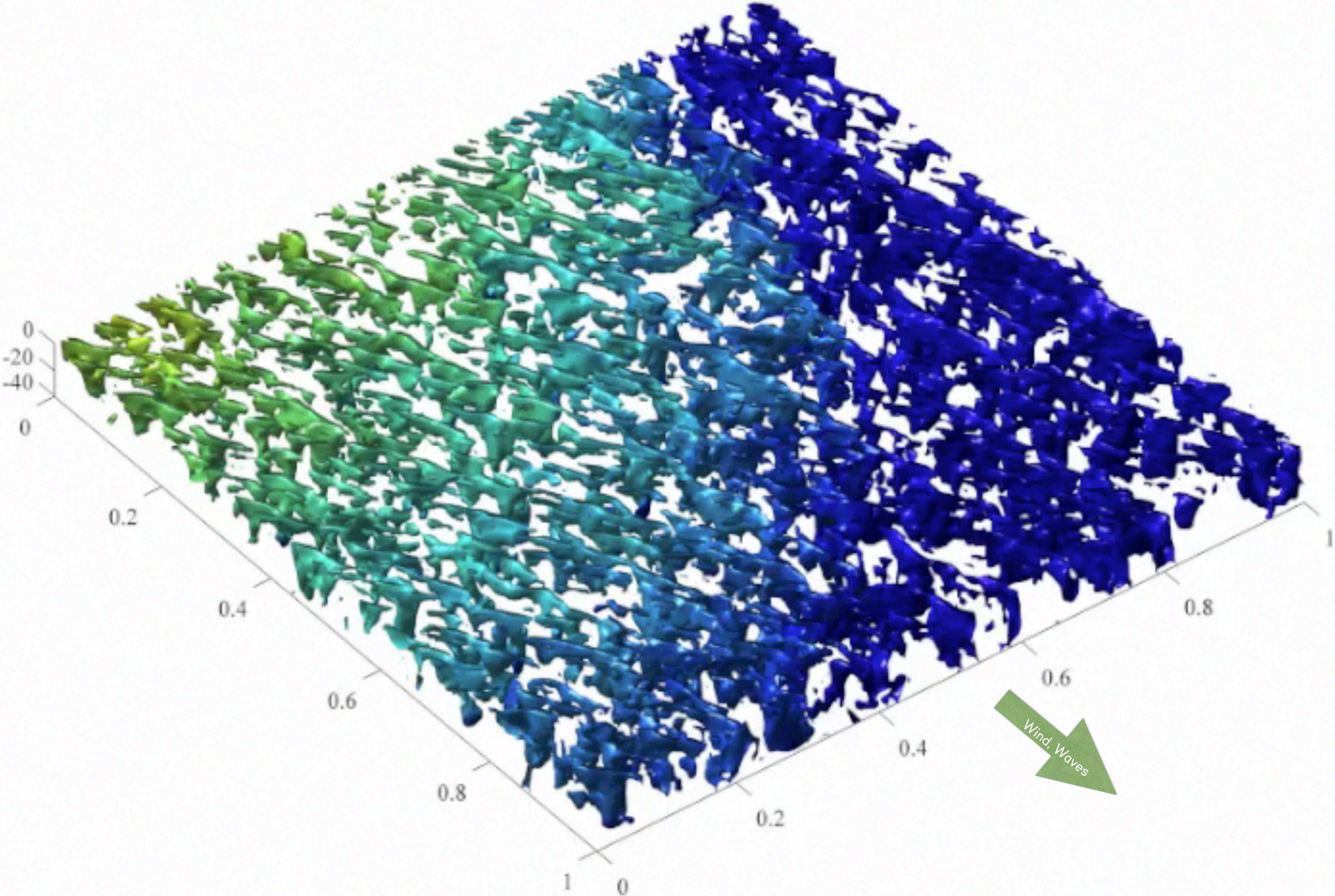
0
-20
-40
0
0.2
0.4
0.6
0.8
1
0
0.2
0.4
0.6
0.8
1
Wind, Waves

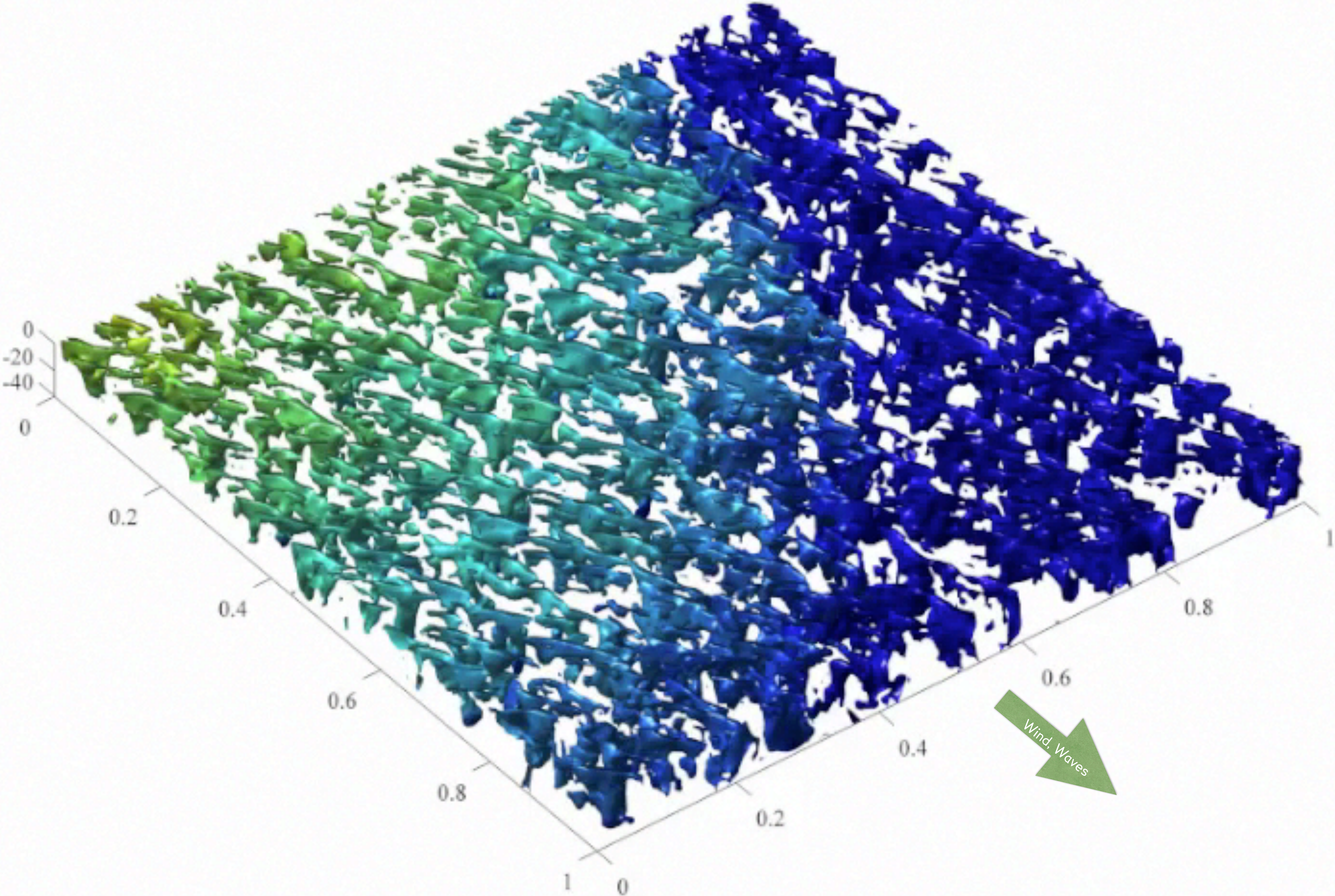
0
-20
-40
0
0.2
0.4
0.6
0.8
1
0
0.2
0.4
0.6
0.8
1
Wind, Waves

image:
Thorpe, 04

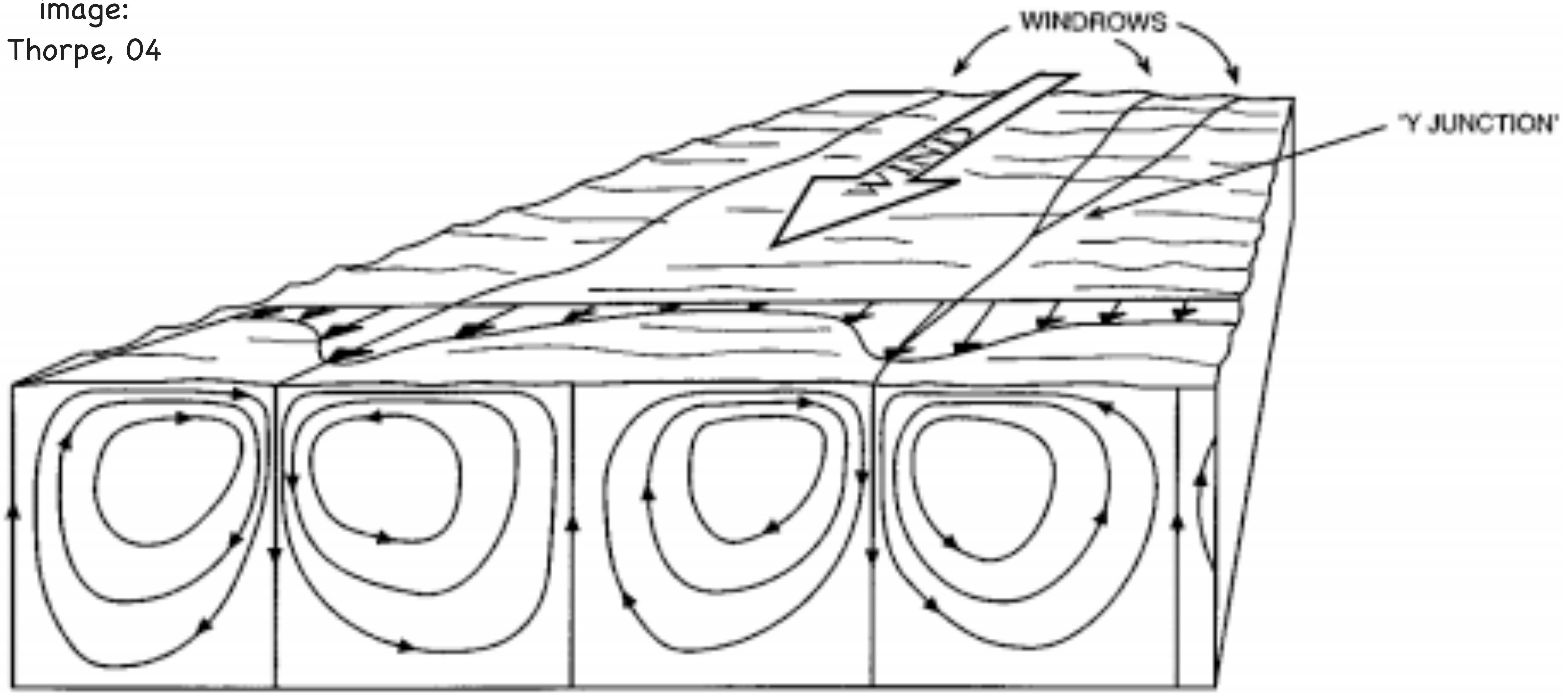

Figure 1 Sketch showing the pattern of mean flow in idealized Langmuir circulation. The windrows may be 2 m to 300 m apart, and the cell form is roughly square (as shown). In practice the flow is turbulent, especially near the water surface, and the windrows (Figure 2) amalgamate and meander in space and time. Bands of bubbles or buoyant algae may form within the downward-going (or downwelling) flow (see Figure 3).

$$\frac{\alpha^2}{Ri}\left[w_{,t} + v_j^L w_{,j} + \frac{M_{Ro}}{RoRi} w w_{,z}\right] = -\pi_{,z} + b - \varepsilon v_j^L v^s_{j,z} + \frac{\alpha^2}{ReRi} w_{,jj}$$

N. Suzuki and BFK. Understanding Stokes forces in the wave-averaged equations. Journal of Geophysical Research-Oceans, 121:1-18, 2016.

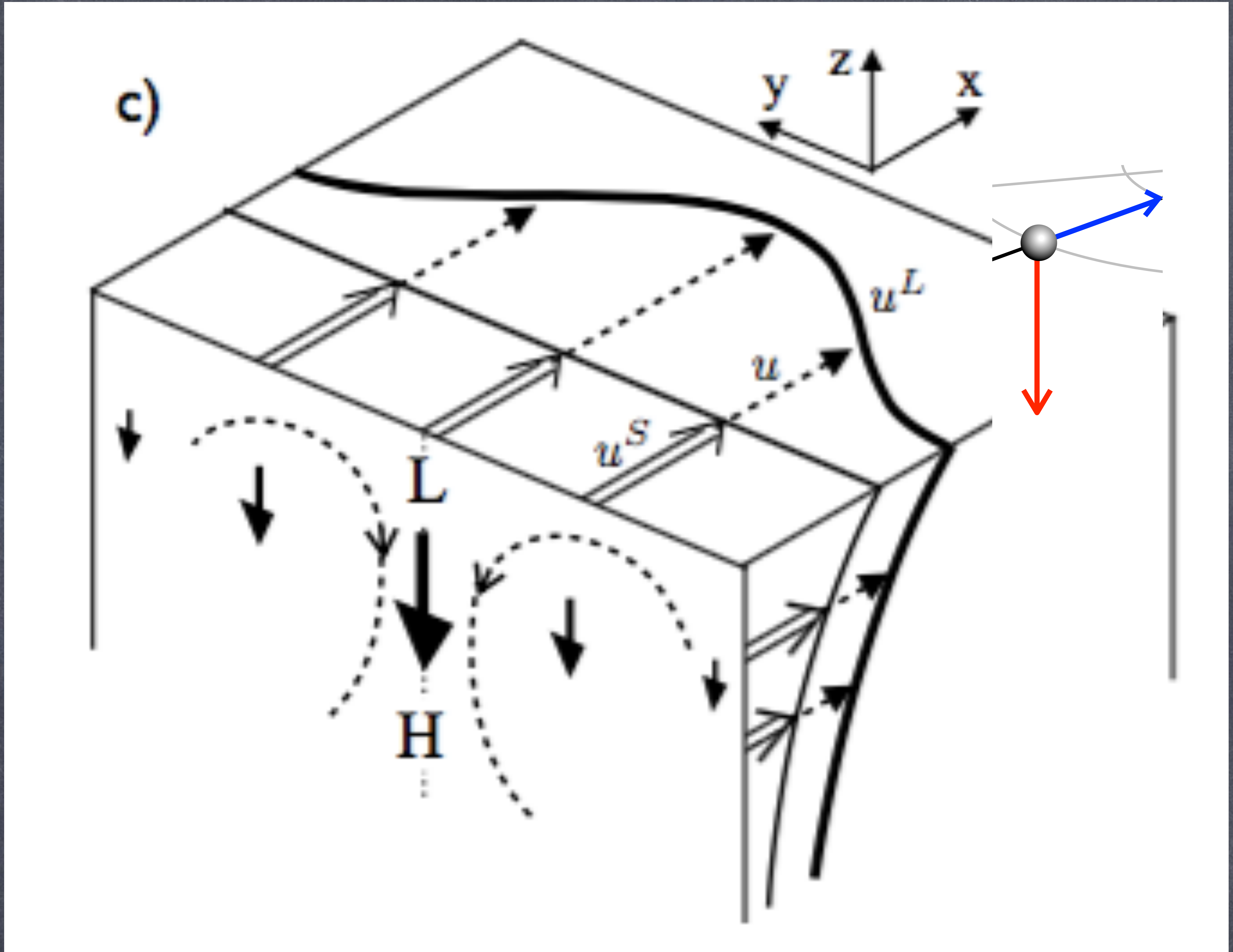

$$\frac{\alpha^2}{Ri}\left[w_{,t}+v_j^L w_{,j}+\frac{M_{Ro}}{RoRi}ww_{,z}\right]=-\pi_{,z}+b-\varepsilon v_j^L v_{j,z}^s+\frac{\alpha^2}{ReRi}w_{,jj}$$

N. Suzuki and BFK. Understanding Stokes forces in the wave-averaged equations. Journal of Geophysical Research-Oceans, 121:1-18, 2016.

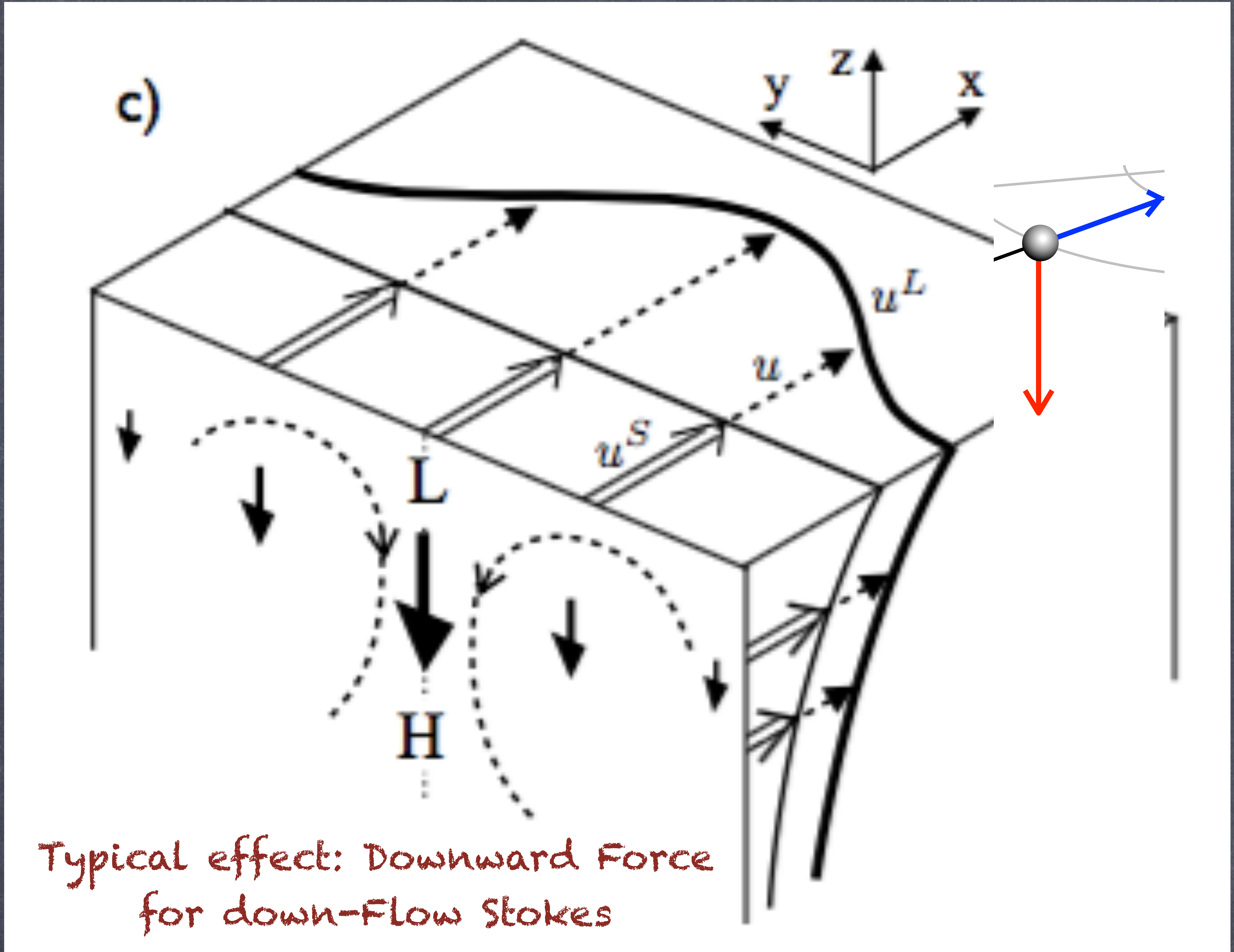

$$\frac{\alpha^2}{Ri}\left[w_{,t} + v_j^L w_{,j} + \frac{M_{Ro}}{RoRi} w w_{,z}\right] = -\pi_{,z} + b - \varepsilon v_j^L v^s_{j,z} + \frac{\alpha^2}{ReRi} w_{,jj}$$

N. Suzuki and BFK. Understanding Stokes forces in the wave-averaged equations. Journal of Geophysical Research-Oceans, 121:1-18, 2016.

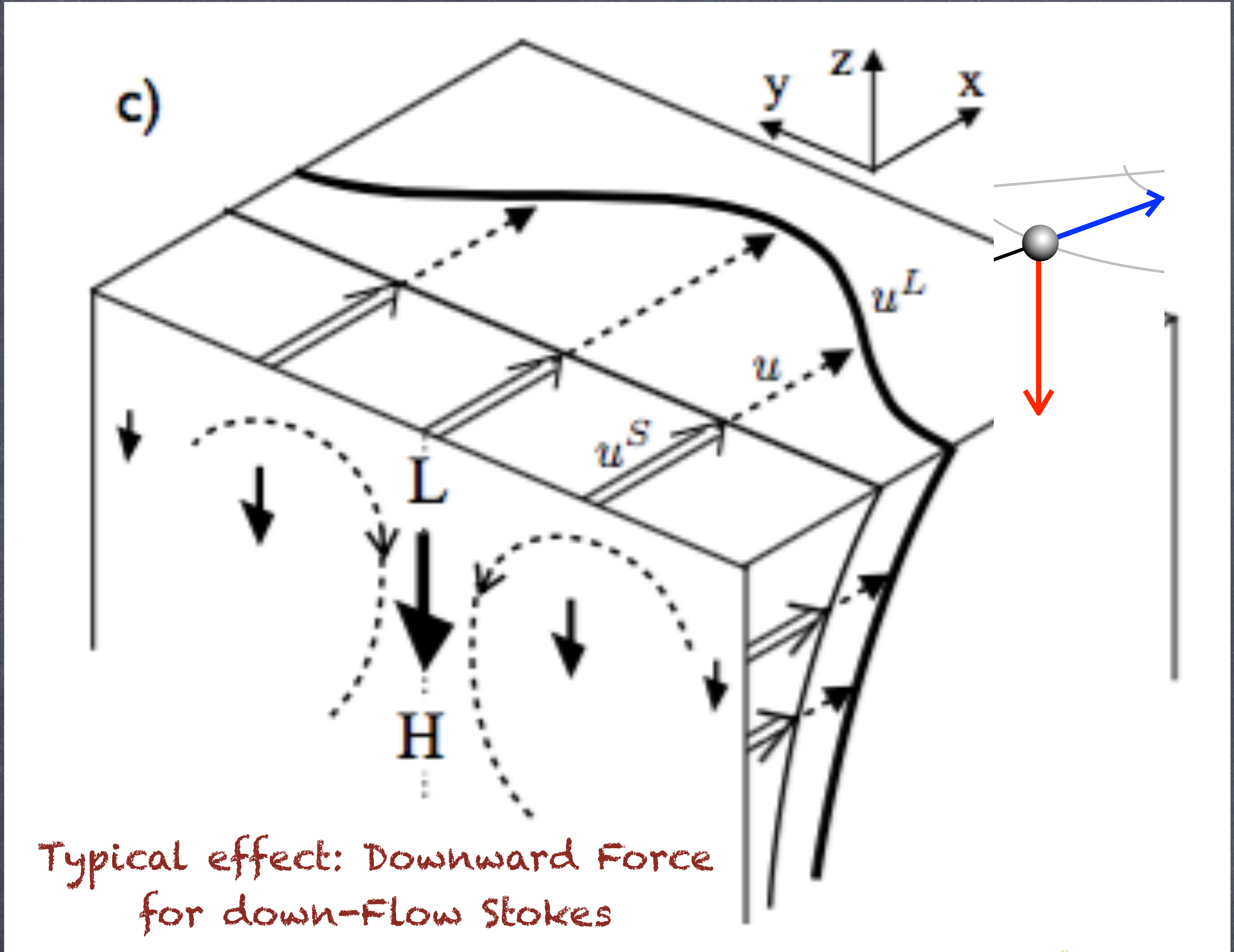

"wavy hydrostatic" if $\epsilon \gg 1$

$$\frac{\alpha^2}{Ri}\left[w_{,t} + v_j^L w_{,j} + \frac{M_{Ro}}{RoRi} w w_{,z}\right] = \boxed{-\pi_{,z} + b - \varepsilon v_j^L v_{j,z}^s} + \frac{\alpha^2}{ReRi} w_{,jj}$$

N. Suzuki and BFK. Understanding Stokes forces in the wave-averaged equations. Journal of Geophysical Research-Oceans, 121:1-18, 2016.

v

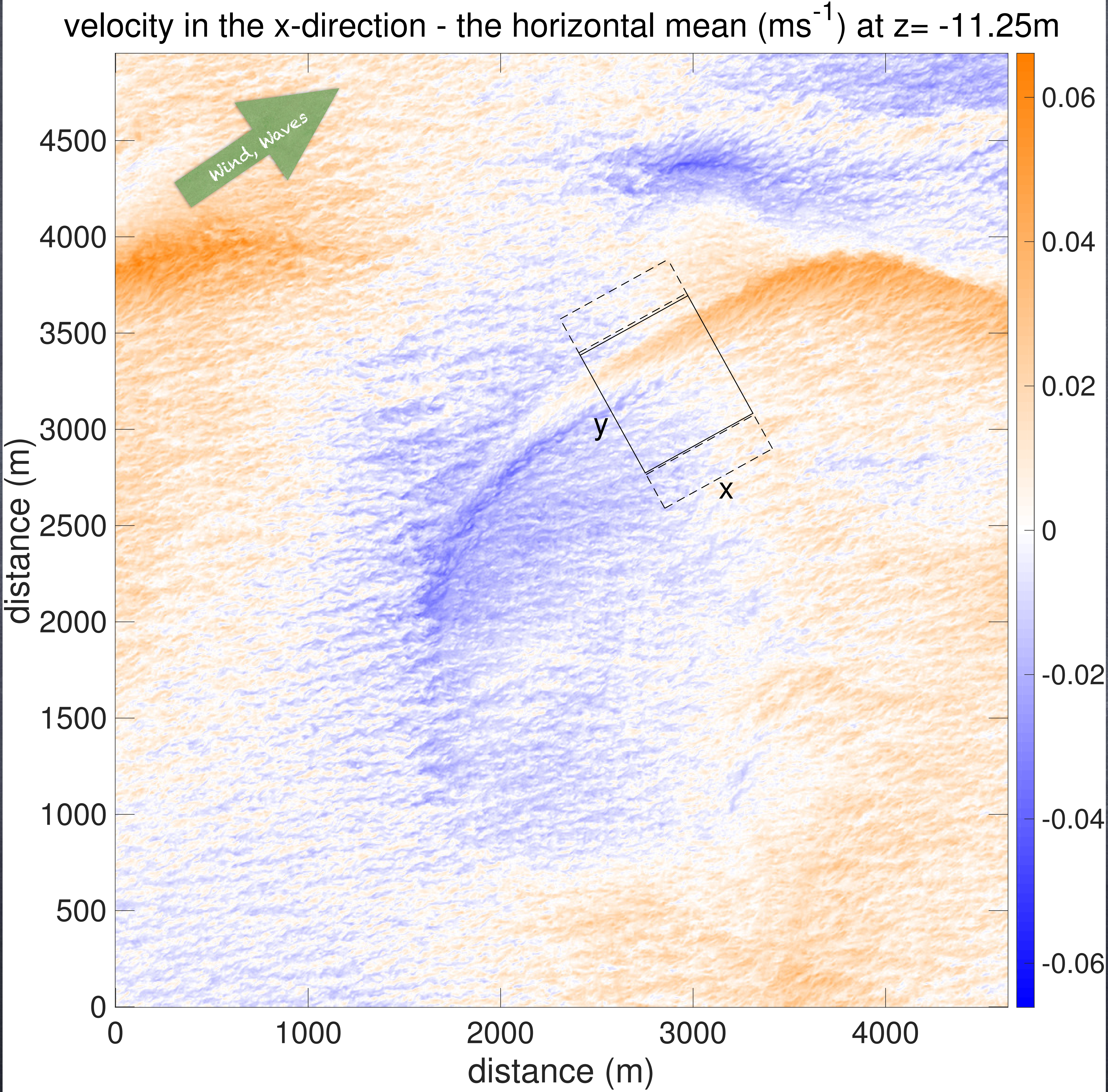

N. Suzuki, B. Fox-Kemper, P. E. Hamlington, and L. P. Van Roekel. Surface waves affect frontogenesis. Journal of Geophysical Research-Oceans, 121:1-28, May 2016.

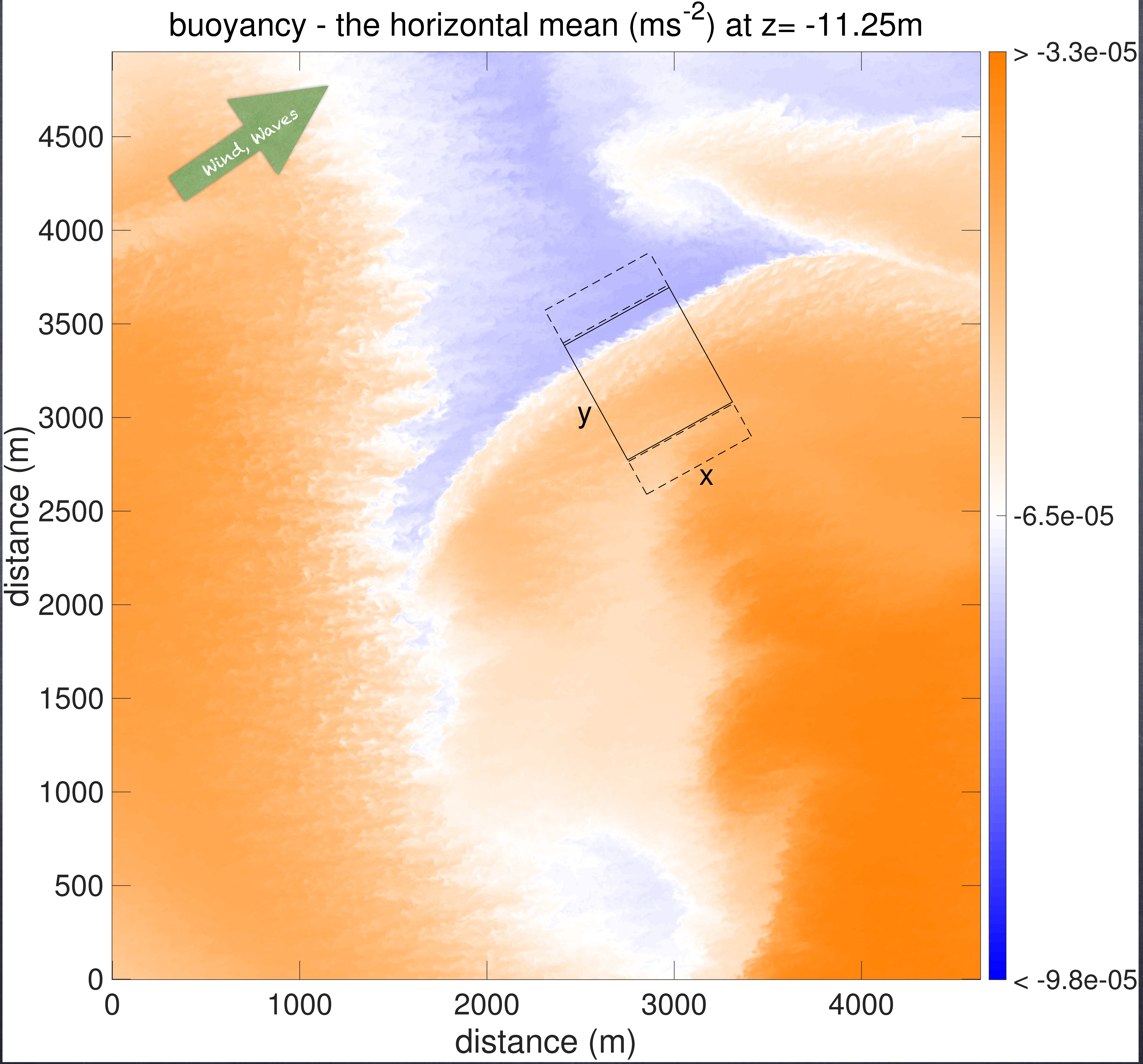

N. Suzuki, B. Fox-Kemper, P. E. Hamlington, and L. P. Van Roekel. Surface waves affect frontogenesis. Journal of Geophysical Research-Oceans, 121:1-28, May 2016.

W

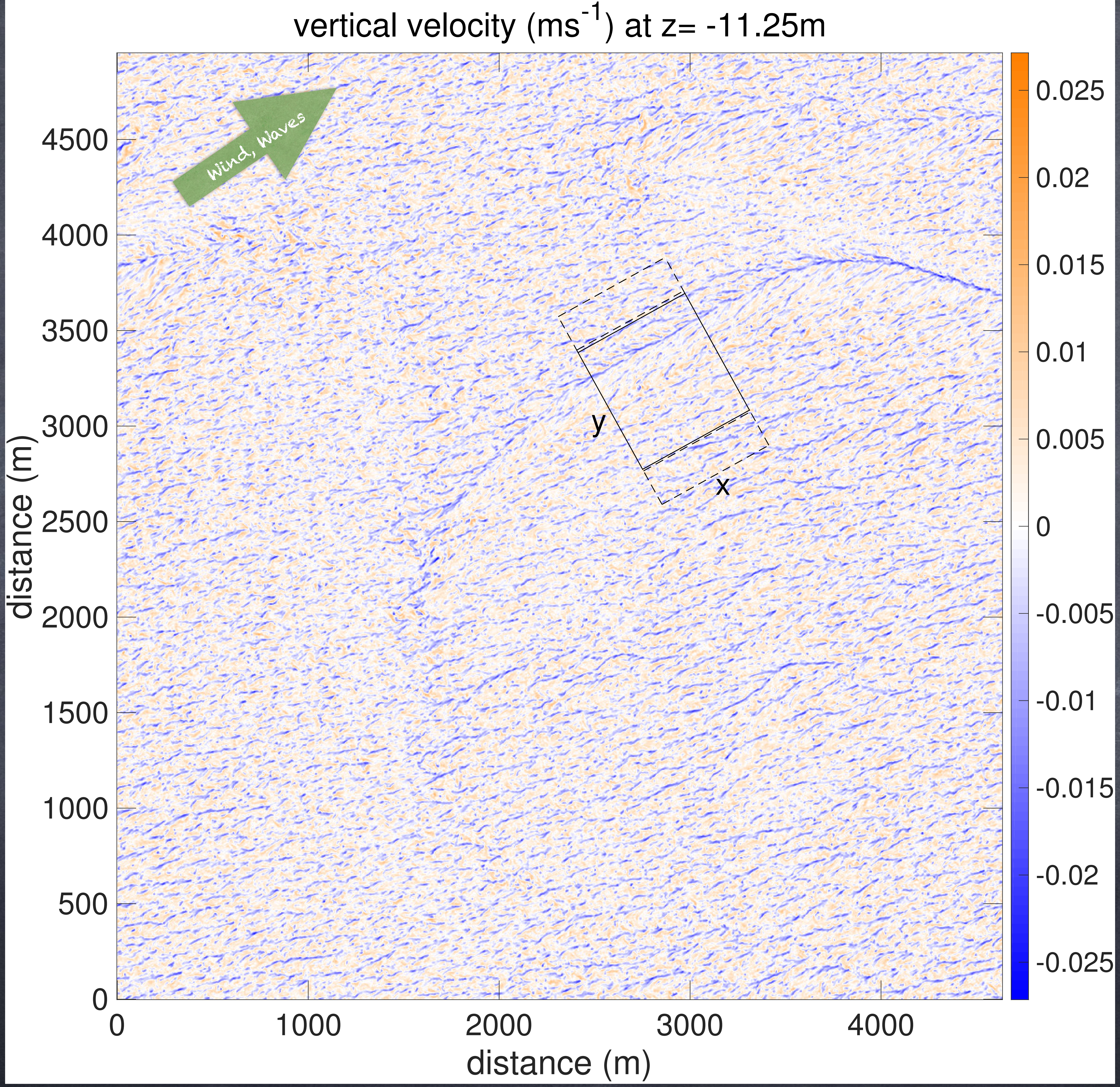

N. Suzuki, B. Fox-Kemper, P. E. Hamlington, and L. P. Van Roekel. Surface waves affect frontogenesis. Journal of Geophysical Research-Oceans, 121:1-28, May 2016.

Initially every surface node has 1 drifter,
so there are 851796 drifters in the picture

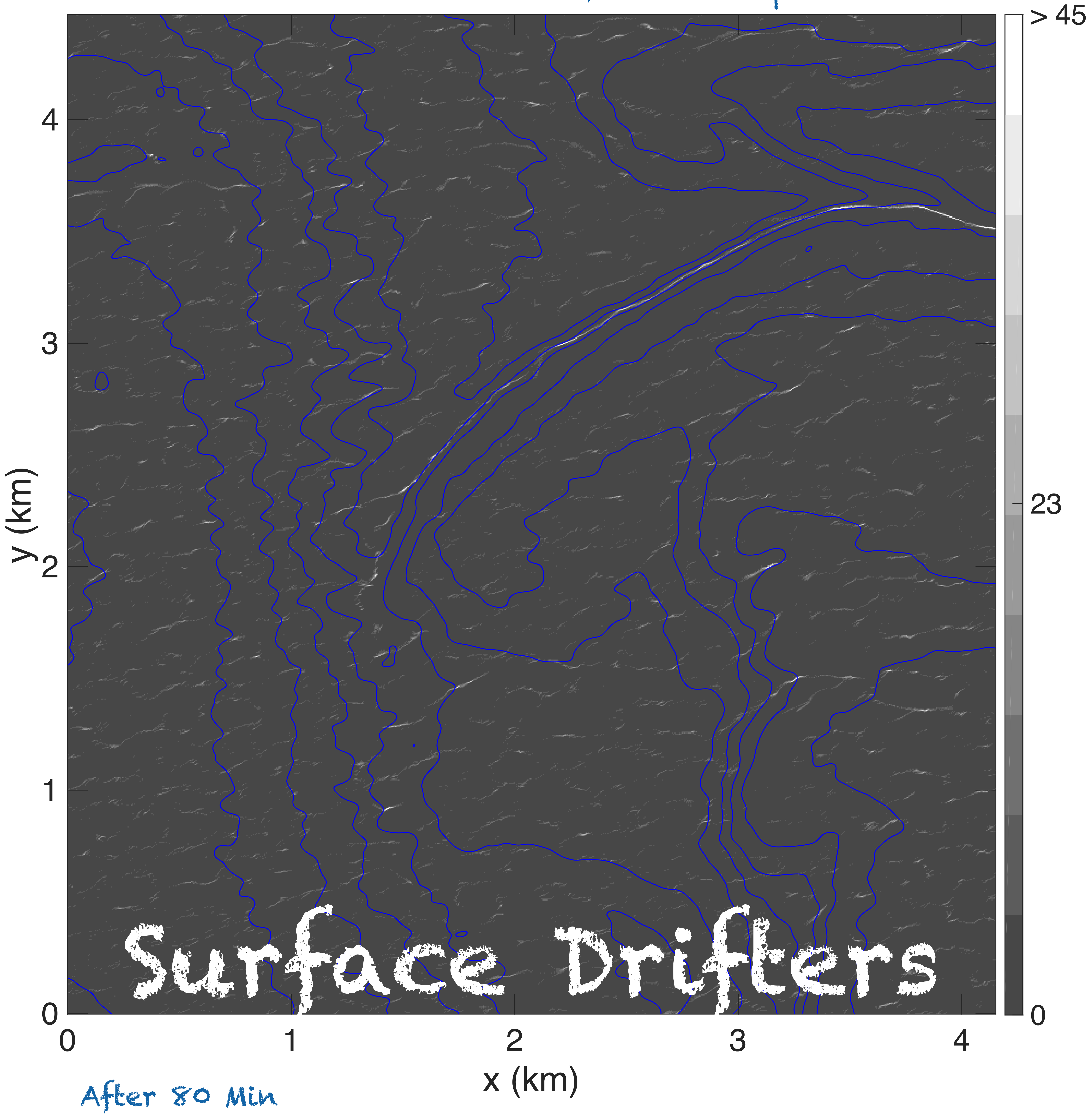

After 80 Min

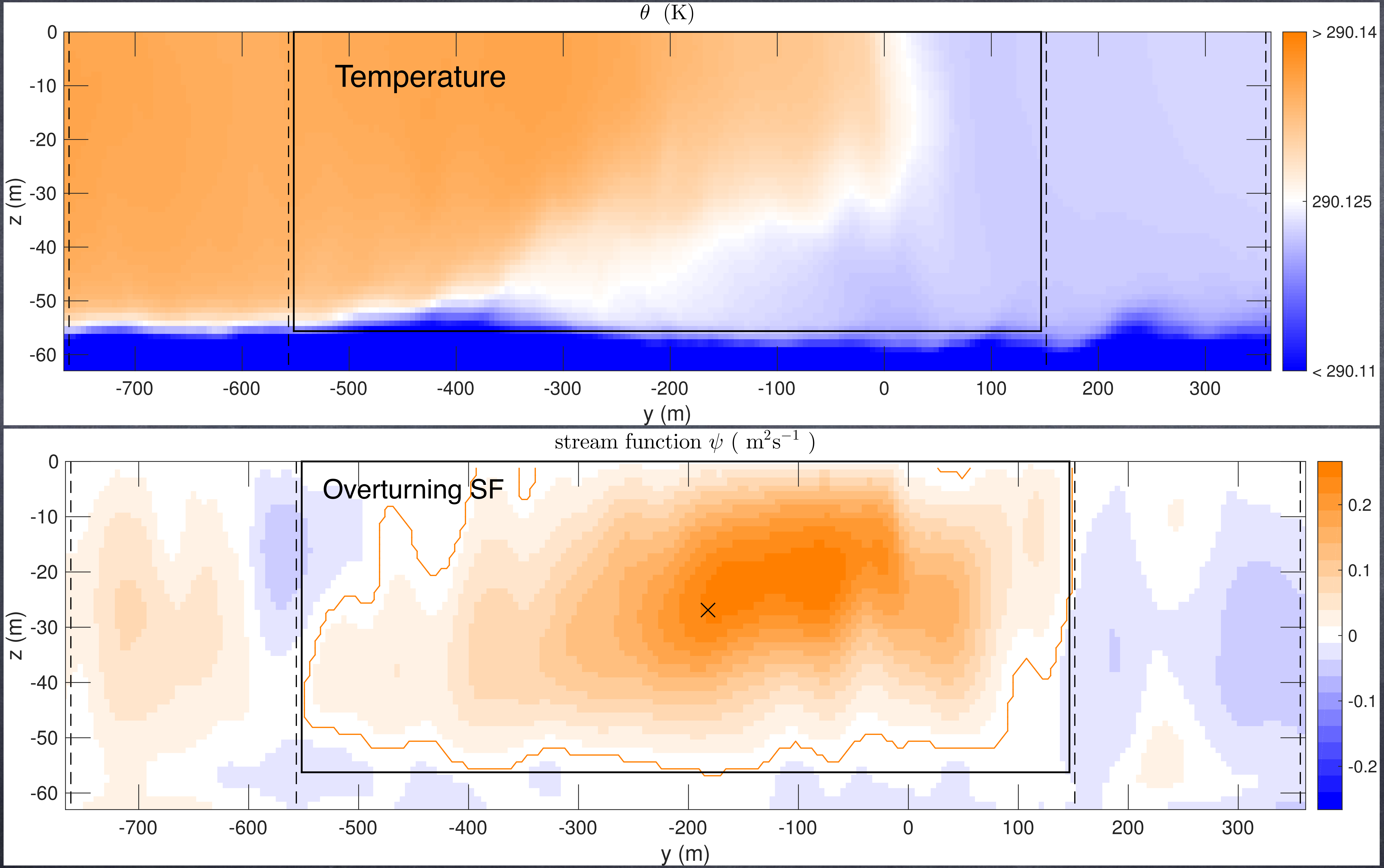

N. Suzuki, BFK, P. E. Hamlington, and L. P. Van Roekel. Surface waves affect frontogenesis. Journal of Geophysical Research-Oceans, 121:1-28, 2016.

Do (wavy hydrostatic) Stokes Forces Matter?

Yes! At Leading Order (in LES)

Table 3. Integrated Budget for Overturning Vorticity[a]

Responsible Force	Relative Value
Relative Tendency of Overturning Circulation along the Cell Boundary	
Net tendency	$11 \pm 8\%$
Sources	
Buoyancy anomaly	100%
Stokes shear force anomaly	$44 \pm 4\%$
Interaction with v^H	$44 \pm 8\%$
Frontal anomaly in pressure gradient	$6 \pm 9\%$
Nonlinear interaction with v^B:	$2 \pm 1\%$
Sinks	
Frontal turbulence anomaly (mostly, imbalance in wavy Ekman relation)	$-82 \pm 11\%$
Coriolis on along-front jet	$-66 \pm 2\%$
Lagrangian advection of (v^ψ, w^ψ)	$-36 \pm 7\%$

N. Suzuki and BFK. Understanding Stokes forces in the wave-averaged equations. Journal of Geophysical Research-Oceans, 121:1-18, April 2016.

N. Suzuki, BFK, P. E. Hamlington, and L. P. Van Roekel. Surface waves affect frontogenesis. Journal of Geophysical Research-Oceans, 121:1-28, May 2016.

For Today

- Vast & Diverse
  - Turbulence
  - Waves
- Breakpoints at the Grid Scale
- Mesoscale, Submesoscale, Boundary Layer
- Navier-Stokes
- Boussinesq
  - Hydrostatic or Not?
- Quasi-Geostrophic?
- Wave-Averaged Equations for Boundary Layer AND Submesoscale!

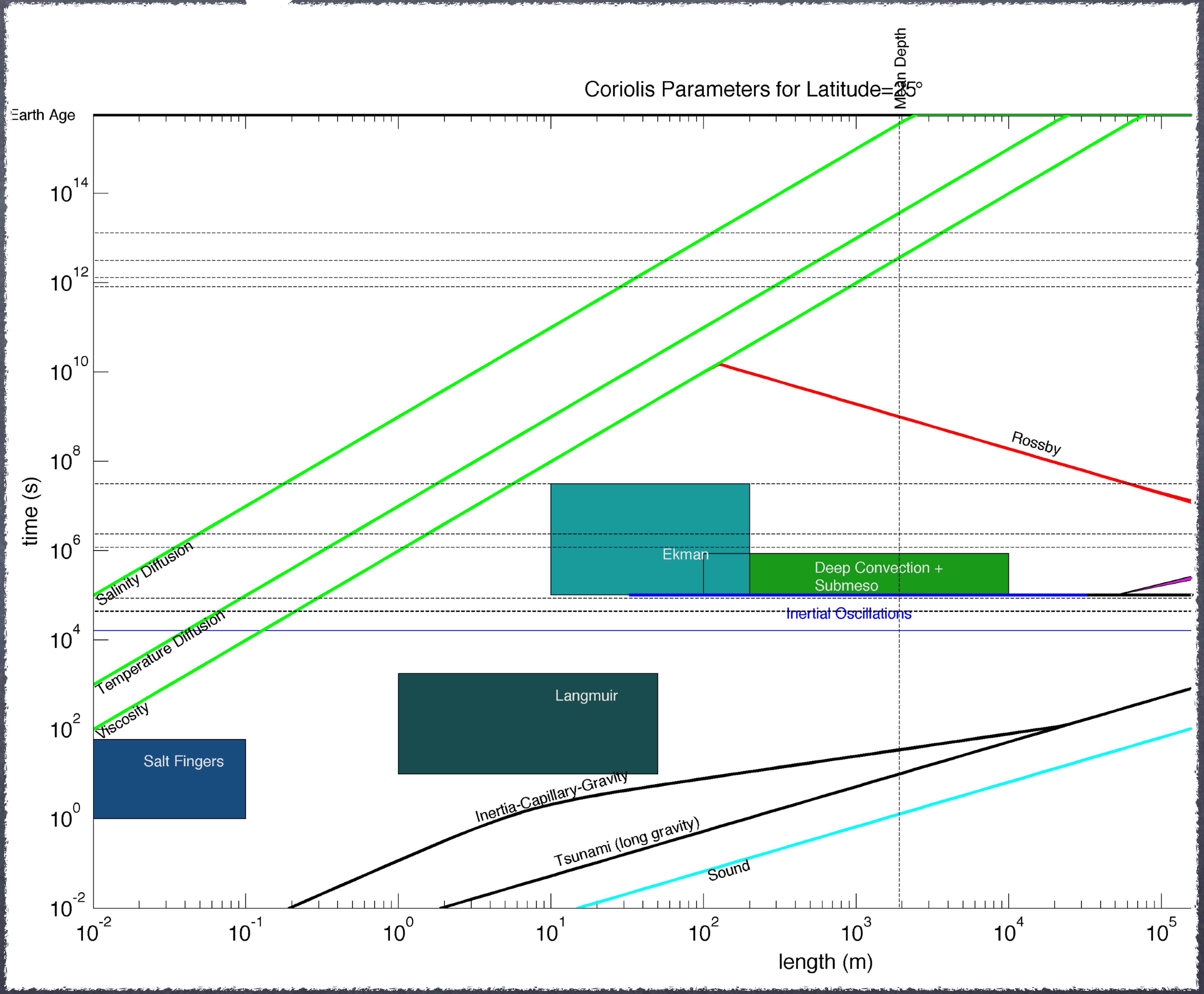

4 Review/Comment Papers: "Notions for the Motions of the Oceans", "Ocean near-surface layers", "Challenges and prospects in ocean circulation modeling", "The small scales of the ocean may hold the key to surprises"